Spectral characterization of paper and print

Wisniewski Dominik

Master's thesis
April 2007
Department of Computer Science and Statistics
University of Joensuu

Dominik Wisniewski

Spectral characterization of paper and print
Department of Computer Science and Statistics
University of Joensuu

Supervisor: Markku Hauta-Kasari

Reviewers: Markku Hauta-Kasari
Raimo Rask

Acknowledgements

This masters thesis was done at Department of Computer Science, University of Joensuu in the time from June 2006 to March 2007. The work related to the thesis is a one of the subprojects of the PAPVISION project (Paper and board printability tests using machine vision) which has been led by Lappeenranta University of Technology. The subproject name is SPECTCHAR, i.e. Spectral Characterization of Paper and Print, and its ultimate goal was to provide novel innovative machine vision solutions based on spectral characterization to paper and printing industry. The main parts of the SPECTCHAR subproject included the following topics: mottling characterization and prediction, inverse color separation process, ink concentration prediction, and basic spectral characteristics of paper and print. The work related to the thesis contained also a confidential part. The confidential issues and results coming from experiments are not publicly available and are not included in this thesis. Also the real names of paper used in the experimental part of the thesis are no publicly available and have been replaced with imaginary names.

In particular, I would like to thank European Union and National Technology Agency of Finland (Tekes) for financial support in the Papvision project. Moreover, I would like to thank our industrial partners including Stora Enso, UPM-Kymmene, Myllykoski Paper, Metso Paper, and Labvision Technologies for their scientific and financial support.

I would like to thank my supervisor and the Director of InFotonics Center at University of Joensuu Dr. Markku Hauta-Kasari for his endless support and overall engagement. Moreover, I would like to thank the reviewer Raimo Rask for his helpful comments and support on the thesis.

I would like to thank professor Jussi Parkkinen for the opportunity to participate the IMPIT program and to work at the InFotonics Center at University of Joensuu.

Special thanks the Project manager of the PAPVISION project Lasse Lensu for many useful comments on this work and support. His advice, suggestions, and willingness to discuss any questions or ideas helped me to complete this work.

In particular, I would like to thank my family and my dear Joanna for giving me their endless support.

Abstract

In the thesis we will investigate possibilities and limitations of spectral imaging systems, mainly equipped with a spectral camera, for spectral characterization of paper and print. Based on spectral reflectance or spectral radiance data being the output of a spectral imaging system, we will investigate possibilities of spectral imaging in the field of printing industry and try to characterize the properties of paper and print from spectral point of view.

The experimental part of the thesis is very extensive and can be divided into three main parts: basic spectral characteristics of paper and print, inverse color separation process of multicolor spectral halftone images, and mottling characterization and its prediction.

The thesis itself has a experimental character. In particular, the author is trying to investigate possibilities and accuracy of spectral imaging systems for characterization of paper and print. This study also tries to show the superiority of spectral imaging over colorimetric imaging systems, i.e. the amount of additional color information accompanying the spectral imaging can be used for better characterization of paper and print. All the conclusions contained in the thesis are based on the results being the output of the experimental part, where the assumptions of a specific spectral imaging system and its setup were done.

The thesis also considers and discusses other equipment which can be used for spectral characterization of paper and print, and which probably would improve the results of the experimental part gained so far.

Keywords: spectral characterization of paper, spectral characterization of print, dot gain, mottling characterization, mottling prediction, inverse color separation, Kubelka-Munk theory, ink concentration prediction.

Contents

1 Introduction

Paper and print are the most common ways of communication. Despite the increasing amount of information available on the Internet, the amount of printed products is not decreasing and is still a very important information media.

"Real world" color is a function of many factors including the spectral power distribution of the illumination, the spectral reflectance or transmittance properties of an objects, and the spectral sensitivity of the observer. Due to the complex nature of light and color there arises a need for better methods for investigating the paper surface properties, and examining the print quality and print characteristics. Accurate color measurements can be obtained by taking into account all the factors which contribute to the physical nature of light and color appearance. However, methods which rely on colorimetric reproductions of real objects, i.e. methods which reduce all the color information to only three signals, are not sufficient for accurate color measurements. The thesis considers and examines the accuracy of using spectral imaging systems for spectral characterization of paper and print. In particular, spectral color reproduction allows us to record and reproduce the true color (exact spectral reflectance properties) of imaged objects with high spatial resolution, whereas the captured color information does not depend on any particular illumination or observer. The thesis is organized as follows:

Chapter 2 introduces the light and color phenomena from physical and psychological point of view, discusses the color formation process and different types of interactions between light and objects. Later, the basis of colorimetry and two main color reproduction types - colorimetric and spectral color reproductions are explained. An extensive comparison of the color reproduction types is given, and basis of spectral imaging systems and measurements are explained. The color halftone printing process is discussed. The chapter finishes with descriptions of samples and setups used in sample measurement phase.

Chapter 3 investigates basic spectral characteristics of paper and print including examinations of average spectra and spectral variances of different kinds of blank papers, spatial variation of blank paper surface, black color formations for different kinds of paper, average spectra and spectral variances of printing inks, and the characterization of the dot gain phenomena. Some theory related to mentioned issues will be given. All the results given in this chapter are based on the experimental part related to the thesis.

In Chapter 4 we will examine whether we can predict some forms of mottling based on spectral reflectance or spectral radiance data. The issue also involves determining the spatial distribution of reflecting and fluorescent substances in paper and print under different lightings and examining spatial variations of printing inks and base paper. All the results given in this chapter are based on the experimental part related to the thesis.

In Chapter 5 we will investigate if the inverse color separation process of multicolor printing inks is possible based on spectral reflectance data: given a spectral

reflectance data of a printing dot image we will try to separate it into four RGB images, where each of them corresponds to one of the printing inks used and contains only printed dots of the same color. In particular, this study will show whether the concentration prediction (what printing inks and in what densities were used to create a particular region) of printing inks is possible based on spectral reflectance data. We will also investigate if it is possible to determine missing or partially missing printed dots in overlapping areas based on spectral reflectance. This study will also show how much information we can get about the printed dot pattern (also in overlapping regions) based on spectral information of printed substrate. Some problems related to concentration prediction and inverse color separation will be discussed and possible solutions will be explained.

Chapter 6 accumulates all conclusions given in Chapters 3 - 5 and gives some hints for further work and investigation related to spectral characterization of paper and print.

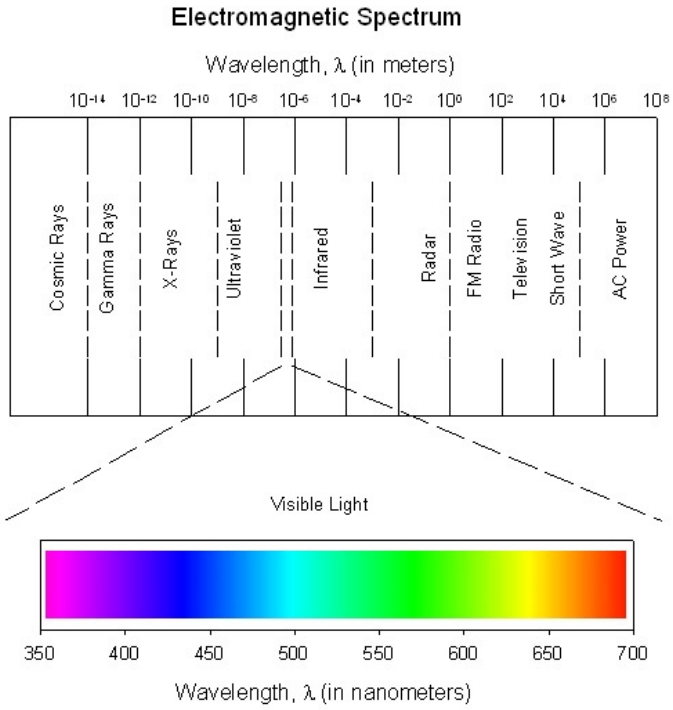

Figure 1: The visible spectrum and its relation to other kinds of electromagnetic radiation (Image taken from http://www.psych.ndsu.nodak.edu).

2 Background

In this chapter we will introduce fundamental concepts related to the nature of light and color. Basis of colorimetry and the multicolor printing process will be discussed. Theory related to colorimetric and spectral imaging systems and their extensive comparison will be given. This chapter finishes with a description of samples and imaging system setups used in the experimental part of the thesis.

2.1 Color and color spaces

2.1.1 Light and color

Visible radiation (spectrum) is a form of energy (part of electromagnetic radiation) which causes a response in the human visual system. The portion of the electromagnetic radiation which we can see is called light and covers a wavelength range in approximately from 400 to 700 nm ($1nm = 10^{-9}m$). The relation of the visible spectrum to other kinds of electromagnetic radiation is shown in Figure 1 [1].

Table 1: Regions and subregions of electromagnetic radiation.

Spectral region	Wavelength range (nm)	Subregion
Ultraviolet	100-280	UV-C
	280-315	UV-B
	315-380	UV-A
Visible	380-430	Violet
	430-500	Blue
	500-520	Cyan
	520-565	Green
	565-580	Yellow
	580-625	Orange
	625-740	Red
Infrared	740 - 1400	Near IR
	1400 - 10000	Far IR

In particular, we can distinguish the following regions and subregions of the electromagnetic spectrum (radiation) shown in Table 1 [25].

Color is the sensation of a visual system (for example the human visual system) caused by a visible physical stimulus (light). Newton's experiment with day light and a prism proved that light can be decomposed into a spectrum of monochromatic components and further decomposition can not be done. According to Newton's experiment light can be characterized by its spectral components, and usually it is done in the form of spectral power distribution which characterizes light by the distribution of power as a function of wavelengths [16].

CIE[1] defines color in the following way:

Attribute of visual perception consisting of any combination of chromatic and achromatic content. This attribute can be described by chromatic color names such as yellow, orange, brown, red, pink, green, blue, purple, etc., or by achromatic color names such as white, grey, black, etc., and qualified by bright, dim, light, dark, etc., or by combinations of such names.

The CIE also adds the following note to the definition of color:

The perceived color depends on the spectral distribution of the color stimulus,

[1]Commission Internationale de l'Eclairage (the International Commission on Illumination - abbreviated as CIE) is the primary organization responsible for standardization of color terminology and color metrics.

the size, shape, structure and surround of the stimulus area, the state of adaptation of the observer's visual system, and the observer's experience of the prevailing and similar situations of observations.

2.1.2 The modification of light by objects

When light strikes an object, spreads in any medium, or interacts with materials, the spectrum of the light can be altered through scattering, reflection, transmission and absorption.

Refractive index The refractive index measures how much the speed of light is reduced in an object (material) in comparison to its speed in the air (vacuum).

At every boundary between two object the speed of light is reduced, and a small amount of the light is reflected or scattered. The direction and the amount of the reflected light beam depends on the initial light beam and the change in the refractive index between these two materials.

Spectral reflectance Spectral reflectance is defined as the ratio of the reflected light to the incident light under specified geometric conditions [12], and usually it is denoted by:

$$R(\lambda) = \frac{I_R(\lambda)}{I_I(\lambda)} \tag{1}$$

, where $I_R(\lambda)$ is the portion of reflected light at wavelength λ, and $I_I(\lambda)$ is the portion of incident light at wavelength λ.

Spectral transmittance The ambient light can go through an object, and then the light is said to be transmitted and the object is said to be transparent. In the case of a colorless object almost the whole light beam is transmitted excepts for a small part which is reflected from the two boundaries of the objects (due to a change in the refractive index).

Spectral transmittance is defined as the ratio of the transmitted light to the ratio of the incident light under specified geometric conditions [12], and is usually denoted by:

$$T(\lambda) = \frac{I_T(\lambda)}{I_I(\lambda)} \tag{2}$$

, where $I_T(\lambda)$ is the portion of transmitted light at wavelength λ, and $I_I(\lambda)$ is the portion of incident light at wavelength λ.

Absorption The ambient light can be absorbed by an object. If the object absorbs a part of the light, then it is colored, but still transparent. On the other hand, if the object absorbs the whole light, then it appears black and is said to be opaque.

In particular, the knowledge about the absorption properties of an object as a function of wavelengths can be used to predict its color.

Scattering Let us consider a homogenous medium with particles which have different refractive indexes (in the case when the medium and the particles have the same refractive indexes no scattering results). Due to the change in the refractive indexes, photons are moved away in different directions, what results in the phenomenon called scattering. The extent of light scattering depends on the difference in the refractive indexes between the two materials and the size of particles in the object.

An object is said to be translucent is some of the ambient light is absorbed, and a part is scattered. If the scattering is so strong that no light can go through an object (material), then the object is said to be opaque (nevertheless, in this case some absorption may occur).

Different pigment sizes and various changes in refractive indexes between the pigments and the resin with which are to be used can give us transparent or opaque coatings. In particular, the knowledge about the scattering and absorption coefficients of colorants as a function of wavelength enables us to predict their colors (for example the Kubelka-Munk theory).

2.1.3 Color formation

There are two kinds of receptors, rods and cones, in the human eye. Rods detect very small amounts of light and are responsible for seeing in the night. Because there is one type of rods, we can only see objects as shades of gray. As the amount of incident light increases rods become inactive and cones begin to send neural signals to the brain. Our sensation of color is caused by three different types of cones which respond differently to light at various wavelengths. The three different types of cone are commonly denoted by L, M, S, and have different spectral sensitivity in the visible spectrum. L cones respond mostly to long wavelength region, M to middle wavelength region, and S to short wavelength region. The spectral sensitivity function related to each type of the cones can be used together with stimulus spectra to determine the response of the cones. The cones, similarly to other detectors, integrate the incident light at all wavelengths, and finally the entire spectrum of incident light is reduced to three cone signals resulting in what is called a trichromacy.

Light coming into the eye can originate in different ways. The simple case occurs when the observer is viewing a self-luminous object and in this situation the light directly originates from the viewed object. More common situation is when

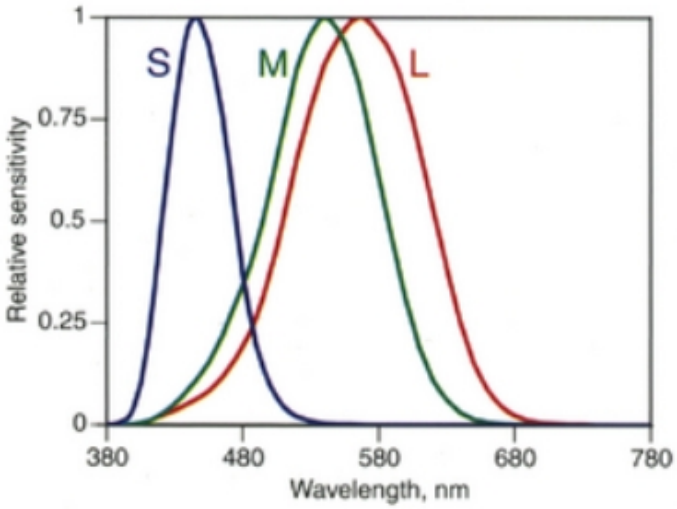

Figure 2: Spectral sensitivity of cones (Image taken from [24]).

objects are illuminated by an external light source and the observer is viewing the objects. In this case, if we assume that the spectral power distribution of the illumination is given by $l(\lambda)$ and an object reflectance is given by $r(\lambda)$, then the amount of light coming into the eye is the product of $l(\lambda)$ and $r(\lambda)$, i.e. $l(\lambda)r(\lambda)$ [16], where λ denotes wavelength. Then, the responses of the three types of cones can be mathematically modelled as:

$$c_i = \int_{\lambda_{min}}^{\lambda_{max}} s_i(\lambda) l(\lambda) r(\lambda) d\lambda \tag{3}$$

, where $s_i(\lambda)$ denotes the spectral sensitivity of ith type of cone at wavelength λ, and λ_{min}, λ_{max} represent the range of wavelength outside of which all these spectral sensitivities are equal to zero. Usually $\lambda_{min} = 360$ and $\lambda_{max} = 830$ [16].

Figure 2 represents spectral sensitivities of different types of cone. The spectral sensitivity of cones L is maximal at 580 nm, for M cone at 545 nm and for S cone at 440 nm. At these wavelengths the observer perceives the color as red, green and blue, respectively [24].

Let us assume that the visible spectrum in the range from λ_{min} to λ_{max} is uniformly spaced by N wavelength values denoted by $\{\lambda_i\}_{i=1}^{N}$, i.e. $\lambda_i = \lambda_1 + (i-1)\Delta\lambda$, where $\Delta\lambda$ is the sampling interval between two successive wavelengths. For computation purposes Equation (3) can be written as:

$$c_i = \sum_{j=1}^{j=N} s_i(\lambda_j) l(\lambda_j) r(\lambda_j) \Delta\lambda = s_i^T f \tag{4}$$

, where $i = \{1, 2, 3\}$, T denotes vector transposition, $f = [l(\lambda_1)r(\lambda_1), ..., l(\lambda_N)r(\lambda_N)]$, $s_i = \Delta\lambda[s_i(\lambda_1), ..., s_i(\lambda_N)]^T$. Let us rewrite Equation (4) as:

$$c = S^T f \tag{5}$$

, where $c = [c_1, c_2, c_3]$, and $S = [s_1, s_2, s_3]$.

Let us now consider two N-vector spectra denoted by f and g. The two spectra produce the same responses in the cones if:

$$S^T f = S^T g \tag{6}$$

Let us notice that the above system of equations has multiple solutions. Furthermore, based on this equation, we can deduce the phenomena called *trichromacy*: for a given stimulus (spectrum) it is possible to produce a color match (the same response in cones under the same viewing conditions) by using light being combinations of three colorimetrically independent (a set of spectra is said to be colorimetrically independent if the color of any spectrum can not be visually matched by a linear combinations of the other spectra) light sources (color primaries). In other words, for any visible spectrum, there exists a linear combination of three color primaries which visually matches the initial spectrum [16].

2.1.4 Basis of colorimetry

In this section we will introduce the standard CIE illuminants and observers, and describe the way of calculating the tristimulus values from spectral reflectance data of a material, a CIE standard illuminant and a CIE standard observer.

As it was mentioned earlier, the color of a visible spectrum can be specified in terms of the tristimulus values. Let us notice that in order to have agreement between different measurement types of color, it is necessary to define a set of standard illuminants and color matching functions for observers with respect to which the tristimulus values will be computed.

CIE standard observers In 1931, the CIE defined standard colorimetric observers by providing two different, but equivalent, sets of color-matching functions (abbreviated as CMFs): the CIE RGB CMFs $(\overline{r}(\lambda), \overline{g}(\lambda), \overline{b}(\lambda))$ and the CIE XYZ CMFs $(\overline{x}(\lambda), \overline{y}(\lambda), \overline{z}(\lambda))$.

The $(\overline{r}(\lambda), \overline{g}(\lambda), \overline{b}(\lambda))$ set of CMFs defines the tristimulus values of the spectrum colors for a fixed set of monochromatic primaries. The primaries were selected at 435.8 nm, 546.1 nm and 700 nm, and the corresponding tristimulus values define the amounts of each of the primaries which will yield a color match to the initial spectrum [12]. Because the CIE RGB CMFs have both positive and negative values, another set of CMFs only with positive values was required. Thus, the second set of CIE XYZ color-matching functions was defined as a linear transformation from CIE RGB CMFs.

Due to some requirements imposed on the new set of CMFs (in particular the color-matching functions are to be all positive), the selected primaries are not physically realizable. The system based on the primaries is called XYZ color system

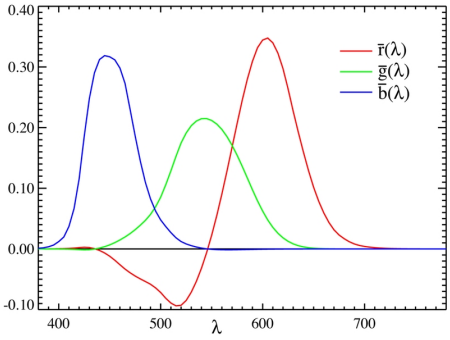

Figure 3: The CIE 1931 RGB color matching functions.

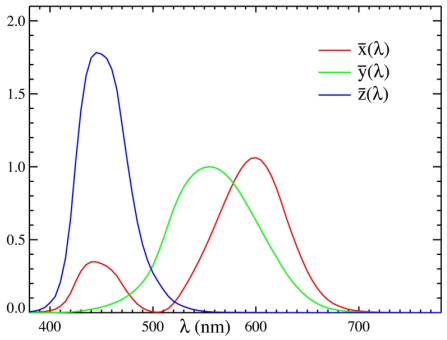

Figure 4: The CIE 1931 XYZ color matching functions (commonly called the 2^o CIE 1931 Standard Colorimetric Observer).

with $\overline{x}(\lambda), \overline{y}(\lambda), \overline{z}(\lambda)$ as color-matching functions, and it is assumed to simulate the color matching results of the average person with normal color vision.

Figure 3 and 4 show the CIE RGB and CIE XYZ color-matching functions, respectively (images taken from [26]). Clearly, the two sets of CMFs are not the cone spectral sensitivity functions, but linear transformations of them.

In particular, the CMFs were derived in such a way that they yield equal tristimulus values for the equi-energy spectrum (equal amounts of X, Y and Z produce white).

The two sets of observers defined in 1931 by the CIE are the 2^o CIE standard observers. Later, in 1964 CIE defined another set of color matching functions for 10^o standard observer which will not be discussed here (see for example [16]).

CIE standard illuminants In addition to CMFs, the CIE also defined a number of standard light sources. These are used in colorimetry of nonluminous reflecting objects, and are known in the CIE terminology as illuminants. There exist the following CIE standards of illuminants:

- CIE standard illuminant A represents the light coming from a blackbody radiator at color temperature of 2856 K. It is used to represent incandescent lighting such as a filament lamp [16];
- CIE Standard Illuminant B emulates noon sunlight at color temperature of 4874 K. The CIE standard illuminant B has been realized by putting double liquid filter in front of light source A [25];
- CIE Standard Illuminant C emulates the average daylight of temperature 6750K, but real daylight contains more ultraviolet than illuminant C. The illuminant has been realized by putting liquid filter in front of light source A [25];

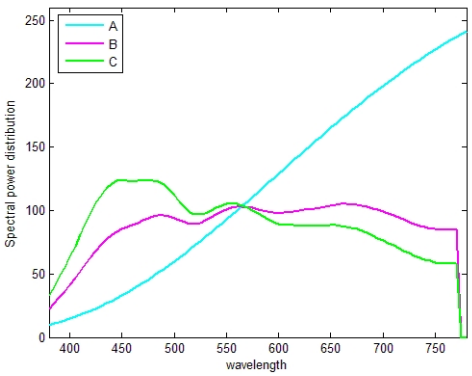

Figure 5: Spectral power distribution of CIE A, B and C illuminants.

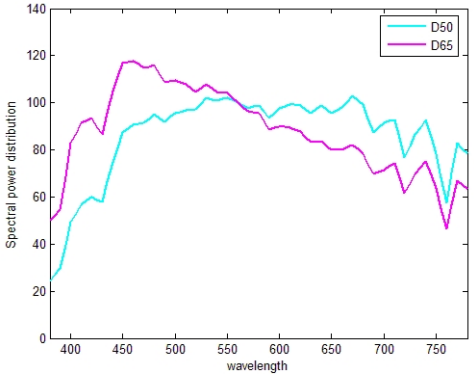

Figure 6: Spectral power distribution of CIE D50, D65 illuminants.

- the D series illuminants are used to represent natural daylight. In particular, the D65 illuminant has the correlated color temperature of 6500 K, D50 of 5000 K and D75 of 7500. They were defined to replace illuminants B and C [25];

- the F series illuminants are used to represent various types of fluorescent lighting. For example, illuminant F2 represents cool white fluorescent, F11 represents narrow-band fluorescent, F7 and F8 represent daylight fluorescent (often used as approximations of D65 and D50, respectively) [27].

Figures 5 and 6 shows spectral power distributions of a couple of CIE standard illuminants.

In particular, the D65 illuminant is one of most important light sources used in day light sample measurements . As mentioned earlier, it belongs to the D series that try to simulate standard illuminating conditions at open air in different parts of the world. The D65 illuminant corresponds roughly to a midday sun in Western/Northern Europe. The CIE 1931 chromaticity coordinates of D65 are $x = 0.31271$ and $y = 0.32902$, and the CIE 1964 chromaticity coordinates are $x = 0.31382$ and $y = 0.33100$.

Calculating the XYZ tristimulus values The tristimulus values calculated with the CIE RGB CMFs are called CIE RGB tristimulus values. Similarly, the tristimulus values calculated with the CIE XYZ CMFs are called CIE XYZ tristimulus values.

Let us assume that S is the spectral power distribution of a light source, R is the spectral reflectance of an object and $\overline{x}$, $\overline{y}$, $\overline{z}$ are the CIE observer color matching functions. Then the tristimulus values calculations for reflecting objects is as follows [12]:

$$X = k \sum_{i=1}^{N} S(\lambda_i) R(\lambda_i) \overline{x}(\lambda_i) \Delta\lambda \tag{7}$$

$$Y = k \sum_{i=1}^{N} S(\lambda_i) R(\lambda_i) \overline{y}(\lambda_i) \Delta\lambda \tag{8}$$

$$Z = k \sum_{i=1}^{N} S(\lambda_i) R(\lambda_i) \overline{z}(\lambda_i) \Delta\lambda \tag{9}$$

$$k = \frac{100}{\sum_{i=1}^{N} S(\lambda_i) \overline{y}(\lambda_i) \Delta\lambda} \tag{10}$$

, where k is a normalizing factor. Let us notice that the normalizing factor has the following implications on the value of Y:

- then dealing with reflecting objects, the value $Y = 100$ will be assigned to ideally nonflorescent white which reflects 100% of the ambient light at all wavelengths;
- then dealing with transparent objects, the value $Y = 100$ will be assigned to perfect colorless materials which transmits 100% of the ambient light at all wavelengths.

The Y value is called the luminance and correlates with the perceived brightness of the radiant spectrum [16]. The CIE XYZ tristimulus values can be thought to be three variables which define a three-dimensional space in which each axis corresponds to a primary, and a set of tristimulus values define a position within the three-dimensional color space. The CIE XYZ color space is special because it is based on experimental measurements of the human visual system, and it serves as the basis from which other color spaces are derived (for example standard-RGB (abbreviate as sRGB)).

Similar equations to Equations (7) - (10) can be defined for the CIE RGB tristimulus values.

2.1.5 Additive and subtractive color mixing

The term additive color mixing refers to the mixing of lights, while subtractive color mixing refers to the mixing of colorants.

It is obvious that different industrial processes (for example printing process and textiles) or devices (for example CRT monitors) use primaries which vary a lot in spectra. We will try to remove these ambiguity and define primaries by their spectra based on theoretical backgrounds. We assume that the visible spectrum is divided into three regions: light below 500 nm is of blue color, light between 500 nm and 600 nm is of green color, and light above 600 nm is of red color [12].

Table 2: Additive color mixing of the theoretical additive primaries.

Primary on	Color	Primary on	Color
No primary	Black	Red + Green	Yellow
Red	Red	Red + Blue	Magenta
Green	Green	Green + Blue	Cyan
Blue	Blue	All	White

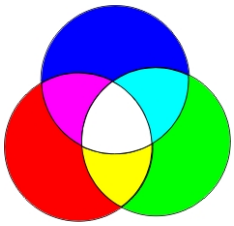

Figure 7: Additive color mixing.

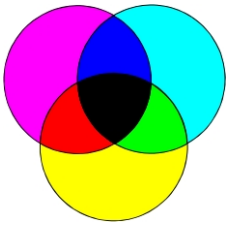

Figure 8: Subtractive color mixing.

The theoretical red, green and blue additive primaries produce light only in the spectral range which corresponds to their color name. Changing the amount of a theoretical primary results in various amounts of light. The spectral shape of the theoretical primary is independent of the current light intensity, and only the amplitude of spectral power of the light changes. As the amount of a theoretical primary increases (the amplitude increase), light is being added. In particular, 0% of a theoretical primary corresponds to the lack of light (black color results), and 100% corresponds to the particular primary [12].

Table 2 contains colors resulting from lights being a combination of different sets of the additive theoretical primaries. Colors which result from combining a pair of primaries are called secondary colors (secondaries).

Figures 7 represents additive primaries and principle of additive color mixing.

The theoretical subtractive primaries are cyan, magenta, and yellow (the complement of additive color mixing). Changing the amount of a theoretical subtractive primary from 100% to 0% results in colors between the particular primary and white. The process of mixing two primaries results in a additive primary (see Figure 8).

Subtractive color mixing can be defined a process of spectrally selective absorption of radiant power of an existing light (white light) by an object. The object (for example ink) causes a light subtraction and the remaining radiant power is reflected or transmitted. For example, cyan and yellow yield green color because cyan absorbs red light, yellow absorbs blue light, and consequently the only not absorbed light is green. Similar conclusions can be made for remaining subtractive

Table 3: Subtractive color mixing of the theoretical additive primaries.

Primary on	Color	Primary on	Color
No primary	Black	Cyan + Magenta	Blue
Cyan	Cyan	Cyan + Yellow	Green
Magenta	Magenta	Magenta + Yellow	Red
Yellow	Yellow	All	Black

primary combinations (see Table 3).

Additive color mixing is applied in coloration systems which are light emitters, and subtractive color mixing is applied in coloration systems which combine unabsorbed light. CRT monitor and televisions are examples of additive coloration systems. Color printing and fiber blending have features of both, additive and subtractive, coloration systems (for example an overprint of two subtractive primary results in additive color primary).

2.1.6 RGB color model

The RGB color model is an additive model in which red, green and blue are the primaries. The primaries are added together in various proportions of intensity to create other colors of the visible radiation according to additive color mixing model.

The RGB color model does not define the "red", "green" and "blue" colors, and the results of mixing them in various intensities (only the additive color mixing is assumed in the model). The color model becomes an absolute color space (such as for example *sRGB* or *AdobeRGB*) when the three primaries are defined, i.e. exact spectral make-up of the primaries is done.

The RGB color model is usually shown as a cube in Cartesian coordinate system as presented in Figure 9. The diagonal of the cube going from $(0, 0, 0)$ - black color to $(1, 1, 1)$ - white color corresponds to the gray scale.

Figure 10 shows a non-linear transformation of the RGB color cube into another color system which is usually known as the HLS color system (stands for Hue, Saturation, Lightness). The HSL color space gives us perceptual ordering of color and can be represented graphically as double hexcone, where the distance along the main axis corresponds to lightness (L) with the two apexes corresponding to black and white colors, the distance from the axis to a particular point corresponds to saturation (S), and the angular parameter corresponds to hue (H).

RGB color spaces are perceptually non-linear, i.e. equal differences in the RGB values do not correspond to equal differences in the perceived color. RGB color spaces are also device-dependent, i.e. the same RGB color values will give different results when viewed on different devices. In particular, if we view the

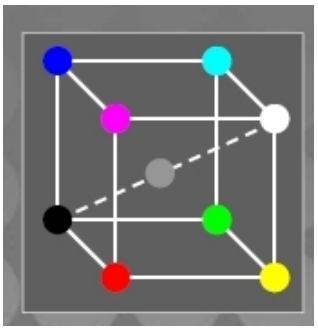

Figure 9: The RGB color model mapped to a cube (Image taken from [28]).

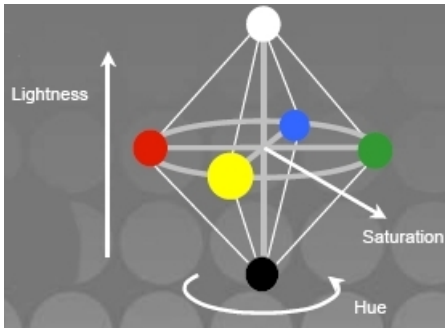

Figure 10: Double hexcone created by rotating the RGB cube (Image taken from [28]).

same RGB image on two different CRT monitors they will probably look different. The difference is mainly caused by slightly various monitor gamut and different monitor settings. Thus, RGB values can be treated a recipe given to a particular device to display a particular color.

RGB color spaces are easy to implement, unintuitive and used for devices such as digital cameras, color displays and scanners.

2.1.7 CMY color model

CMY (refers to cyan, magenta and yellow) is a subtractive color model used in color printing process, where various colors are being created according to subtractive color mixing. Similarly to RGB color model, CMY color model is device-dependent, i.e. the output colors corresponding to particular CMY vales will vary when sent to two different printers or applied to papers with various characteristics.

Theoretically, the relation between RGB values and CMY values in CMY color model is as follows:

$$Cyan = 1 - Red \qquad Magenta = 1 - Green \qquad Yellow = 1 - Blue \tag{11}$$

, where Red, Green, and Blue indicates intensities of RGB primaries which are expressed as fractional values in the range from 0 to 1. In reality, the process of calculating the cyan, magenta and yellow values from the RGB values is more complex, and in particular it involves device-specific, ink-specific, and paper-specific considerations.

2.1.8 CIELAB color space

The CIE XYZ color space is not uniform[2] in that sense that equal perceptual differences in color do not correspond to equal distances in the color space [16]. In 1976 the CIE defined the CIE 1976 $L^*a^*b^*$ uniform color space (called also CIE Lab or CIELAB color space). The color space were defined in terms of transformations from the CIE XYZ color space.

The color space employs a lightness scale L^* which depends only on the illuminance value Y of the CIE XYZ color space. $L^* = 0$ corresponds to black and $L^* = 100$ indicates white (i.e. constant reflectance equal to one). Positive values of a^* represents the amount of purplish red, and negative values of a^* indicates the amount of green. Positive values of b^* represents the amount of yellow, and negative values of a^* indicates the amount of blue.

The L^*, a^* and b^* values corresponding to X,Y,Z values from the CIE XYZ system are given by:

$$L^* = 116 f(\frac{Y}{Y_n}) - 16 \tag{12}$$

$$a^* = 500(f(\frac{X}{X_n}) - f(\frac{Y}{Y_n})) \tag{13}$$

$$b^* = 200(f(\frac{Y}{Y_n}) - f(\frac{Z}{Z_n})) \tag{14}$$

, where

$$f(x) = \begin{cases} \sqrt[3]{x} & x > 0.008856 \\ 7,787x + \frac{16}{116} & x \leq 0.008856 \end{cases} \tag{15}$$

X_n, Y_n, Z_n correspond to CIE XYZ tristimulus values of the reference white point (for example the CIE D65 standard illuminant).

Figure 11 shows a 3D representation for the CIE Lab color space, and Figure 12 shows the CIE Lab color space for $L^* = 25$.

The CIE Lab is the fundamental color space in color management systems and as a device-independent color space it is used for translations between different device-dependent color spaces (a conversion of color data between the native color space of one device and the native color space of another device, for example between two different monitors). In particular, a device-independent color space is not dependent on any particular device, and such a system is meant to be a true representation of colors as perceived by the human visual system.

The reverse transformation i.e. from the CIE Lab color space to the CIE XYZ color space will be skipped here and can be found for example in [12][16].

[2]As mentioned earlier, RGB and CMY systems are also examples of not uniform color spaces.

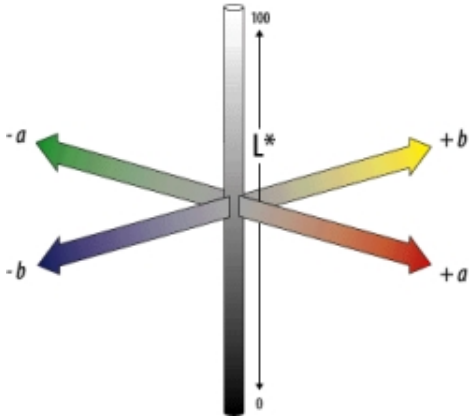

Figure 11: CIE Lab color space.

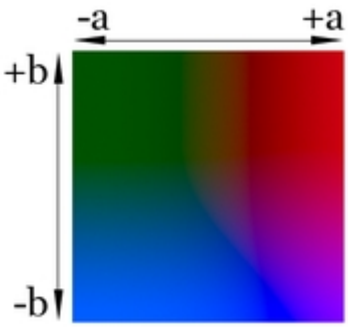

Figure 12: CIE Lab color space at $L^* = 25$ (Image taken from [31]).

Color differences Let us suppose that we have two points $(L^*_{meas}, a^*_{meas}, b^*_{meas})$ and $(L^*_{ref}, a^*_{ref}, b^*_{ref})$ in CIE Lab color system which corresponds to a measured and reference colors, respectively. Let us define the differences in lightness (ΔL^*), redness-greenness (Δa^*) and yellowness-blueness (Δb^*) as follows:

$$\Delta L^* = L^*_{meas} - L^*_{ref} \tag{16}$$

$$\Delta a^* = a^*_{meas} - a^*_{ref} \tag{17}$$

$$\Delta b^* = b^*_{meas} - b^*_{ref} \tag{18}$$

A positive value of ΔL^* means that the measured sample is lighter than the reference one. A negative value of ΔL^* indicates that the measured sample is darker than the reference one. A positive value of Δa^* means that the measured sample is more reddish than the reference one. A negative value of Δa^* indicates that the measured sample is more greenish than the reference one. Finally, a positive value of Δb^* means that the measured sample is more yellowish than the reference one, and a negative value of Δb^* indicates that the measured sample is more bluish than the reference one.

The total color difference between the two samples is given by (Euclidean distance between two colors in the CIE Lab color space):

$$\Delta E^*_{ab} = \sqrt{(\Delta L^*)^2 + (\Delta a^*)^2 + (\Delta b^*)^2} \tag{19}$$

There exist more sophisticated color difference formulas, in particular including the CIEDE200 color difference formula [6].

2.2 Color reproduction

Color reproduction can be broadly defined as acquisition and replication of color information of a scene (object) on another media. [17] gives the following definition of color reproduction process:

Color reproduction can be defined as an optical process of producing a close color representation of some original scene or object. Photography, electronics, and the physical transfer of a colorant to a substrate may each play a role in this process, depending on the form of the reproduction. In a broad sense, the process includes making photographic transparencies and prints, television images, and printed reproductions.

We are especially interesting in two kinds of color reproduction: spectral and colorimetric imaging.

Spectral color reproduction The objective of spectral color reproduction is to achieve identical spectral power distribution between the reproduction and the original object. In this case, the colors of the original and the reproduction will match for all observers and for all illuminants (independence from any observer and any illumination is achieved). Moreover spectral color reproduction is the only way to diminish or eliminate the effect of metamerism.

Colorimetric color reproduction Colorimetric color reproduction is achieved when the CIE tristimulus value (X, Y, Z) of the reproduction and the original are the same. This kind of color reproduction does not guarantee that the spectra of the original and the reproduction are the same (virtually it is almost impossible to achieve the match in spectra). The reproduced colors fully depend on the illumination and the observer used, and the image match the original as long as the viewing conditions do not change. In the case, when the viewing condition are changed, the color acquisition process and the calculation of the CIE tristimulus values must be repeated to achieve colorimetric match to the original.

2.2.1 Colorimetric imaging

Traditional (colorimetric or metameric) imaging is based on the physiology of the human eye.

In traditional imaging systems a limited number of channels is used (usually three), but careful system design still enable us to reproduce images with sufficient fidelity for most of applications. The phenomena of reducing all color information to only three signals has been applied to many used in practice color reproduction system including television, printing and photography. As described in Section 2.1.3, the human visual system can not sense the individual contributions each

wavelength of a particular stimuli makes, but instead it can just sense the aggregate effect.

Advantages Since traditional imaging quantizes the whole spectral information into 3 channel color image, the amount of information in colorimetric imaging is relatively small in comparison with the spectral information. Small amount of data makes image data processing fast, and minimizes the storage requirements. As mentioned earlier, careful colorimetric system design still enable us to reproduce images with sufficient fidelity for most of applications.

Disadvantages The most important problem of colorimetric imaging systems is metamerism. The phenomena is described in details in the next section. Colorimetric imaging systems make color reproductions which are metameric to the originals. In particular, it means that color matching of the original and the reproduction is relative to the viewing conditions (illumination and observer). They can much under one set of viewing conditions, but mismatch under another set of viewing conditions. In particular the acquired color information about an object is "dirty", i.e. the color information of the object is the color of the object under specified light source and observer. It diminishes very much the possibilities of faithful reproduction of the imaged object under different viewing conditions. In particular two physical stimuli with different spectral compositions can look identical under one set of viewing conditions and different under another set of conditions.

Colorimetric systems quantize spectral data coming from physical stimuli to produce three-color scene and therefore a large number of different spectral distributions in the scene can produce the same response (physically different color stimuli are transformed to the same color information).

In particular, [18] enumerates the following limitations of RGB-based systems:

1. the RGB values obtained in conventional imaging systems can have different meaning for different devices. The output values depend on the device characteristics, illuminants, pre-processes involved in the imaging systems and user preference settings. Therefore, RGB values do not give the objective and correct color information;

2. the spectral sensitivity characteristics of conventional imaging systems are different from the human vision system;

3. image retrieval based on color information in image archives and databases is limited since RGB values depend on imaging devices and illuminants. In particular, the target object could not be found in a databases, if the imaging system or the illuminant has been changed;

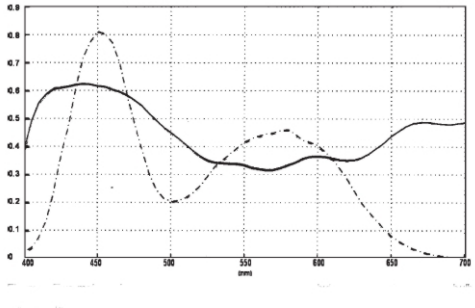

Figure 13: Two metameric spectra that look the same in daylight, but different under tungsten bulb illumination. (Figure taken from [22]).

Figure 14: Objects under daylight and tungsten bulb.

4. calculating the color under different illuminant and for different observers is impossible. Image acquisition phase under the specific viewing conditions must be repeated.

2.2.2 Metamerism - the blessing and the curse

Metamerism is a phenomenon in which spectrally different stimuli match to a given observer [12]. Stimuli do not have to have identical physical properties in order to match in color. If two spectrally different stimuli match in color under specified illumination and observer then they can mismatch due to change in light source or observer.

A pair of objects which have different spectral reflectance curves, but the same color coordinates for a specified illumination and a specified observer is called a metameric pair or metameric objects [12]. The pair of objects is said to exhibit a metamerism. If the pair exhibits metamerism upon a change in observer (illumination), then the pair is said to exhibit a observer (illuminant) metamerism.

A pair of objects, whose spectral reflectance curves differ in visible spectrum, is a metameric match, if their colors match under specified illumination and viewing condition. Similarly, a pair of objects, whose spectral reflectance curves are the same in visible spectrum is a spectral match. Such a pair of objects match under all illuminations and for all observers.

[22] proves the need for multispectral imaging by introducing the problem of metamerism, and showing a clear example when traditional colorimetric imaging systems fail.

Figure 13 shows two spectra from two different objects. Under daylight illumination the objects have the same CIE Lab values equal to $L^* = 66.90$, $a^* = 11.94$ and $b^* = -24.60$. Under tungsten bulb illumination the two objects have different

CIE Lab values. These are $L^* = 66.37$, $a^* = 5.27$ and $b^* = -24.16$ for one object, and $L^* = 66.51$, $a^* = -5.80$ and $b^* = -22.84$ for another.

There are many examples of applications in which metamerism effect is employed and also many examples where the phenomenon is not desired. In particular, metamerism allows us for easy color reproduction and the phenomena has enabled various color image technologies to exist. Most color reproduction systems including television, photography, movies and printing rely on three or four primaries to represent our chromatic world [12]. For example, the three phosphors used in color CRT displays can generate a wide range of colors that match many objects. On the other hand, the majority of color reproductions on paper substrates utilize combinations of cyan, magenta, yellow and black inks (called colorants). No combination of these inks can generate spectral matches to the original scene. Therefore, a printed reproduction of an original scene is usually a metameric match to the former, and accurate viewing is thus dependent upon a specified illumination and upon a specified observer.

2.2.3 Spectral imaging

Since colorimetric imaging does not provide sufficient amount of information to accurately reproduce color, another approach using more spectral dimensions is needed. Spectral imaging allows us to record the true color (exact spectral reflectance) of imaged objects with high spatial resolution, whereas the color does not depend on any particular illumination or observer.

Spectral imaging can be defined as acquiring, processing, displaying and interpretation of images with a number of spectral channels exceeding three found in colorimetric (traditional) color imaging. Thus, the key feature of spectral imaging distinguishing it from colorimetric imaging is the number of sampled image dimensions exceeding the 3-D color resolution of the human visual system [19]. Spectral imaging systems, unlike to colorimetric imaging systems, are based on the physics of light and its interaction with real-world objects. The range of wavelengths is not necessary confined to the visible spectrum and mostly depends on a particular application. Multispectral imaging allows us to determine (compute) the color of a imaged object for any arbitrary observer and illumination.

Advantages Spectral imaging systems give us a possibility for acquiring more information about color and thus allow us for high-fidelity color reproduction.

Spectral imaging systems are able to divide signals of imaged objects into two categories: a category which is due to the object and a category which is due to the illumination itself. Thus the spectral reflectance of the imaged objects can be distinguished effectively from the other factors. Having reflectance spectra of imaged objects gives us, in particular, the ability of reproducing the image under different viewing conditions, i.e. for different illuminations and observers, without repetition of the image acquiring stage. It should be also noticed that traditional

Table 4: Storage requirements for spectral image data

Image size	Colorimetric imaging	Spectral imaging
1024×768	2,25 MB	91,1 MB

colorimetric imaging systems are not able to recognize which image signals are due to the illumination and which are due to object itself.

Spectral imaging enables us to diminish or eliminate the effect of metamerism. As the spectra of original and the reproduction become closer, the effect of metamerism problem is reduced. Due to acquired spectral reflectance[3] of imaged objects, the original and the reproduction will match under any illumination and any observer - about such pair of objects we say that they are isomers instead of metamers.

Responses of spectral imaging systems can also be used to estimate CIE tristimulus value more accurately (colorimetry-based reproduction on the basis of multispectral data).

Spectral models for devices (such as printers), in principle, can achieve more accurate characterizations of corresponding devices than corresponding colorimetric models.

Disadvantages We can suspect that along with the large amount of additional image data in a spectral imaging, the storage requirements for spectral images will be considerably higher. Table 4 shows sample storage requirements of spectral imaging in comparison with colorimetric imaging. It is assumed that the size of sample image is 1024×768, colorimetric imaging uses three channels with 8 bits per channel, and spectral imaging uses 81 channels (5 nm visible spectrum sampling from 380 nm to 780 nm) with 12 bits per channel.

Another consequence of considerably larger amount of data in case of spectral imaging is slower image data processing. In the case of colorimetric imaging, image processing can be performed in real-time and does not require expensive hardware. When the spatial size of sample scene and number of channels increases, then real-time processing of spectral image data becomes impossible or significantly slower.

In general multispectral images produced by spectral imaging systems can not be directly viewed, but they make up a base from which derivative images are produced, and then displayed or printed.

Extensive usage of multispectral technology in color imaging is still diminished by high cost and usually is confined to applications which can not tolerate metamerism phenomena and for which cost is not a crucial ingredient (for example medical imaging, artwork reproduction and others).

[3]We can also say that an exact spectral match between original and reproduction is achieved.

2.3 Acquisition of spectral color information

Much of research has been done in investigating issues such as efficient spectral representation of spectral images, the optimum number of spectral channels and the optimum number of bits per channel. In this section we will try to address all of the problems, answer the questions, and make explanations for our choice.

2.3.1 Spectral camera

Unlike to spectrometers and spectrophotometers, spectral camera images a line of a sample (scene) at a time and disperses light to its spectral sensitive components in each spatial location in the line. Thus, the output of a spectral camera is a two dimensional image (image frame) with spatial axis in one direction (imaged line sample) and spectral axis in another direction (spectral information in each spatial location (pixel) of the line). Thus, the whole sample (scene) can be imaged by moving either the camera relative to the sample or the sample relative to the camera. After measuring the whole sample and joining together the acquired image frames corresponding to line images, a three dimensional image will result with two spatial axes (corresponding to the two dimensional nature of the sample), and one spectral axis (corresponding to the spectral information in each spatial location of the sample). Figure 15 shows main parts of a spectral camera and the underlying operating principle of it [20].

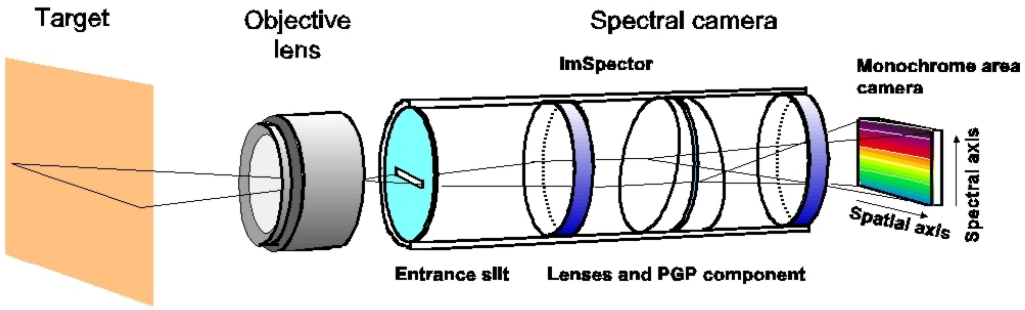

Figure 15: Operating principle of a spectral camera (Image taken from [20]).

Figure 16 shows the intuitive structure of one line captured by a spectral camera. As mentioned earlier, the line is internally represented by a two dimensional image with a spectral axis in one and spatial axis in another direction. The determination of spectral reflectance value for a particular spatial location (pixel) is done on the basis of values which lie along the spectral axis corresponding to the examined pixel.

Figure 17 shows spectral image formation by a spectral camera. As we can see, the second spatial axis (determined by successive lines which are to be measured) can be considered as the time axis. Nevertheless, the time axis corresponds to

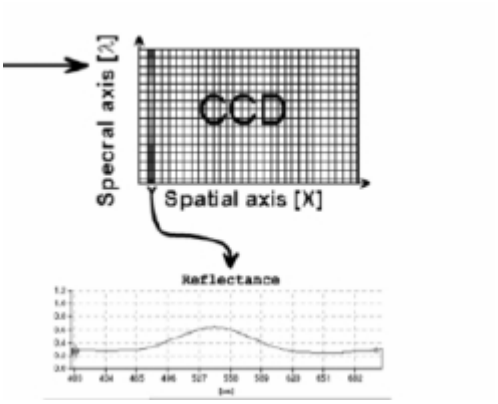

Figure 16: Spectral and spatial axes and spectral reflectance formation.

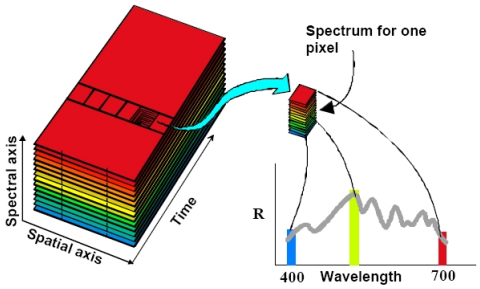

Figure 17: Spectral image formation by a spectral camera. (Figure taken from [20]).

the total number of measured lines which have been measured by the spectral camera. After the scene is imaged, a three dimensional image is the output of the measurement phase.

Spatial resolution Spatial resolution of a spectral camera is determined by the number of pixels which make one captured sample line. Usually spatial resolution of spectral cameras is between 1200-1600 pixels per one imaged line.

The line width which is imaged by a spectral camera depends on several factors including the distance of the spectral camera from the sample, the adjustment of objective lens, and effective slit length. Let us notice that the line width and the spatial resolution of a spectral camera affect the final spatial image quality. To achieve high spatial image reproduction, the line width should be minimized. The minimum line width is determined by optics elements of a spectral camera and clearly it can not be smaller than the effective slit length. Since the effective slit length is approximately equal to 9-10 mm. Thus, we can get a spatial accuracy about 1200-1600 pixels per each 9-10 mm of the original sample.

Spectral resolution The optimal number of channels used can vary from application to application, and usually it depends on the imaged object or scene, illumination, imaging system, and techniques used for reconstructing the original spectral image form the output values of the spectral camera.

Typically spectral cameras are able to give spectral responses in the visible wavelength range, i.e. from 380 nm to 780 nm. Spectral cameras with broader range exceeding the visible spectrum wavelengths are also available.

Spectral information sampling scheme can be usually controlled by software managing the spectral camera. [21] reports that reflectance of natural objects under illuminants which do not have sharp spectral peeks are smooth functions of

wavelengths, and thus it suffices to sample spectral information with wavelength intervals equal to 5, 10 or 20 nm. Number of bits per each channel, similarly like in traditional imaging, is of big concern in spectral imaging as well. It has been reported that 12 bits per channel is sufficient to achieve high-fidelity spectral color reproduction. It should be also noticed that 12 bits per channel is the top limitation of most of spectral cameras.

Spectral camera focusing [20] is a spectral camera user manual which introduces the concept of spectral camera, its operating principle, and its advantages and disadvantages. A mechanical construction and detailed specification of different kinds of spectral cameras are given. The document describes also focusing and spatial alignment principles of a spectral camera with respect to a sample.

As mentioned earlier, the spectral camera is a line-scan system, i.e. it measures a line of a sample at a time. The goal of the spatial camera alignment with respect to the sample is to ensure that:

- the imaged line is at desired position of the measured sample;
- the sample is evenly illuminated;
- the objective lens are focused properly.

These above goals can be achieved by using a special test target (see Figure 18) and then applying the alignment procedure described below. The test target is placed on the same surface where the imaged object will be placed, and after the alignment procedure is finished it is removed from the surface.

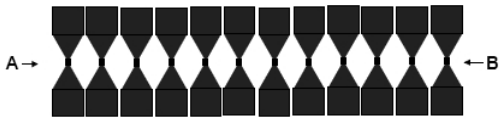

Figure 18: Test target for spectral camera alignment (Figure taken from [20]).

Figure 18 shows a typical test target for spectral camera alignment procedure. As already described, the spectral camera measures a single line of a sample at a time, and the output is a two dimensional image with spatial axis in one and spectral axis in another direction. Thus, a color image would be a bad candidate for the test target due to spatial and spectral variations of the output image. Hence, black-white image will be used as the target, where black areas correspond to the lack of signal at all wavelengths, and white areas give signal at all wavelengths.

Figures 19 and 20 (Figures taken from [20]) show typical output images from a spectral camera. The former image indicates a situation when the spectral camera

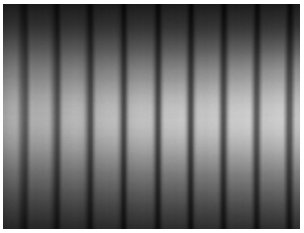

Figure 19: Spectral camera is out of focus.

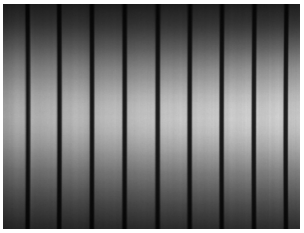

Figure 20: Spectral camera is in focus.

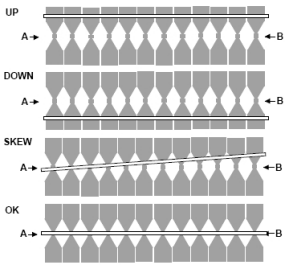

Figure 21: Spectral camera alignments.

is out of focus, and the latter image indicates a situation when the configuration of the spectra camera is right i.e. the spectral camera is in focus.

Figure 21 (Figure taken from [20]) shows a typical alignment errors and proper configuration of the spectral camera. The line A-B shown in Figure 18 is the desired measurement line and the goal of the alignment procedure (see [20] for detailed description of the alignment procedure).

Data processing in spectral imaging In this paragraph we will explain basic data processing steps for precise spectral color acquisition with a spectral imaging system consisting of a light source (illuminant), lens or fiber optics connected to a spectral camera, an imaged sample and a PC computer. The basic camera preparation steps include the following:

1. spectral camera calibration and adjustment (see previous paragraph);
2. acquire and store black reference (typically by blocking the light which enters the lens and then measuring the spectral radiance);
3. acquire and store white reference.

The basic steps of image acquisition and spectral reflectance calculations involve [20]:

1. image acquisition;
2. averaging step (binning), optionally;
3. calculating spectral reflectance for pixels of interest based on the following equation:

$$R_\lambda = \frac{sample_\lambda - dark_\lambda}{white_\lambda - dark_\lambda} \tag{20}$$

, where $sample_\lambda$ is the output value of the spectral camera for a particular pixel p at wavelength λ, $dark_\lambda$ is the reflectance of black reference at wavelength λ, $white_\lambda$ is the reflectance of white reference at wavelength λ, and R_λ is reflectance value of pixel p at wavelength λ.

The formula corrects the output images of the spectral camera by separating the sample reflectance (real reflectance of measured object) from the system response and also compensates for the following attributes: offset due to CCD dark current, light source color temperature drift, and lighting spatial nonuniformity across the scene line.

[20] gives also a formula for CCD frame shift smear and optical stray light compensations. These steps are rarely required and detailed description will be skipped here.

[23] explains possible sources of errors in color measurements which can occur using photometers. They also introduce and compare several calibration, and error correction techniques to improve the accuracy of imaged samples. They explain that the human eye can perceive color difference between two objects, if they differ in color at least about 0.5 CIE Lab error. Thus the threshold should be an objective to achieve accurate color reproduction. In particular, they suggest that the following errors can affect the final color of reproduction: wavelength error, photometric non-linearity, integrating sphere dark level error, and integrating sphere error in both specular included and specular excluded modes. They explained how to measure values corresponding to the errors and give correction equations for them.

Spectral microscopy Undoubtedly, the best solution for spectral measuring with high fidelity and high resolution (for example printing dots) is to employ the spectral microscopy concept. Figure 22 shows an imaging system which is a connection of a microscope and a spectral camera attached to it.

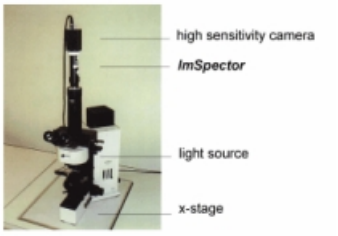

Figure 22: Spectral microscopy.

This kind of imaging system enables us to measure samples with microscopic accuracy and, in particular it can be employed to measure printing dot structure.

2.4 Color halftone printing

Printing is a reproduction of texts and images usually with inks on paper substrate. Color printing employs usually cyan, magenta, yellow and black inks to produce colors (four-color printing process), however, three-ink printing systems have also been used with cyan, magenta and yellow inks. Theoretically, black color is not needed (CMY color model), but when cyan, magenta and yellow inks at maximum densities are mixed together on paper, the result is not usually a black color. Practically, dyes and printing inks have spectral absorption curves that overlap significantly and are much different from the theoretical spectral absorption curves. Due to the spectral overlap among the colorants (inks), converting RGB values to CMY values using $the\ one - minus - RGB\ method$ (see Equation (11)) works in unacceptable way in reality. Mainly, the unwanted absorptions among printing inks, optical processes in paper substrate (optical dot gain), and physical interaction between paper and ink (mechanical dot gain) introduce nonlinearity which can not be easily analyzed or compensated.

Due to the large extent of literature about printing process and related phenomena, in the remaining part of the section and next sections we will describe only a couple of relevant concepts and problems which have direct connection to the experimental part of the thesis. Readers interested in this topic are referred to [1], [7], [33] and [34].

2.4.1 Image processing for color printing

Color printing process involves a sequence of steps and image transformations in order to generate good quality color reproductions. The following are the main steps when reproducing a color image in four-color (CMYK) printing [1]:

Color separation process The amounts of red, green and blue colors are measured in each spatial location of the original image with the help of special red, green and blue filters. Each of the filters sees its own color in the original image as white and opposite color as black (for example blue filter sees all blue regions of the original image as white and other regions with opposite color as black). For subtractive color formation, the black filter values are taken into account. The color separation for black ink is calculated based on the three color signals resulting from the filters or by applying a yellow "gold" filter.

[1] suggests that the result of color separation process depends on illumination used to illuminate the original image, reflectance or transmission properties of the original object, and transmission characteristics of the separation filters.

Color correction process Color correction process is performed due to non-ideal light absorption characteristics of printing inks. The goal of the process is to compensate for color distortions caused by insufficient and incorrect light absorption properties of printing inks.

If we assume that the paper surface reflects all the incoming light, each printing ink absorbs one-third of the visible spectrum and totally transmits the remaining two-thirds of the visible spectrum (the transmission spectra of printing inks do not overlap), then the color correction process would not be needed. However, in reality printing inks do not absorb a sufficient amount of desired parts of visible spectrum and absorb some undesired parts of the spectrum.

The main criteria for successful color correction is to keep the gray tone of the original image in the final reproduction. If the correction of color signals is not done, then gray areas of the original image will result in brown and darker areas in the reproduction than in the original. Thus, the main goal of color correction process is to eliminate these deficiencies. The process is called gray balancing and determines a equivalent neutral density (END) curve for each printing ink which shows how much of a particular ink should be used to obtain neutral gray colors of different darkness levels in the final print. As suggested by [1], in general cyan dots should be bigger than magenta and yellow dots.

In a typical set of printing inks, yellow ink absorption is very close to the ideal. Unfortunately, for magenta and cyan inks secondary absorption are considerable (for a particular ink, secondary absorptions exist in the parts of the visible region where the ink should be totally transparent for incoming light), and thus should be compensated by the color correction process to achieve acceptable final results. Let us consider for example a magenta ink which due to non-ideal light absorption looks slightly yellowish and cyanic. To correct this color distortion, cyan and yellow signals could be reduced locally by:

$$Y = Y - M_Y \qquad C = C - M_C \tag{21}$$

, where Y is the yellow separation signal, C - is the cyan separation signal, M_C - is the amount of cyan component in magenta signal and M_Y - is the amount of yellow component in magenta signal [1].

Thus, in general case, three inks require correction with two secondary absorptions, what suggests that six corrections are needed.

Screening (halftoning) Screen printers usually can not reproduce continuous tone images[4] due to the inability to lay down continuously variable densities of inks. Halftoning (screening) is the process of conversion of continuous tone image to a halftone image [1]. A halftone image is made of small dots of varying sizes which simulate the original continuous tone image and which can be produced by a screen printer.

Figure 23 shows an example of binary halftone process. The halftone process usually creates patterns of small black printing dots of varying sizes on a white

[4]A continuous tone image is an image which contains smooth gradations of tone between the lightest and the darkest image areas (for example photographs, artist's paintings and airbrush illustrations).

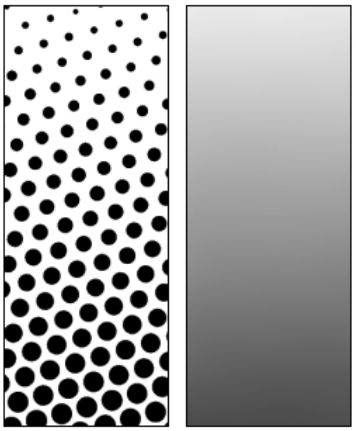

Figure 23: Left: halftone dots. Right: how the human eye sees the halftone dots when viewed from a sufficient distance (Image taken from [30]).

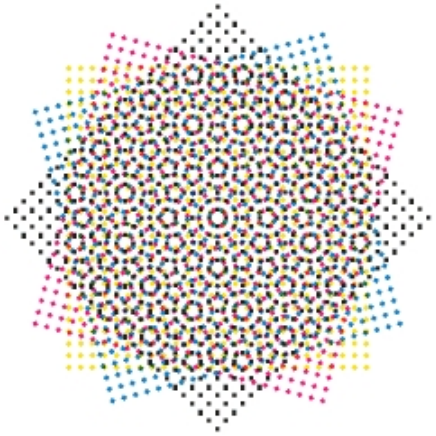

Figure 24: Traditional screen angles for color plates (Image taken from [29]).

background (paper). When viewed from a sufficient distance, the human visual system will not be able to see the printing dots structure, but instead the human will have the illusion of a continuous tone gray image. The darkness of the image will depend on the area coverage and the amount of black printing dots laid down on the substrate, i.e. many black printing dots or black dots with high level of area coverage will create the illusion of a darker gray, while few or small black dots will create the illusion of a lighter gray [30].

In four-color printing process, the halftone pattern is generated for each printing ink used (usually cyan, magenta, yellow and black). Then the halftone patterns (color planes, screens) are superimposed and printed one over another.

The rows of printing dots on the screens used for each color separation must be positioned at a specific angle [29]. As shown in Figure 24 the angles are as follows: 45^o for black dots, 75^o for magenta dots, 90^o for yellow dots and 105^o for cyan dots. The screens form a rosette pattern which is merged into one continuous tone image by the human visual system. On the other hand, in the case when the screen angles are wrong, the rosette pattern is not correct and a moiré pattern appears which results in images having no more smooth gradations of color.

Figure 25 shows example of color halftoning process with CMYK separations. The cyan, the magenta, the yellow and the black separations (color planes) are combined together to form the halftone pattern (superimposition of the color planes). The appearance of the combined halftone pattern when viewed by the human eye from a sufficient distance is also shown.

[1] enumerates the following variables which control the halftoning process:

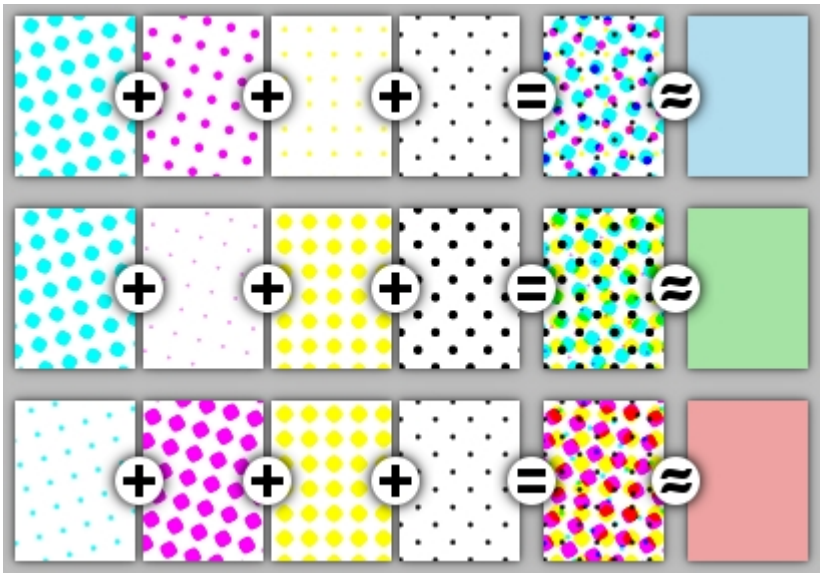

Figure 25: Examples of color halftoning with CMYK separations. From left to right: the cyan separation, the magenta separation, the yellow separation, the black separation, the combined halftone pattern and the appearance of the combined halftone pattern when viewed by the human eye from a sufficient distance (Image taken from [30]).

1. halftone dot size - the minimum and maximum dot area coverage in a halftone cell. Printing usually avoids having no dots (0% area coverage) and solid areas (100% area coverage);

2. screen frequency (screen ruling, screen density) - is the measure of the frequency (number) of the lines of dots per inch (or centimeter) on the halftone screens. It directly affects the printing dot size i.e. the higher the screen frequency the smaller and less visible the printing dots what, in particular, gives more detailed and sharper prints with smoother tonal changes. On the other hand, the following factors limit the screen density level: the type of paper (smooth and coated paper can carry more information than newspapers and uncoated paper), more advanced printing process, and smaller dots are more susceptible to dot gain phenomena;

3. screen (halftone) angle - as mentioned earlier, it defines the angles of the halftone screens;

4. halftone dot structure - defines the halftone dot shape inside a halftone cell. When the halftone positives (halftone screens) are produced using the optical screening process, then diamond dots will usually result with minor possibilities to any modifications. Generating the halftone screens using the

digital halftoning process enables us to choose the halftone dot structure from several different dot shapes.

Nowadays, most of the print technologies are not limited to binary output (full area coverage and no coverage), but have multilevel printing capabilities. It means that the printer is capable of putting an intermediate amount of ink on the paper surface, thus increasing the color gamut considerably.

Restoration and enhancement The operations are usually performed to improve the final reproduction result. The image enhancement processes are attended to improve the final reproduction to give better visual quality in the intended use, for example they consider the preferences and properties of the final viewers. The restoration processes, however, try to equalize the output reproduction to the original image [1].

2.4.2 Halftone dot placement techniques

Color printing process requires mixing three or four inks to make an output print. Color gamut of a printing process and the output print are usually affected by different dot placement techniques including dot-on-dot, dot-off-dot and rotated dot schemes [7].

Color planes composed of printing dots of various sizes can be superimposed in various ways:

1. dot-on-dot technique - dots of one printing ink are placed on the top of dots of other printing inks, where the number of layers is limited by the number of printing inks. In the dot-on-dot screen the cyan, magenta, yellow and black dots are placed at the same screen angle usually equal to 45^o;

2. dot-off-dot technique - the scheme places dots of one printing ink adjacent to dots of other printing inks. This technique has limited applications in color printing because of the existence of overlapping areas in the case of dots at high densities;

3. rotated dot technique - the dots for each printing ink are arranged in a color plane with different screen angles. Superimposition of the screens and their different screen angles cause the printing dots to partially overlap.

Figure 26 - 28 show example of dot-on dot, dot-off-dot and rotated dot techniques respectively.

The dot placement techniques affect the printer color gamut and in the case of dot-on-dot and rotated-dot techniques the order in which the dots or screens are superimposed has significant effect on the output print appearance.

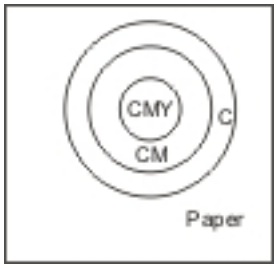

Figure 26: Dot-on-dot model.

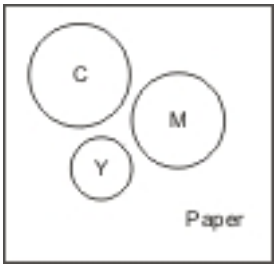

Figure 27: Dot-off-dot model.

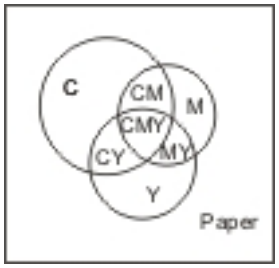

Figure 28: Rotated-dot model.

2.5 Experimental part

In this section we will give a description of samples which have been used in the experimental part of the thesis. The setups for the sample measurements will be described and some applications for spectral data analyses will be discussed. Based on the data coming from the experimental part we examined the following aspects:

1. basic characterization of paper and print (Chapter 3);
2. mottling characterization and prediction (Chapter 4);
3. concentration prediction and inverse color separation process (Chapter 5).

2.5.1 Sample description

In the experimental part four types of paper were considered and measured:

1. paper type A;
2. paper type B;
3. paper type C;
4. paper type D;

For each type of paper, three sheets coming from different parts of the sheet pile were considered: the first sheet of paper was taken from the top of the sheet pile, the second sheet from the middle part, and the third from the bottom of the pile. Thus, twelve sheets of papers constituted the input to the experimental part of the thesis.

The measurement phase was divided into two turns:

1. blank paper turn - some areas of blank paper sheets were carefully chosen and measured with the spectral imaging system described later;

2. printed paper turn - papers were printed and the same areas as in the previous step were measured with the same settings of the spectral imaging system (measuring the same areas of the papers before and after the printing process has significant meaning to mottling prediction experiments). Other areas were also measured in this phase and the spectral data were later used as input for experiments concerning ink concentration prediction, printing dot separation process, and basic characteristics of paper and print.

The samples were measured under two different illuminants. In the case of measurements under D65 illumination, all the data have been collected and saved in the form of spectral reflectance data files. In the case of measurements under UVA illumination, all the data have been collected and saved in the form of spectral radiance data files.

2.5.2 Setups for sample measurements

In the experimental part, three setups were used to acquire spectral and RGB images of samples:

- spectral imaging system with ImSpector V8 as the spectral camera to acquire spectral images of printing dots;
- spectral imaging system with ImSpector V10 as the spectral camera to acquire spectral images of large sizes;
- Epson Perfection V700 scanner - high resolution scanner used to acquire RGB images of printing dots. Its maximum optical resolution is 6400 dots per inch (DPI).

Figure 29 shows the spectral imaging system at InFotonics Center which was used to acquire spectral images. The imaging system consists of a spectral camera, an illuminant, a PC computer and a sample mover with attached table. During measurement phase a sample will be attached to the table.

Light sources GretagMacbeth SpectraLight III was used as the illumination source (see Figure 29). It provides five selectable light sources:

- Simulated Daylight including D75, D65 or D50;
- Horizon (early morning sunrise/afternoon sunset simulation);
- Illuminant A (incandescent home lighting);
- Cool White Fluorescent;
- Custom Fluorescent (TL84 or U30);
- Ultraviolet (can be used in conjunction with another source).

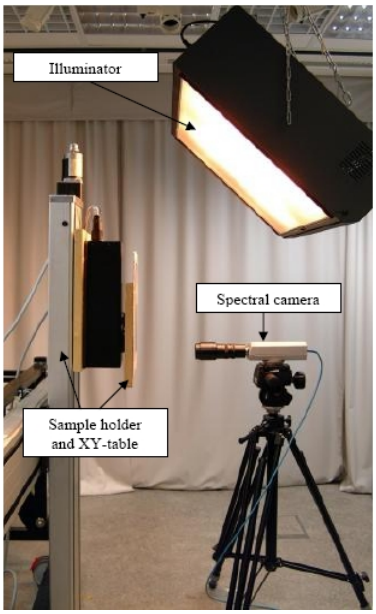

Figure 29: Spectral imaging system at InFotonics Center.

Sample mover Isel Automation C10C-E/A was used as the sample mover. As mentioned earlier, a spectral camera is able to acquire only one line of a measured sample at a time. Thus, the sample mover was used to assure continuous moving of a sample while measuring. It enables 2D linear movements and is the place where the sample is attached. During the measurement phase, it is used to adjust the sample alignment with respect to the spectral camera.

Reference levels and geometry Before actual measuring of samples, it is common to measure reference white and reference black spectra in the same ambient illumination as the samples will be measured (see Section 2.3.1). These reference spectra are further used to diminish the influence of the ambient illuminant on the measured samples in the final image data. Thus the final image data is the reflectance image data in which the effect of the light source is eliminated (see Equation (20)).

The standard imaging geometry was used to measure the sample i.e. the angle of the spectral camera with respect to the sample is equal to 0^0 and the angle of the light source with respect to the sample is equal to 45^0.

Spectral cameras The ImSpector V8 spectral camera was used to acquire spectral images of printing dots with the help of a magnifying optics and lens which give us the possibility to come very close to a sample. The ambient D65 illumination was artificially generated by a SpectraLight III illuminator. As mentioned earlier the spectral camera can measure one line of a sample at a time. The

width of the line depends on the distance of the spectral camera from the sample board and the adjustment of the camera lens. Nevertheless the optical parts of the camera impose some limitations on the minimum line width. The minimum line width is about 12 mm and the maximum spatial camera resolution is 1280 pixels. It means that in the final spectral image we can got 1280-pixel resolution per each 12 mm of measured sample. The camera is able to give spectral responses in the range between 380-780 nm, thus covering the whole visible spectrum.

The setup of the ImSpector V8 spectral camera used for measurements is as follows:

- light source - D65 illumination generated by SpectraLight III illuminator;
- geometry - standard;
- spatial resolution - 1280 pixels;
- wavelength range - 380-780 nm;
- sampling interval - 5 nm;
- spectral resolution after spectrum quantization - 81 channels;
- bit per channel - 12;
- line width - 12 mm;
- output files - spectral reflectance values.

The ImSpector V10 spectral camera were used to acquire spectral images of the samples under D65 and UVA illuminants depending on the current measurement purpose. In this case, the line width was fixed to be 160 mm. The maximum spatial camera resolution is 1600 pixels. It means that in the final spectral image we got 1600-pixel resolution per each 160 mm of measured sample. The camera is able to give spectral responses in the range between 400-1000 nm, thus exceeding the visible spectrum range. The quality of spectral images captured with the ImSpector V10 spectral camera is much better than with ImSpector V8 spectral camera. Unfortunately, the ImSpector V10 spectral camera does not work properly with the magnifying optics and lens which must be used to see and measure the printing dot structure.

The setup of the ImSpector V10 spectral camera used for measurements under D65 illumination is as follows:

- light source - D65 illumination generated by SpectraLight III illuminator;
- geometry - standard;
- spatial resolution - 1600 pixels;

Table 5: Characterization of spectral cameras

Spectral camera	Spectral range	Spatial resolution	Slit length
ImSpector V8	380 - 780 nm	up to 1280	9.8 mm
ImSpector V10	400 - 1000 nm	up to 1600	9.8 mm

- wavelength range - 400-1000 nm;
- sampling interval - 5 nm;
- bit per channel - 12;
- spectral resolution after spectrum quantization - 121 channels;
- line width - 160 mm;
- output files - spectral reflectance values.

The setup of the ImSpector V10 spectral camera used for measurements under UV illumination is as follows:

- light source - UVA illumination generated by SpectraLight III illuminator;
- geometry - standard;
- spatial resolution - 1600 pixels;
- wavelength range - from 288 nm to 1181 nm (exceeding the visible spectrum considerably);
- sampling interval - 0.7 nm;
- spectral resolution - 1200 (for each spatial location of the imaged line 1200 values constituting the color information are given);
- bit per channel - 12;
- line width - 160 mm;
- output files - spectral radiance values - raw data being the output of the spectral camera (not corrected data).

Table 5 contains basic description of the spectral cameras used in the experimental part (see www.specim.fi for more detailed description).

Software managing the spectral imaging system The spectral camera and the sample mover is fully controlled by special kind of software installed on a PC computer to assure exact reconstruction of the acquired line-sliced spectral images. In particular, the software is responsible for the following issues:

- the spectral camera and the sample mover synchronization during the measurement phase;
- acquisition of reference white and reference black for current imaging system adjustments;
- spectral image post-processing phase - image correction after the spectral image is acquired (converting from spectral radiance to spectral reflectance data according to Equation (20) using measured black and white levels);
- camera settings: exposure time settings (depends on the level of illumination and spectral camera settings) and data depth (possibility to choose between 8 or 12 bit per each spectral channel);
- spectral image previewing in sRGB color space;
- raw data and corrected (spectral reflectance) data can be saved (the output file consists of a simple header and raw data);
- possibility to select an area of interest which is to be measured. (the shape of the area is always rectangular and given by start point, width, and height. The route by which to scan the rectangular area of a sample can be selected);
- wavelength range and quantization step can be selected (it will directly affects the spectral reflectance data file);
- hardware binning - combines pixel responses to give average response for particular pixels. The higher the binning ratio, the less noise in the final spectral image.

The software managing the spectral camera does not impose any fixed limitations on the vertical resolution of the final spectral image. Nevertheless, the vertical resolution is determined in the following way: suppose that the spectral camera is adjusted in such a way that we can measure a line of a mm width at a time, and suppose that the height of the final image is b mm. Then, the width of one pixel in the final image will be a/res, where res is the current spatial resolution of the spectral camera. The software makes the pixels in the final spectral image to be squares, so the height of pixels in the final image is also a/res. This implies that the vertical resolution of the final reproduction is $b/(a/res)$ pixels.

The software also allows us to adjust the sampling step of the visible spectrum. If for example the sampling step is equal to c, then we are examining the visible spectrum of a measure sample in intervals of length c, starting from 380 nm and

finishing at 780 nm. The less the sampling interval the bigger the output file size. Thus, usually the sampling step is equal to 5 mm what was shown by researchers to be a optimal choice between the image quality and the output file size [21].

Printing dot measurements The resolution of a spectral camera, and the line width (which is dependent on the current spectral camera optic and setup) impose some limitations on minimum sizes of printing dots which can be measured. As mentioned above the ImSpector V8 spectral camera was used to measure printing dot structure. The minimum line width is about 12 mm and the spatial resolution is 1280 pixels. This implies in straightforward way that in the final image a pixel will be a square with 0.0095 mm side length.

Usually a printed dot diameter size is between 10-30 microns (1 micron = 1/1000 mm) in good quality printing. If we assume for now that the diameter of a printed dot is equal to 20 microns = 20/1000 mm and the length of a pixel side is 0.0095 mm, then in approximately one printed dot will be represented by 16 pixels in the final image.

However, the main concern about printing dot measurement is the quality of the acquired spectral images. In this situation, the ImSpector V8 spectral camera was equipped with a magnification optics and lens and located at very close distance to the imaged sample to be able to see the structure of printing dots. Due to the fact that the spectral camera is very close to the sample the final spectral images were very noisy and the color information (spectral reflectance) is changed in comparison to the original images. In particular, the problem will directly affect the concentration prediction and inverse color separation processes and will make them hard to perform (see Chapter 5). A straightforward solution to the problem of noisy spectral images of printing dots is the spectral microscopy discussed in Section 2.3.1.

Figure 30 - 32 show black printing dots at different densities. We can see by naked eye the color distortions in the RGB representations of spectral images. In particular, the black color of the printing dots is lighter than it was intended to be and the paper surface areas are much darker than they were intended to be. Consequently, the spectral reflectance of the dots and the paper surface is inaccurate and can influence the correctness of the concentration prediction and color separation processes.

Spectral image post-processing phase For further analyses of acquired spectral images a number of applications were used. Figure 33 shows an example application which plays a significant role in post-processing phase of acquired spectral images. The application enables us to select individual pixels of acquired imaged and examine spectral reflectance or spectral transmittance of the pixel at that spatial location (corresponding spectrum is drawn in the form of a plot). Simulations of the appearance of the imaged objects (spectral images) under different illuminations (the CIE A, C, D50 and D65 standard illuminants) and observers

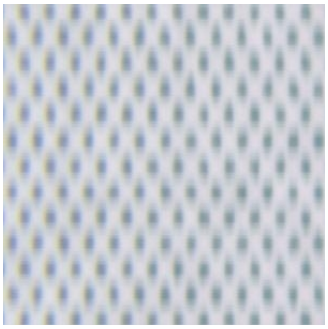

Figure 30: Black dots at 10% density.

Figure 31: Black dots at 40% density.

Figure 32: Black dots at 80% density.

(the CIE 1931 standard observer and the CIE 1964 standard observer) can be done and then spectrum investigation of each spatial location can be performed. The application also allows the user for magnification options which enable detailed view of the acquired spectral images.

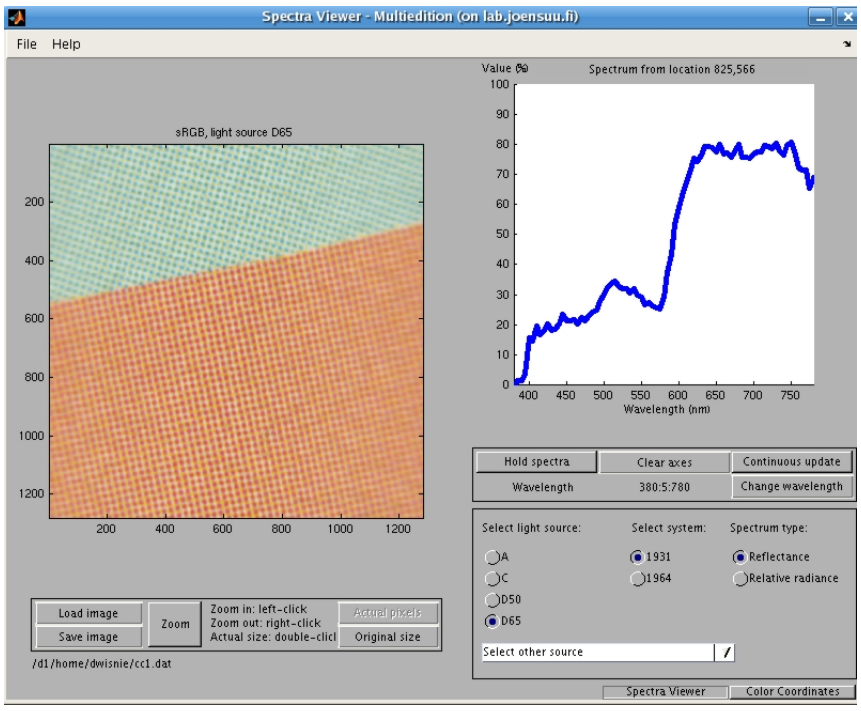

Figure 33: An application for processing of spectral images.

3 Basic spectral characteristics of paper and print

In this chapter we will examine basic characteristics of paper and print. In particular, our investigation will include average spectra and spectral variances of different kinds of blank paper, spatial variations of blank paper surface, black color formations for different kinds of paper, average spectra and spectral variances of printing ink and dot gain characteristic. These basic characteristics will be examined for each kind of paper used in the experimental part.

3.1 Average spectrum and spectral variance of blank paper

The whiteness of a plain paper mainly depends on the amount and the distribution of whitening agents in the paper structure. Thus, we suspect that the spectral reflectance properties of different kinds of blank paper will vary. In this section we will examine average reflectance spectrum and spectral variation of different kinds of paper.

Figure 34 presents average spectral reflectance of four kinds of plain paper under D65 illumination. For each kind of paper spectral reflectances of a region of 45 mm by 45 mm were measured by the ImSpector V10 spectral camera in the range from 400 nm to 1000 nm with 5 nm intervals. Then average spectrum of the measured region was calculated[5]. It is clear that for a particular type of paper there exist regions with higher spectral reflectance values and regions with lower spectral reflectance values than the corresponding spectrum presented in the figure. This is mainly due to uneven distribution of whitening agents in paper surface, and in particular, it is connected with the print unevenness phenomena.

Figures 35 - 38 shows the corresponding RGB images for each type of paper. Directly from the RGB representations of papers we can conclude some information about the amount of whitening agents in paper and classify them according to their whiteness.

Table 6 shows coordinates in RGB and CIE Lab color spaces of different kinds of plain paper.

The X, Y, Z tristimulus values were calculated based on the average spectral reflectance data of plain papers under the CIE D65 standard illuminant and with the 1931 CIE Standard Observer (see Section 2.1.4). Then Equations (12), (13) and (14) were used to calculate values in CIE Lab color space corresponding to a given set of tristimulus values. Furthermore, the RGB values are actually coordinates in the sRGB color space (standard-RGB color space - one of the absolute color space

[5]If not stated otherwise, the setup will be assumed for other measurements carried out in the experimental part of the thesis.

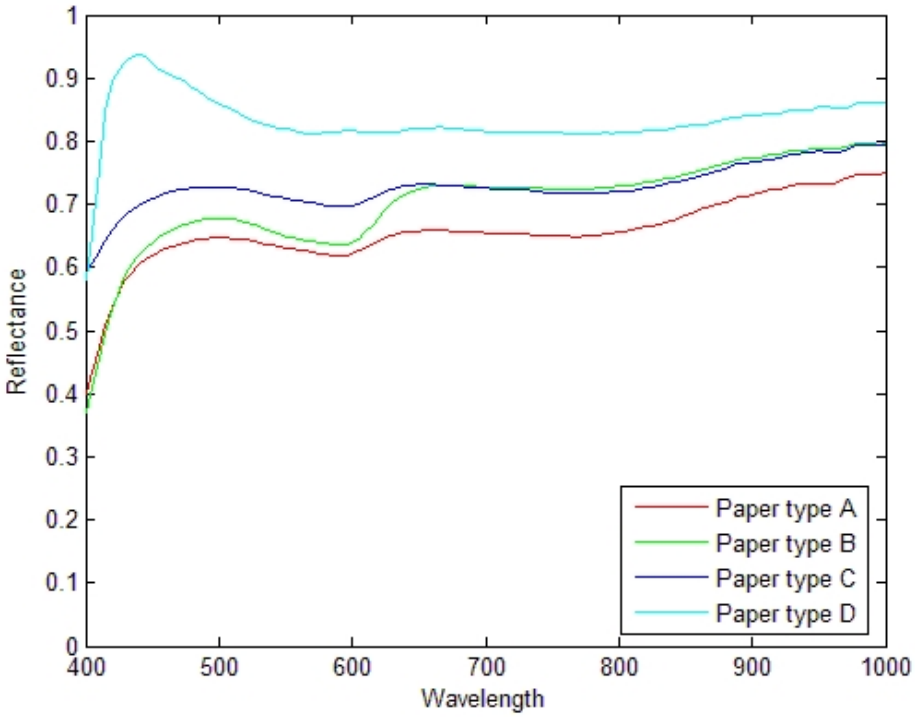

Figure 34: Average spectral reflectance of different kinds of paper under D65 illumination.

Figure 35: Paper type A under D65 illumination.

Figure 36: Paper type B under D65 illumination.

Figure 37: Paper type C under D65 illumination.

Figure 38: Paper type D under D65 illumination.

for the RGB color model)[6].

Table 6: Values in RGB and L*a*b* color spaces for different kinds of paper.

Color space	RGB			L*a*b*		
Paper kind	R	G	B	L*	a*	b*
Paper type A	0.8130	0.8198	0.8027	83.6113	-1.2996	1.8222
Paper type B	0.8311	0.8322	0.8138	84.8427	-0.8545	2.1556
Paper type C	0.8548	0.8625	0.8561	87.5463	-0.8739	0.4265
Paper type D	0.9094	0.9181	0.9615	92.8609	1.3612	-5.7447

In the experimental part we were investigating three sheets of each kind of paper - the first sheet was taken from the top of a paper pile, the second sheet was taken from the middle region of the pile and the last one was taken from the bottom of the pile. In this section we will examine if there are any differences in spectral reflectance between these sheets for each kind of paper, i.e. we will try to estimate the pressure magnitude on the middle sheet and bottom sheet in comparison to the top one from spectral point of view. To carry out this experiment average spectrum of a region of 45 mm by 45 mm was taken from each sheet of each kind of paper. Then, for a particular kind of paper the average spectra of the sheets were compared together.

[6]These scheme for calculating the CIE Lab values and RGB values will be employed in the remain part of the thesis, if not stated otherwise. For simplicity, in the thesis we will be using the expression "values in RGB color space" to denote a set of values which actually are from sRGB color space.

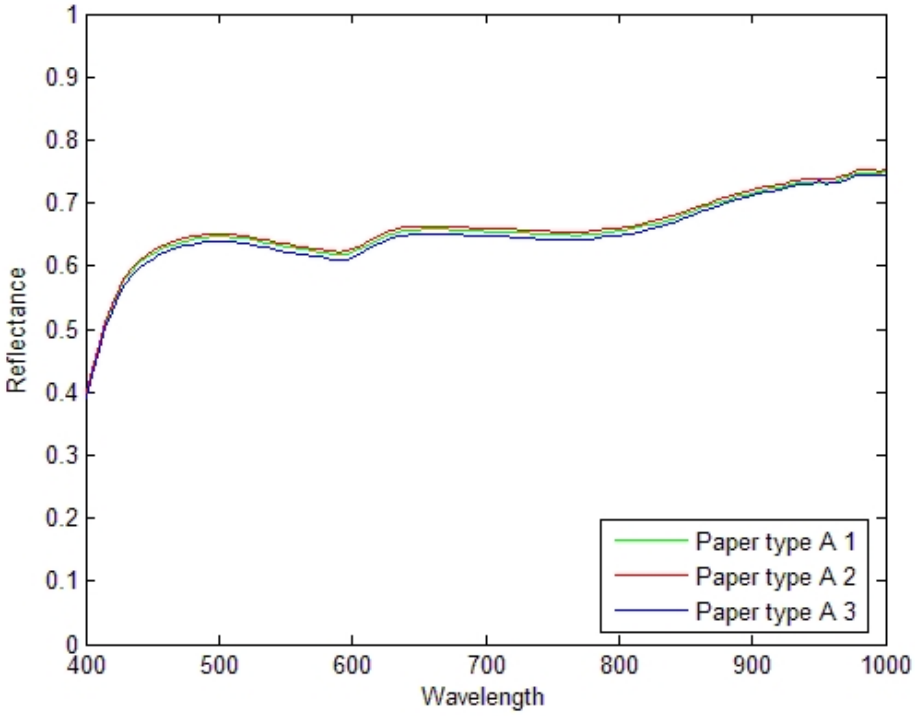

Figure 39: Paper type A sheets under D65 illumination.

Figure 39 shows the spectral reflectances of three sheets of paper type A. The top sheet denoted by green line is very similar from spectral point of view to the middle sheet denoted by red line. The bottom sheet spectral reflectance curve goes lower than the others, and thus we can conclude that the bottom sheet is darker than the other sheets. In spite of this difference the sheets can not be visually discriminated from each other.

Figure 40 shows the spectral reflectances of three sheets of paper type B. The middle sheet denoted by red line is very similar from spectral point of view to the bottom sheet denoted by blue line. The top sheet spectral reflectance curve is going higher than the others, and thus we can conclude that the bottom and middle sheets are darker than the top one. These results suggest that there can exist minor difference in perceived brightness between the top sheet and the other sheets.

Figure 41 shows the spectral reflectances of three sheets of paper type C with the top sheet spectrum denoted by green line, middle sheet by red light and bottom sheet by blue line. Spectral reflectance curves are very similar what suggests that there is no pressure impact on bottom and middle sheets in comparison to the top one.

Figure 42 shows the spectral reflectances of three sheets of paper type D with the top sheet spectrum denoted by green line, middle sheet by red light and bottom

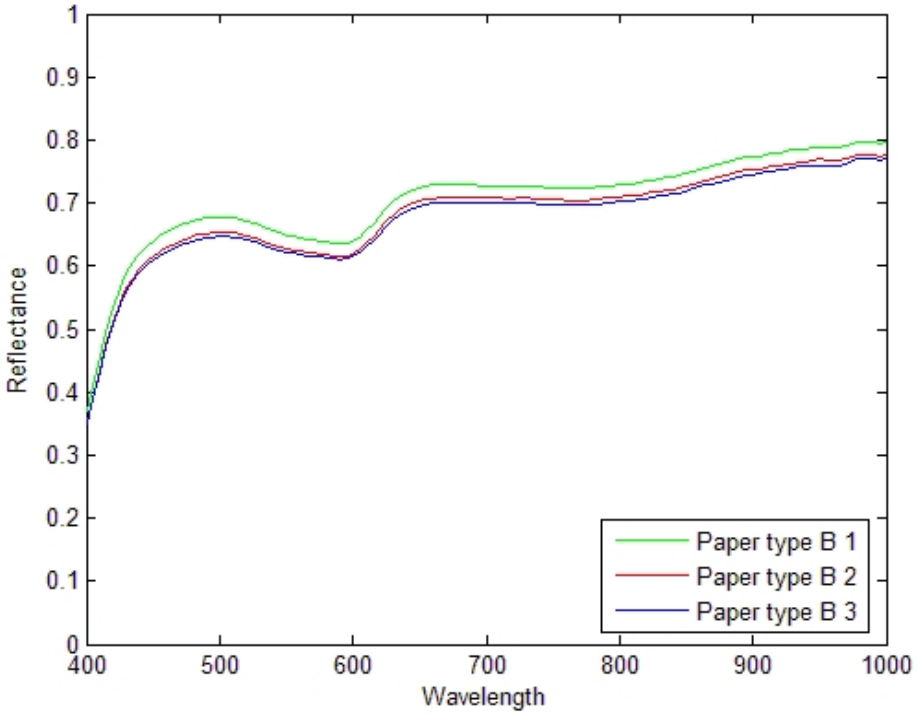

Figure 40: Paper type B sheets under D65 illumination.

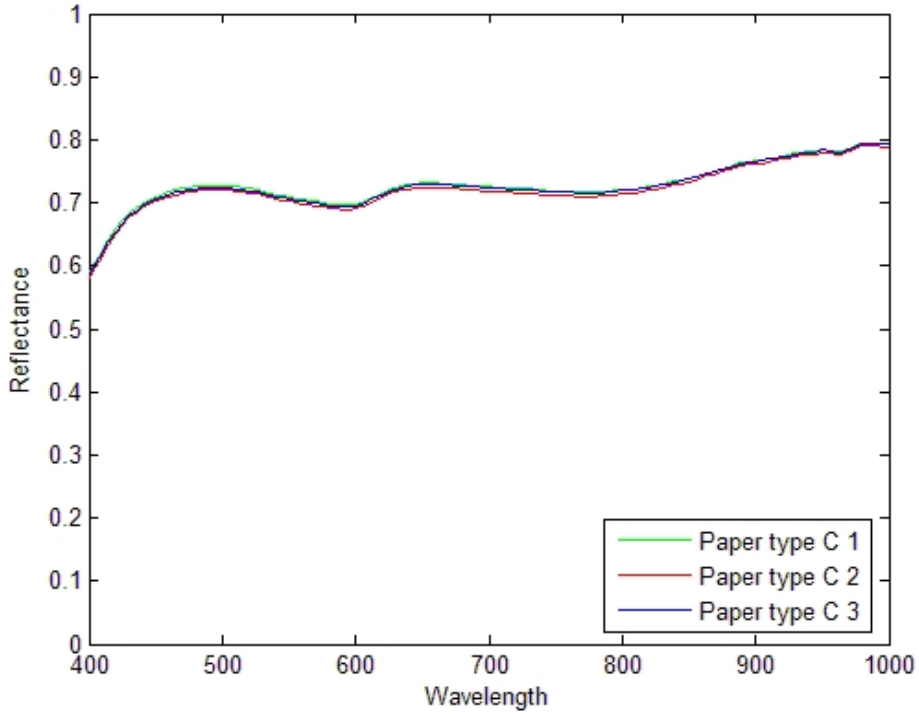

Figure 41: Paper type C sheets under D65 illumination.

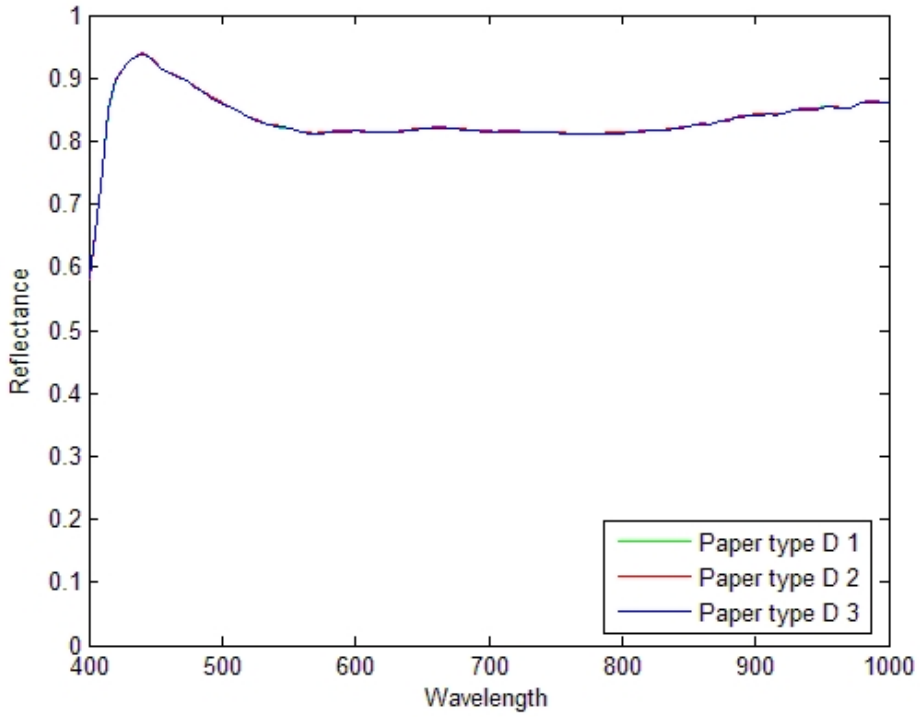

Figure 42: Paper type D sheets under D65 illumination.

sheet by blue line. Spectral reflectance curves are identical what suggests that there is no pressure impact on bottom and middle sheets in comparison to the top one.

Now we will investigate standard deviations of spectral planes for different kinds of plain paper. To compute the standard deviations for a particular type of paper the following procedure will be used:

1. let R be a spectral image of a region of plain paper;
2. for each spectral plane which corresponds to wavelength λ compute standard deviation for the plane;
3. draw figure which presents standard deviations as a function of wavelengths.

In this case the size of the region was 30 mm by 30 mm, and we considered wavelengths (planes) in the range from 400 nm to 780 nm.

Based on the results shown in this section we come to the following conclusions:

1. average spectral reflectance of different kinds of paper vary significantly;
2. pressure impact on bottom and middle sheets in comparison to top sheet is visible for paper type B and paper type A (low quality papers);

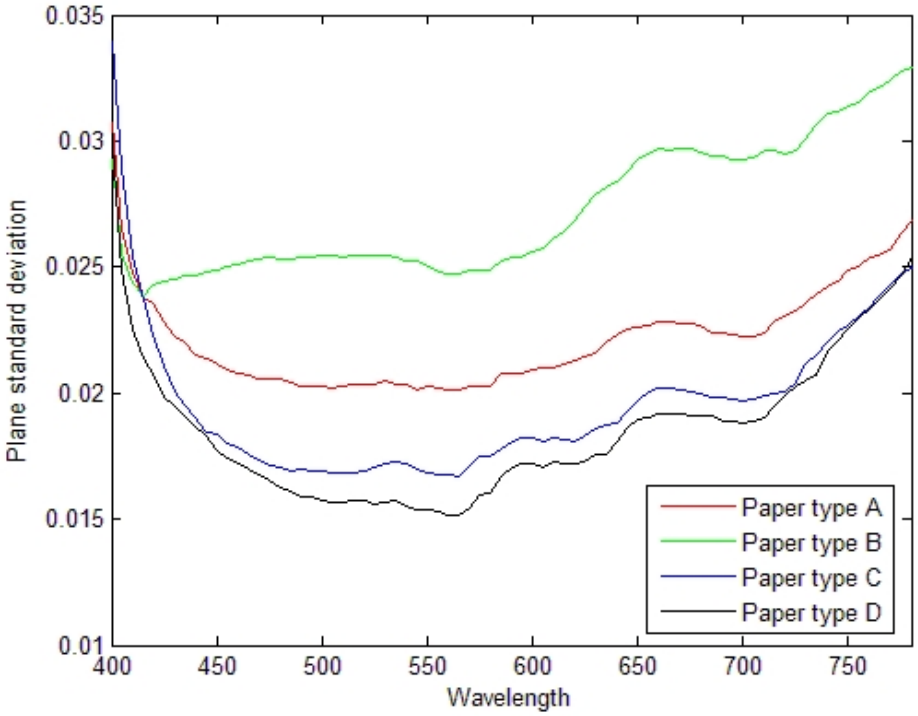

Figure 43: Standard deviations of spectral planes for different types of plain paper

3. there is no pressure impact on bottom and middle sheets in comparison to top sheet for paper type C and paper type D from spectral point of view (good quality papers);

4. plane standard deviations for paper type D and paper type C (good quality papers) are much lower than for paper type A and paper type B (bad quality paper). It means that for paper type D and paper type C values corresponding to a particular spectral plane are not spread widely;

5. paper type D and paper type C have similar standard deviation curves. The biggest standard deviations occur in paper type B and then in paper type C. Let us notice that the shape of the standard deviation curves are similar for all paper types.

In Section 3.3 we will analyse if spectral differences between plain paper sheets (coming from different parts of a pile) for a particular kind of paper have some influence on later prints on these sheets, i.e. "Do prints on different sheets vary if there are some variances in average spectral reflectance between plane sheets?".

3.2 Unevenness of blank paper surface

Inhomogeneities in the paper surface are usually caused by unevenly spreading of whitening agents in the paper structure. Thus, the spectral reflectance properties of different spatial regions of a sheet of base paper can vary, and finally the printing process can result in inhomogeneous distribution of ink and ink penetration into the substrate due to the fact that the background of the ink varies in thickness and lightness. Visually this inhomogeneity may be perceived as print mottle (optical inhomogeneity due to varying light absorption over the printed surface - print unevenness) especially visible in the presence of UV illumination [3].

Figures 44 - 47 shows paper surfaces for different kinds of paper. A 3D view of a paper surface was created in the following way:

1. let R be a spectral image of a selected paper region;

2. for each spatial location (x, y) of image R let us denote by $v = (v_1, ..., v_N)$ the spectrum corresponding to the location and compute the mean value $(value)$ of vector v according to the following equation:

$$value = \frac{\sum_{i=1}^{N} v_i}{N} \tag{22}$$

3. draw the computed values as a function of spatial locations of region R.

Based on contours depicted under Figures 44 - 47 we can come to the following conclusions:

1. paper type A surface and paper type B have uneven surface structure from spectral point of view (contours for Figure 44 and Figure 45 reveal many large areas of cyan and red color what suggests high spectral variations between these regions);

2. paper type C and paper type D have considerably more even surface structure than paper type A and paper type B (contour for Figure 46 and Figure 47 reveal lower spectral variations in comparison to paper type B and paper type A);

3. finally, we come to the following conclusion: the better the paper quality the lowest the spectral reflectance variations of the base paper.

3.3 Print variations between different sheets of the same kind of paper

In this section we will analyse if spectral differences between plain sheets of the kind of paper taken from different parts of a pile (see Section 3.1) have some influence on later prints on these sheets, i.e. we pose the following question: "do the existence of spectral variations between plain sheets of the same kind of paper causes any variations between later prints applied to the sheets?".

To carry out this experiment, we calculated average spectra of a 45 mm by 45 mm region covered by cyan ink at 100% density for each sheet of a particular kind of paper, and then we compared them. The procedure was carried out for each type of paper.

Figures 48 - 51 present the results. Based on these figures we conclude that there is no visible print variations between different sheets for a particular kind of paper used in the experiment even though, there could exist some spectral variations between these sheets before the printing process (especially when considering low quality papers).

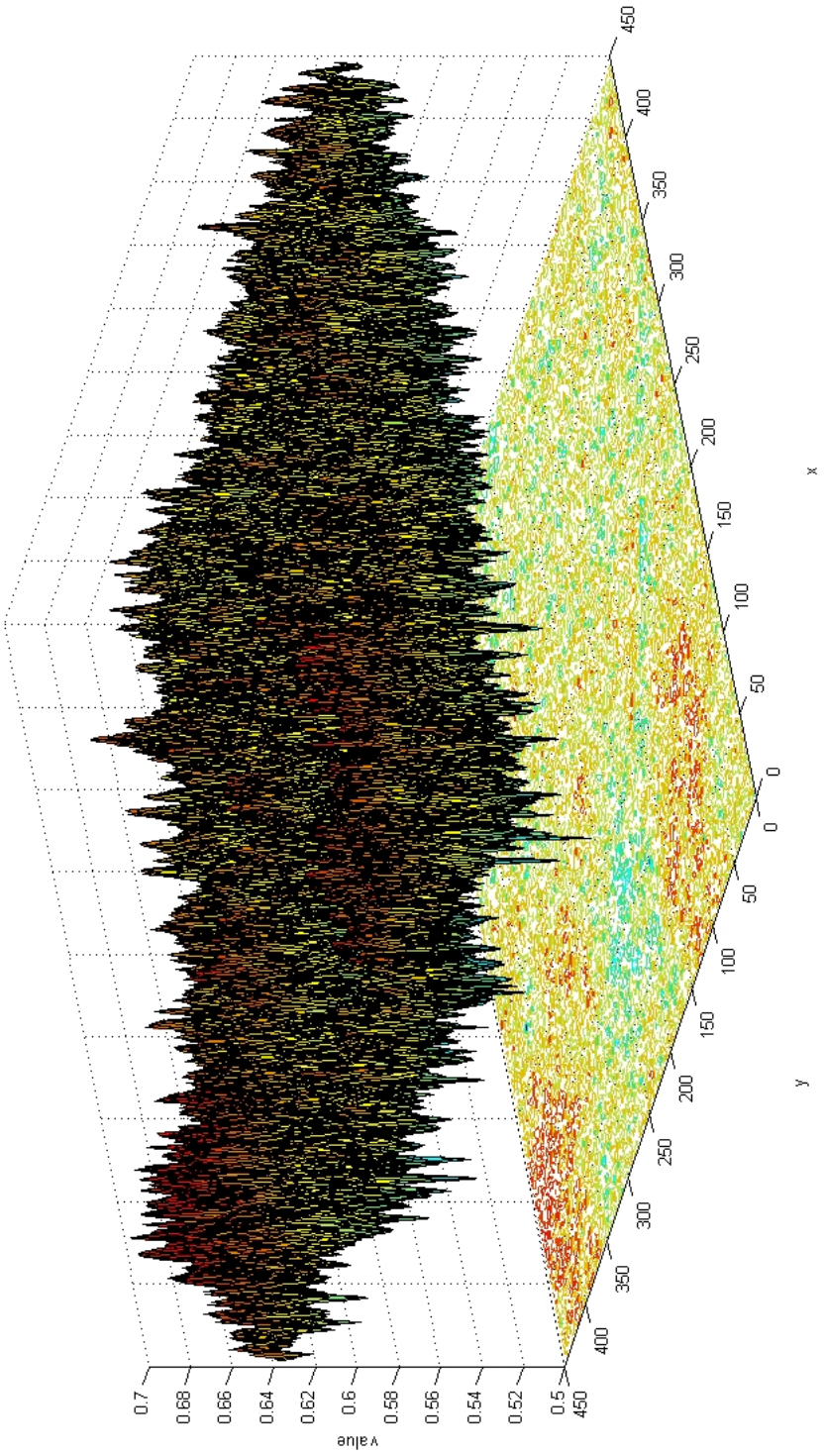

Figure 44: Paper type A surface.

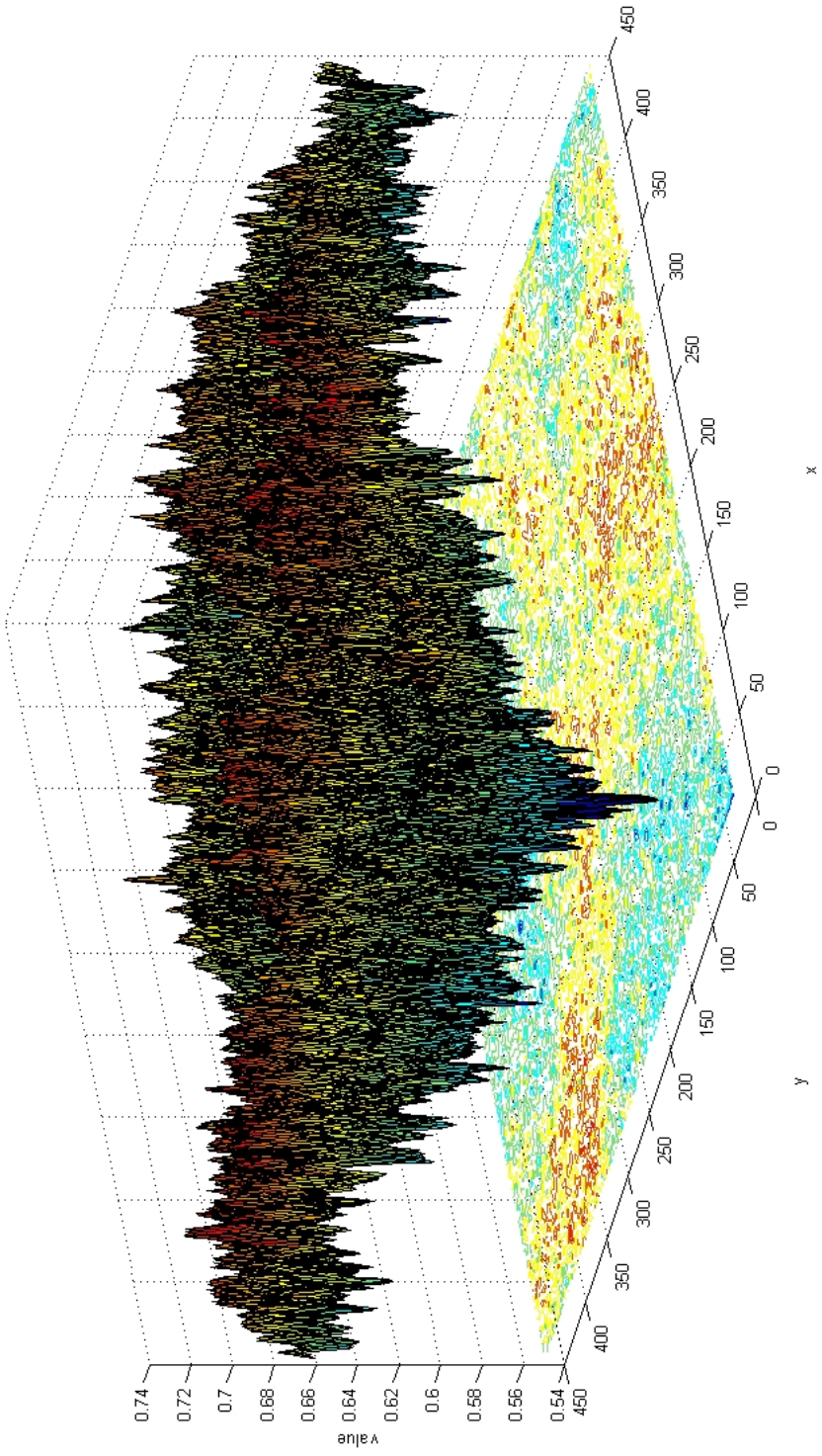

Figure 45: Paper type B surface.

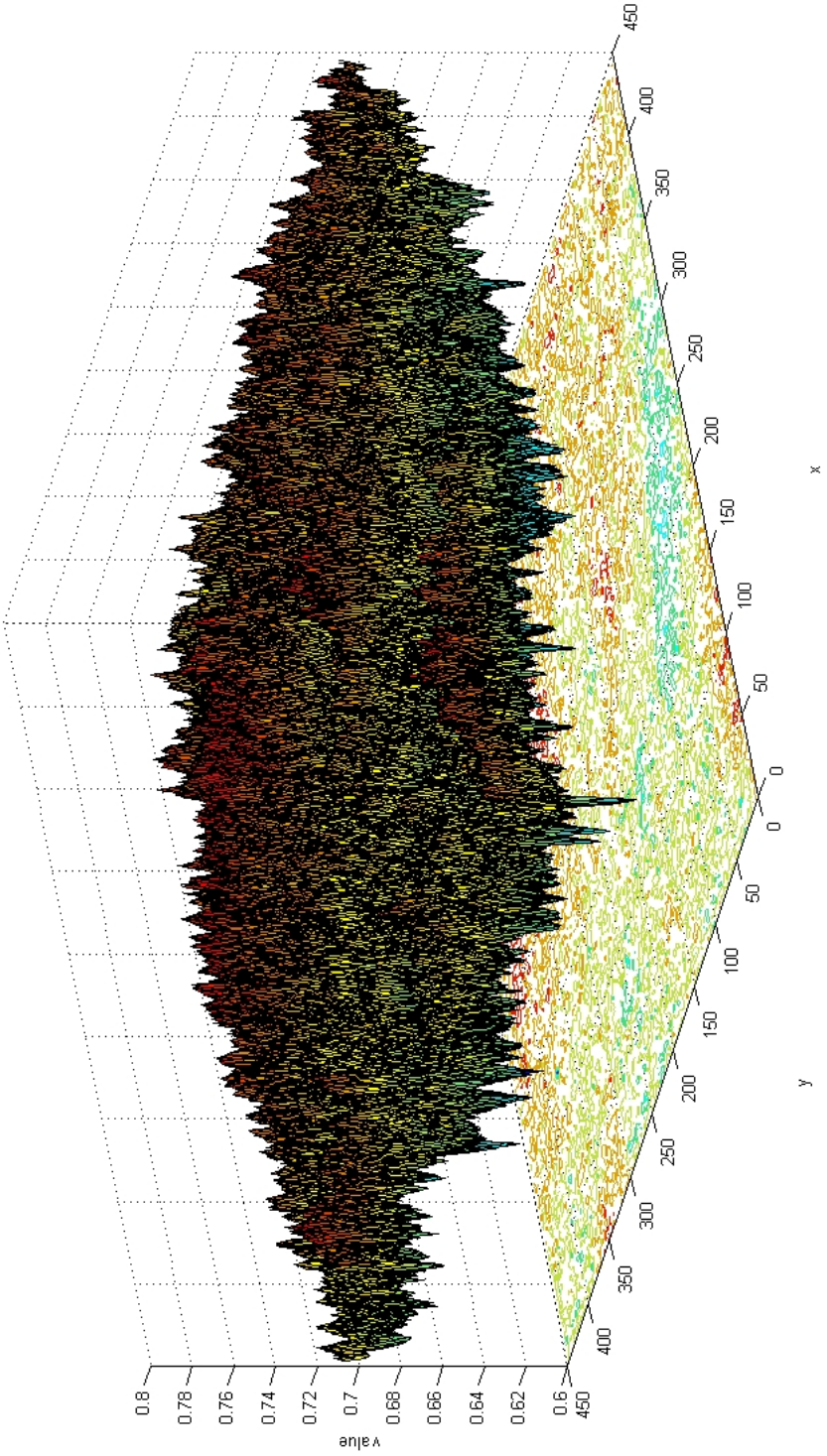

Figure 46: Paper type C surface.

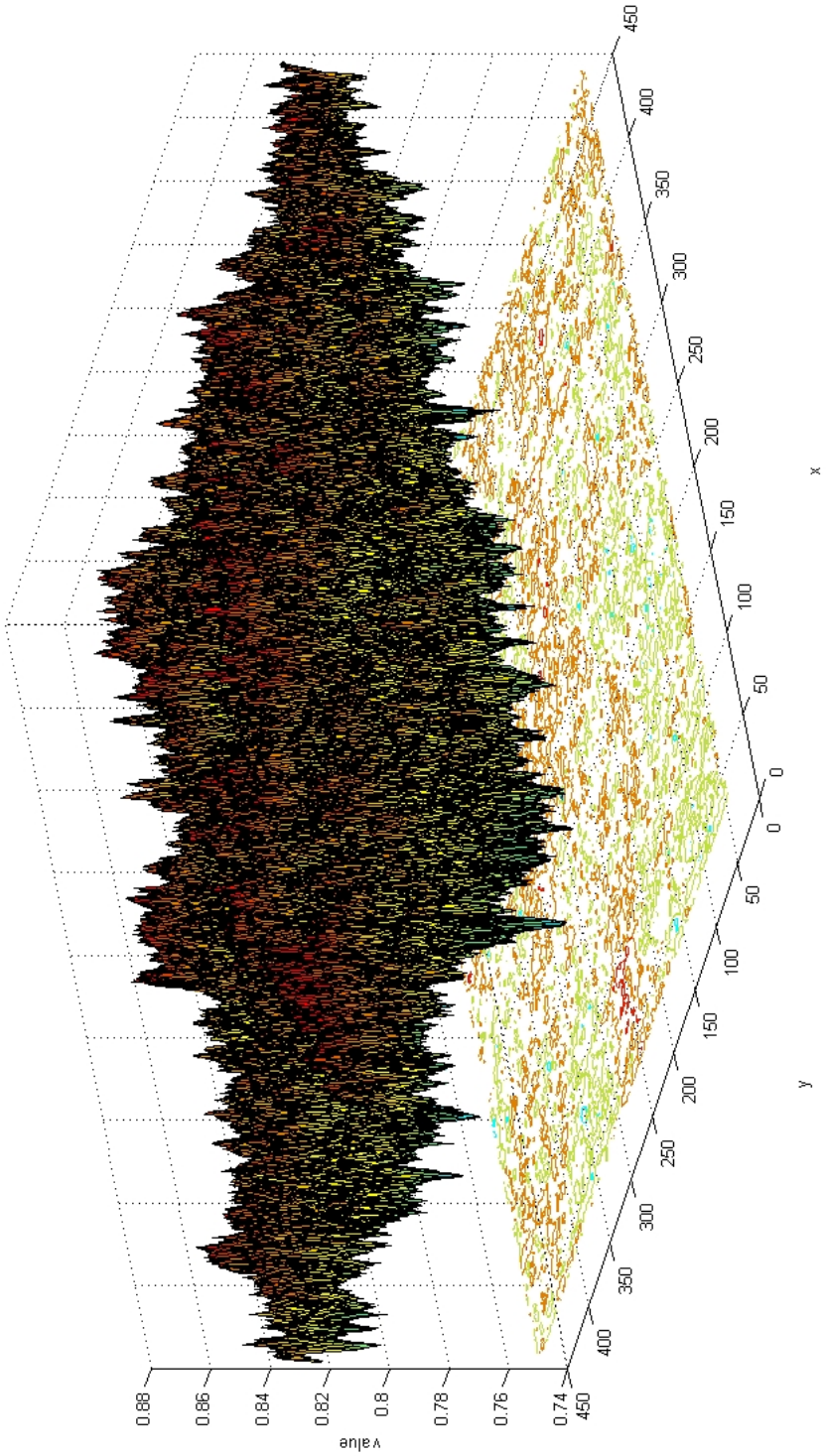

Figure 47: Paper type D surface.

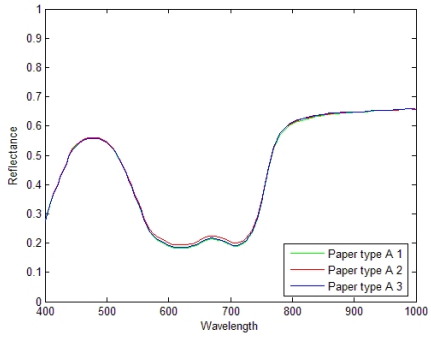

Figure 48: Print variance between different sheets of paper type A.

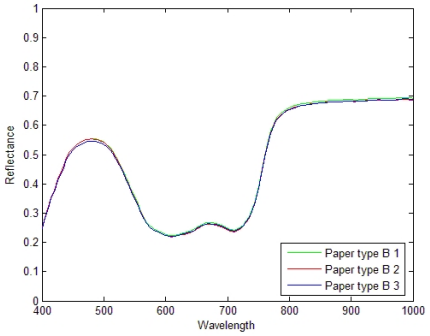

Figure 49: Print variance between different sheets of paper type B.

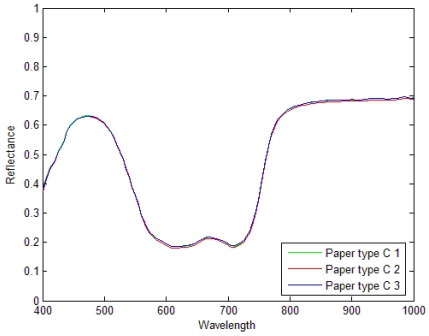

Figure 50: Print variance between different sheets of paper type C.

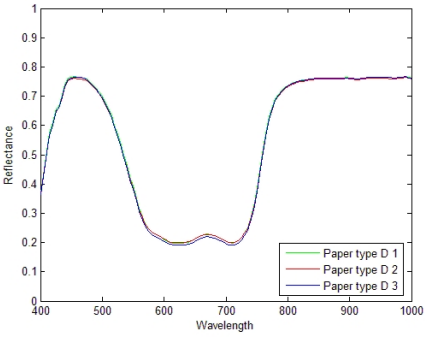

Figure 51: Print variance between different sheets of paper type D.

3.4 Black color formation for different kinds of paper

In Sections 2.1.7 and 2.4 we discussed CMY and CMYK subtractive color spaces used in three-color and four-color printing, respectively. Traditionally, the three-color printing process has used three inks (including cyan, magenta and yellow) to reproduce images. In this case black ink was formed by a mixture of cyan, magenta and yellow pigments. Additionally, in the four-color printing black ink has been added. The reasons for the addition of the black ink in four-color printing in comparison to three-color printing are the following [1][4]:

- a mixture of color inks (cyan, magenta and yellow) rarely produces pure black ink (theoretical (ideal) and real (practical) light transmission spectra for printing inks vary a lot - it is nearly impossible to create sufficiently pure pigments);
- mixing all three color inks together merely to make black can make the paper wet. In poor quality papers (such as newsprint) it can damage paper surface and in high speed printing wet paper sheet can make some markings on the next printed sheet;
- text is usually printed in black, and gray areas of an image can be printed with the use of black ink instead of using three color inks;
- tonal density range of the print and color gamut will increase;
- using black ink to produce black rather than three color inks can lead to cost savings (black ink amount on gray regions of images is only one-third of total amount of color inks required for these regions).

The formation of black color can be carried out according to different scenarios:

- a mixture of cyan, magenta and yellow inks at 100% density (denoted by CMY100);
- a mixture of cyan, magenta, yellow and black inks at some fixed densities (for example cyan, magenta, yellow and black ink at 76%, 67%, 67%, 90% densities, respectively, denoted by C76M67Y67K90);
- black ink at 100% density (denoted by B100);
- a mixture of cyan, magenta, yellow and black inks at 100% density (denoted by CMYK100).

Now we will examine the average spectral reflectance curves for different kinds of black color formation for each type of paper used in the experimental part. The average spectral reflectances are the mean value of spectral reflectance values taken from an area of 45 mm by 45 mm.

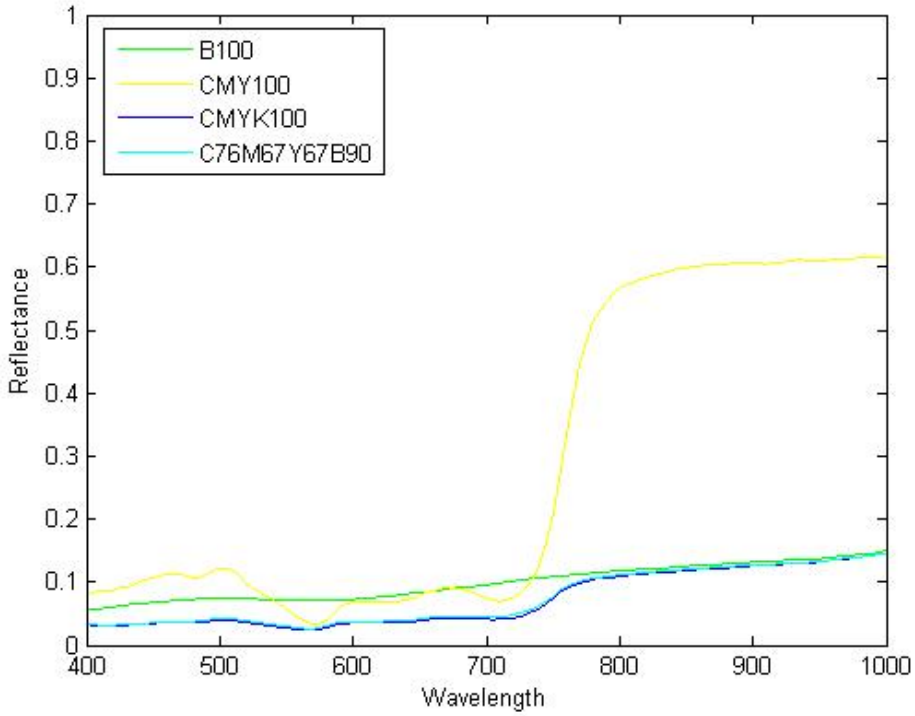

Figure 52: Average spectral reflectance of different black color formations for paper type A.

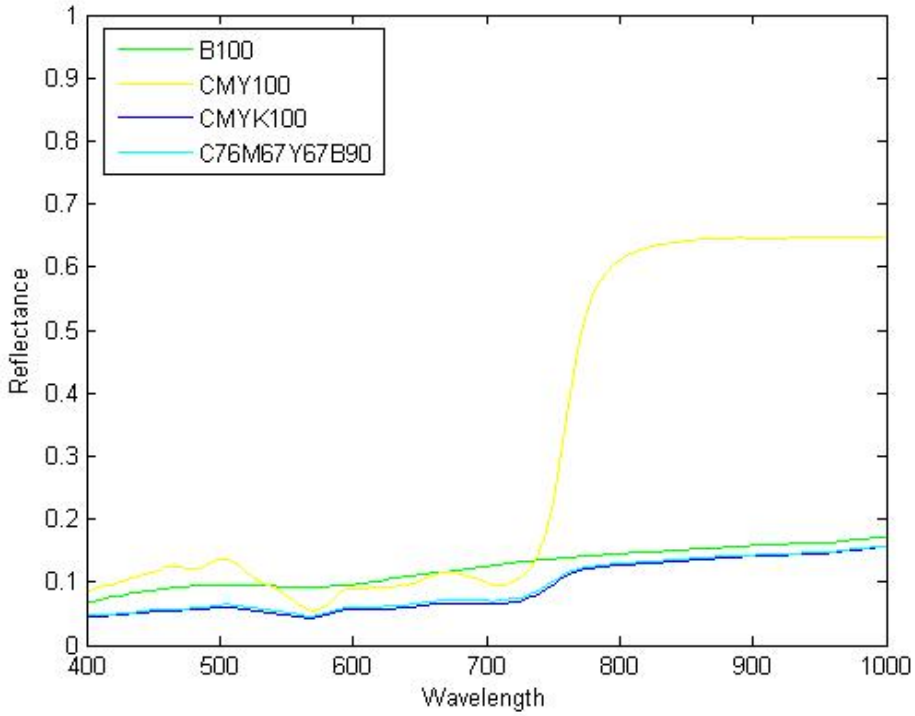

Figure 53: Average spectral reflectance of different black color formations for paper type B.

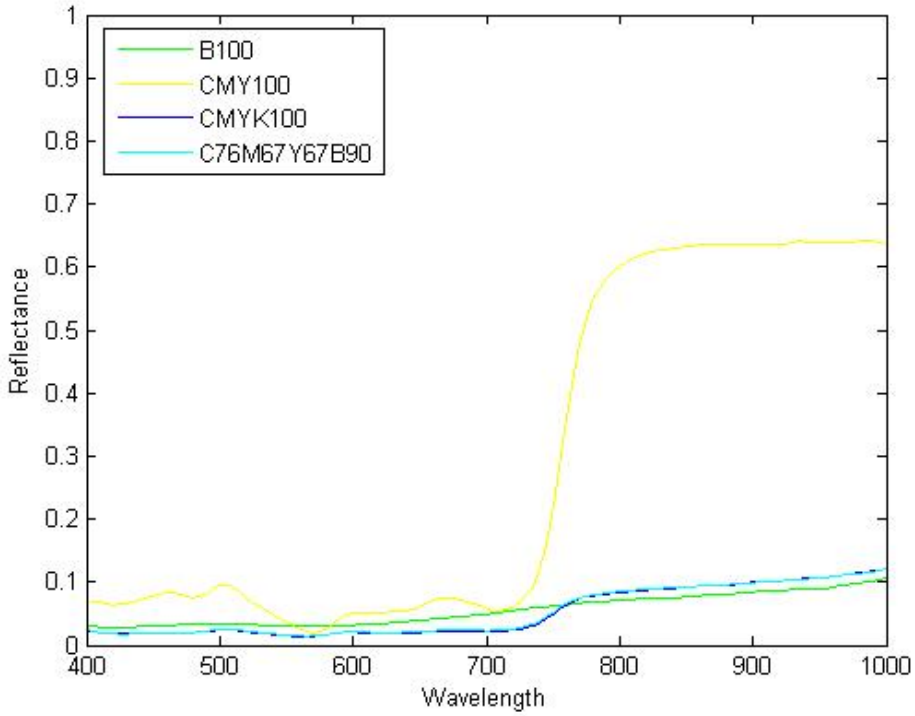

Figure 54: Average spectral reflectance of different black color formations for paper type C.

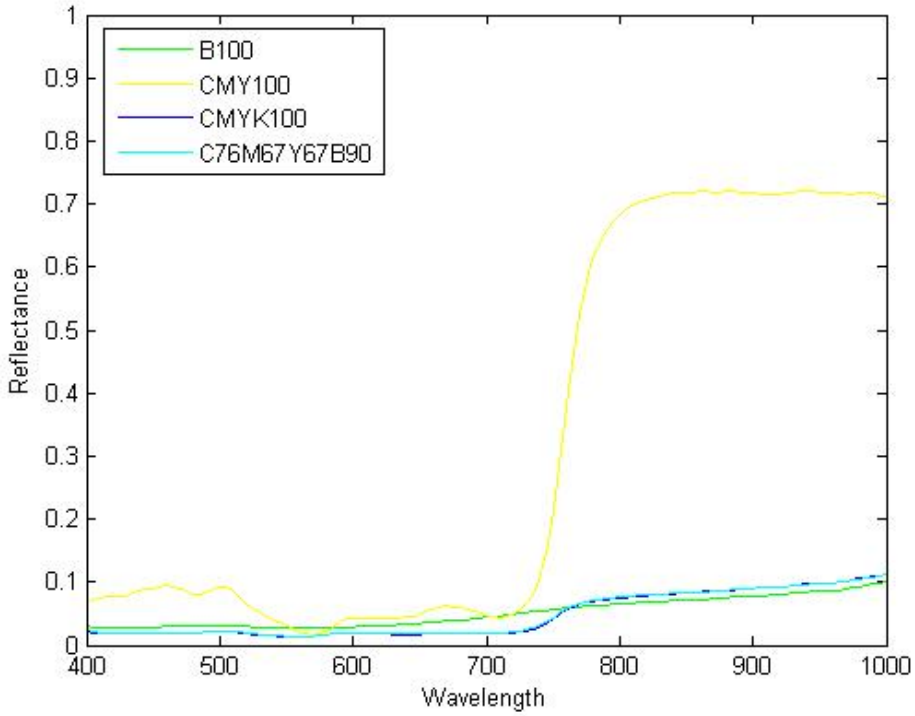

Figure 55: Average spectral reflectance of different black color formations for paper type D.

Figures 52 - 55 present spectral reflectance curves for different black color formations for various kinds of paper.

Based on the results of spectral differences between various black color formations for different kinds of paper we make the following observations:

1. CMYK100 (400% total density) and C76M67Y67K90 (300% total density) black color formations have exactly the same spectral reflectance curves for all kinds of paper, and their color will be perceived identical. There is no need to use a set of inks at 400% total density, if another set of inks at 300% total density gives the same result (from spectral point of view) for all kinds of paper;

2. spectral reflectance curve of B100 black color formation is close to spectral reflectance curves of CMYK100 and C76M67Y67K90 black color formations for paper type C and paper type D. Nevertheless, there is visible difference in color between B100 and CMYK100, and between B100 and C76M67Y67K90;

3. spectral reflectance curve of B100 black color formation is far from spectral reflectance curves of CMYK100 and C76M67Y67K90 black color formations for paper type A and paper type B in comparison to paper type C and paper type D. There is significant visible difference in color between B100 and CMYK100, and between B100 and C76M67Y67K90;

4. spectral reflectance curve of CMY100 black color formation is far from spectral reflectance curves of other black color formation methods, what suggests very significant visible difference in color between CMY100 and other methods;

5. there exist big differences in spectral reflectance curves between CMY100 and other methods outside the visible spectrum range (CMY100 gives significant spectral responses in the infrared region of the electromagnetic radiation in comparison to other black formation methods).

Tables 7 and 8 show coordinates in RGB and CIE Lab color spaces for different kinds of black color formations for paper type A and paper type D respectively. These coordinates were calculated based on spectral reflectance values, the CIE D65 standard illuminant and the 1931 CIE Standard Observer (see Section 3.1).

The results of representation of various black colors for different kinds of paper in RGB and CIE Lab color spaces confirm the observations made based on results of spectral reflectance differences between various black color formations for different kinds of paper, and furthermore we come to the following conclusions:

1. black colors for paper type A (low quality paper) seem to be much brighter than for paper type D (good quality paper)[7];

[7]Let us remind that L parameter in the CIE Lab color space represents the lightness of a color (L=0 yields black color and L=100 indicates white color).

Table 7: Different black color formations for paper type A and their coordinates in RGB and CIE Lab color spaces.

Color space	RGB			L*a*b*		
Paper type A	R	G	B	L*	a*	b*
B100	0.3044	0.2985	0.2884	32.4242	0.1094	1.6873
CMY100	0.2420	0.2996	0.3646	31.8656	-1.2570	-11.6969
CMYK100	0.1990	0.1920	0.2061	20.6108	1.6602	-2.0542
C76M67Y67K90	0.2058	0.2013	0.2098	21.5804	1.0348	-1.2488

Table 8: Different black color formations for paper type D and their coordinates in RGB and CIE Lab color spaces.

Color space	RGB			L*a*b*		
Paper type D	R	G	B	L*	a*	b*
B100	0.1905	0.1837	0.1864	19.5282	0.9541	-0.2009
CMY100	0.1782	0.2317	0.3368	24.8671	2.6401	-17.9706
CMYK100	0.1399	0.1344	0.1500	13.6472	1.6738	-2.4688
C76M67Y67K90	0.1405	0.1373	0.1489	13.9054	1.1411	-1.8847

2. CMY100 black color is much more bluish in comparison to other blacks for all kinds of paper (large value of blue channel in RGB color space, and equivalently large negative value of b parameter in CIE Lab color space).

3.5 Average spectrum and spectral variance of printing inks

Printing presses are usually able to deliver different amounts of printing ink on the substrate. In this section we will examine spectral reflectance variance of printing inks when applied to the substrate surface at different densities.

For each paper type, the spectral reflectance of each printing ink at a particular density was calculated as the average spectrum of a region of 10 mm by 10 mm. It must be noticed that the computed spectra do not correspond to spectral reflectances of printing dots, but they are combinations of spectral reflectances of particular printing dots and paper surface (the influence of paper surface is not removed). Conversely, in Section 5.1.1 we will consider printing dot spectra, i.e. the spectrum of a printing dot will be computed as the average spectrum over the printing dot area.

Figures 56 - 59 show spectral reflectance variation of printing inks for paper type A.

Figures 60 - 63 show spectral reflectance variation of printing inks for paper

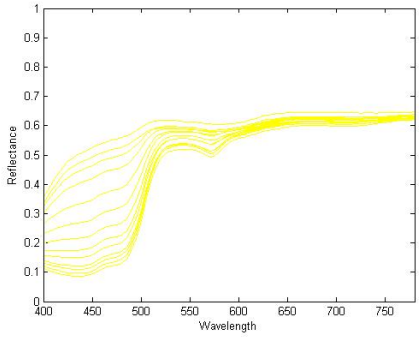

Figure 56: Yellow inks for paper type A.

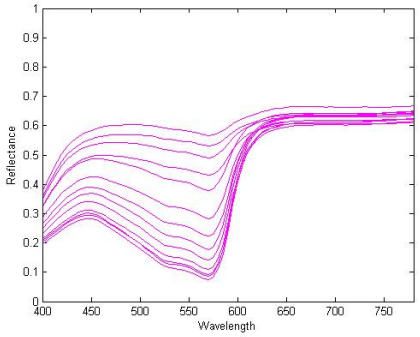

Figure 57: Magenta inks for paper type A.

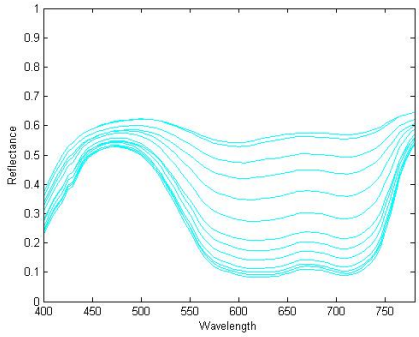

Figure 58: Cyan inks for paper type A.

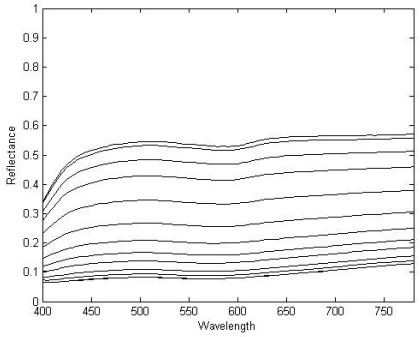

Figure 59: Black inks for paper type A.

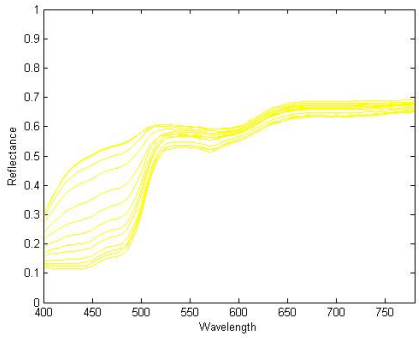

Figure 60: Yellow inks for paper type B.

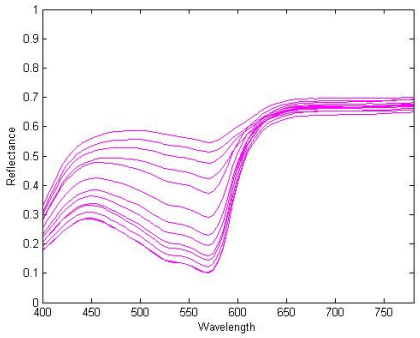

Figure 61: Magenta inks for paper type B.

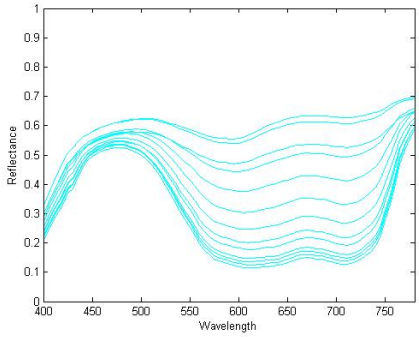

Figure 62: Cyan inks for paper type B.

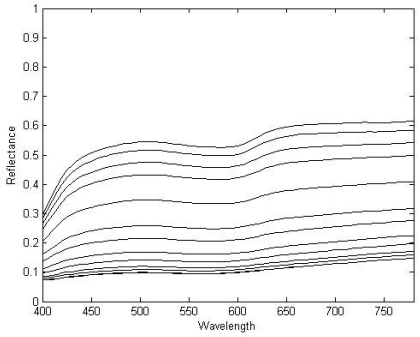

Figure 63: Black inks for paper type B.

type B.

Figures 64 - 67 show spectral reflectance variation of printing inks for paper type C.

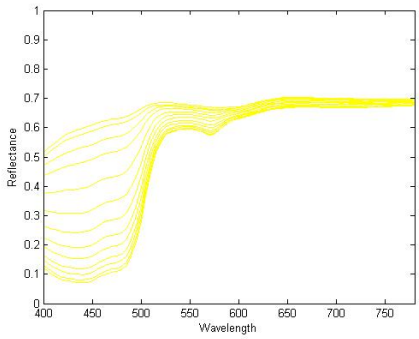

Figure 64: Yellow inks for paper type C.

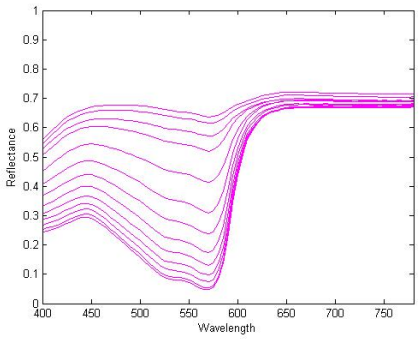

Figure 65: Magenta inks for paper type C.

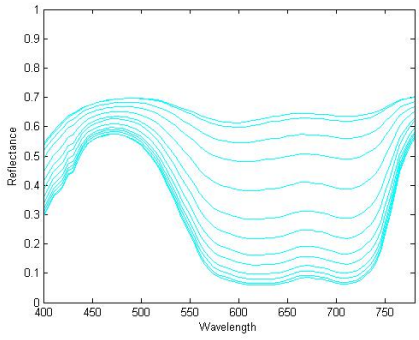

Figure 66: Cyan inks for paper type C.

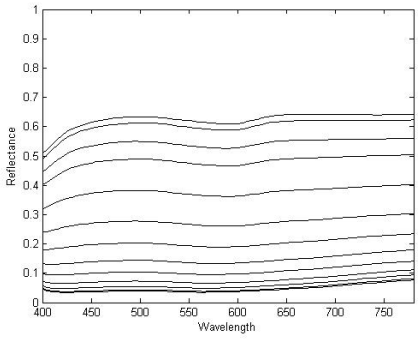

Figure 67: Black inks for paper type C.

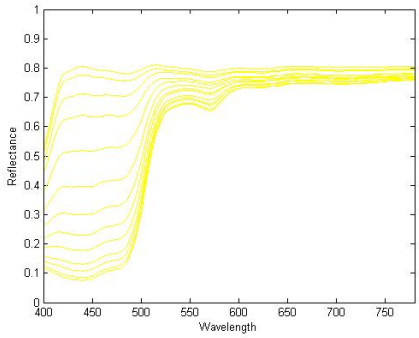

Figure 68: Yellow inks for paper type D.

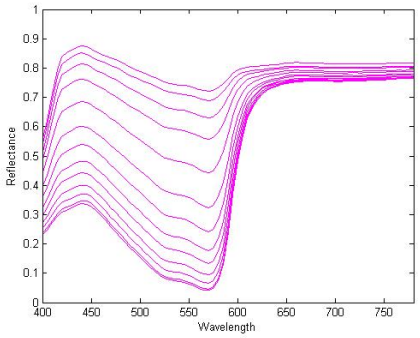

Figure 69: Magenta inks for paper type D.

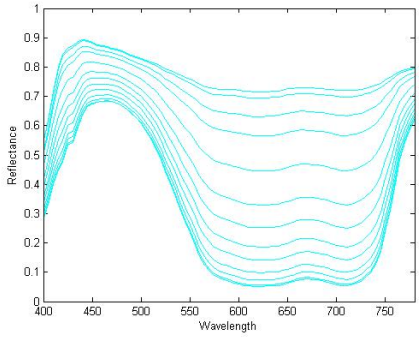

Figure 70: Cyan inks for paper type D.

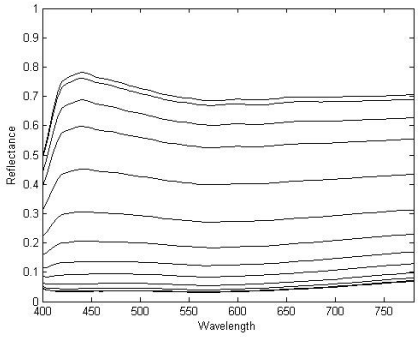

Figure 71: Black inks for paper type D.

Figures 68 - 71 show spectral reflectance variations of printing inks for paper type D.

Tables 9 and 10 show coordinates of yellow ink at different densities in RGB and CIE Lab color spaces for paper type B and paper type D respectively.

An analysis of the results gives us the following conclusions:

1. R and G channel values do not have significant variations ($\sigma(R) = 0.0053$ and $\sigma(G) = 0.0210$ for paper type B, and $\sigma(R) = 0.0027$ and $\sigma(G) = 0.0327$ for paper type D, where $\sigma(X)$ is the standard deviation of variable X);

2. B channel values decrease evenly with the increase of successive ink densities with $\overline{B} = 0.0344$ for paper type B, and $\overline{B} = 0.0614$ for paper type D (where $\overline{X}$ is the average decrease in B channel between successive ink densities calculated from 10% to 100%);

3. L^* values decrease evenly with the increase of successive ink densities (see also Figure 72) with $\overline{L}^* = 0.5208$ for paper type B, and $\overline{L}^* = 0.7011$ for paper

Table 9: Coordinates of yellow ink at different densities for paper type B in RGB and CIE Lab color spaces.

Paper type B	RGB			L*a*b*		
Yellow ink	R	G	B	L*	a*	b*
1%	0.8063	0.7959	0.7300	81.4564	-1.9302	8.5850
2%	0.8110	0.7994	0.7271	81.7675	-2.1013	9.4374
5%	0.8152	0.7991	0.7042	81.7003	-2.6115	12.4611
10%	0.8093	0.7896	0.6712	80.7648	-3.2084	15.6081
20%	0.8053	0.7778	0.6135	79.6022	-4.1831	21.8096
30%	0.8165	0.7805	0.5605	79.7726	-5.2568	29.1977
40%	0.8164	0.7738	0.5110	79.1171	-5.8846	34.8898
50%	0.8159	0.7680	0.4708	78.5641	-6.2929	39.4249
60%	0.8197	0.7671	0.4411	78.4845	-6.5507	43.1592
70%	0.8109	0.7537	0.3995	77.2613	-6.6750	46.8473
80%	0.8057	0.7462	0.3761	76.5789	-6.7486	48.8924
90%	0.8068	0.7452	0.3599	76.4919	-6.8364	50.7591
100%	0.8038	0.7397	0.3405	76.0052	-6.8138	52.4847

type D respectively (where $\overline{X}$ is the average decrease in L^* values between successive ink densities calculated from 10% to 100%). Nevertheless, paper type D is much brighter than paper type B (see L^* parameters);

4. a^* and b^* values increase evenly with the increase of successive ink densities with $\overline{b}^* = 3.8298$ for paper type B, and $\overline{b}^* = 6.6123$ for paper type D respectively. Paper type D is less yellowish than paper type B between 1% and 30% densities, and much more yellowish between 30% and 100% densities (see b^* parameter);

5. the span of spectral reflectance curves of printing inks for paper type D is much bigger than for paper type B. This suggests that the gamut of colors produced on paper type D is much bigger than on paper type B.

Figure 72 shows L^* and b^* parameter variations for different yellow ink densities for paper type B and papers type D. As suggested earlier, paper type D (red-squared curve) is less yellowish than paper type B (blue-squared curve) between 1% and 30% densities, and much more yellowish between 30% and 100% densities. Let us notice that at 30% density of yellow ink both papers have the same amount of yellow color (b* parameter).

Another property of printing inks which can be measured is their spectral reflectance span (already mentioned earlier). For example, let us compare yellow inks shown in Figures 60 and 68. We can easily see that the span (in spectral

Table 10: Coordinates of yellow ink at different densities for paper type D in RGB and CIE Lab color spaces.

Paper type D	RGB			L*a*b*		
Yellow ink	R	G	B	L*	a*	b*
1%	0.9036	0.9057	0.8998	91.5479	-0.3631	0.5267
2%	0.8994	0.8996	0.8856	90.9867	-0.5732	1.6017
5%	0.8996	0.8950	0.8514	90.4761	-1.4535	5.4179
10%	0.8953	0.8851	0.8087	89.5051	-2.3627	9.7076
20%	0.8991	0.8773	0.7329	88.6560	-3.9955	18.6273
30%	0.9006	0.8672	0.6423	87.5933	-5.7233	29.1598
40%	0.9011	0.8571	0.5578	86.5938	-6.9351	38.8393
50%	0.9053	0.9053	0.4831	86.0585	-7.7379	47.6163
60%	0.9020	0.8405	0.4155	85.0610	-8.1323	54.6034
70%	0.9033	0.8331	0.3405	84.4128	-8.3990	62.3980
80%	0.9047	0.8297	0.2917	84.1265	-8.5374	67.1695
90%	0.9016	0.8220	0.2378	83.4653	-8.5327	71.5408
100%	0.9013	0.8193	0.2063	83.2343	-8.5292	73.9377

reflectance sense) for yellow inks for paper type B is much lower than for paper type D - the difference between the top level spectrum and the low level spectrum in Figure 60 is much smaller than for spectra in Figure 68. In this paragraph we will investigate the differences in spectral reflectance span of printing inks for different kinds of paper. The following scheme will be utilized to carry out the experiment:

1. choose a printing ink;
2. calculate the spectral reflectance span of the printing ink for each paper of interest in the following way:
   (a) take reflectance spectra of the printing ink at 100% density and 1% density denoted by $R_{100\%}$ and $R_{1\%}$, respectively;
   (b) calculate the difference spectrum as $R_{diff,\lambda} = R_{1\%,\lambda} - R_{100\%,\lambda}$ for each wavelength λ of interest;
   (c) plot a curve of the difference spectrum R_{diff} as a function of wavelength.

Figure 73 - 76 show the results of the above scheme applied to cyan, magenta, yellow and black printing inks respectively. The spectral spans have been calculated for all printing inks and all papers used in the experimental part.

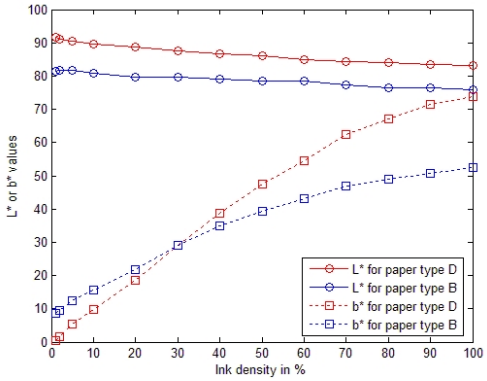

Figure 72: L* and b* parameter variations for different yellow ink densities for paper type B and paper type D.

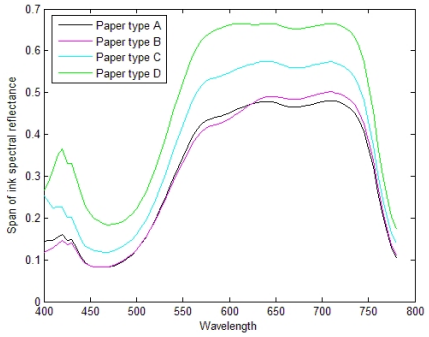

Figure 73: Spectral reflectance span for cyan inks.

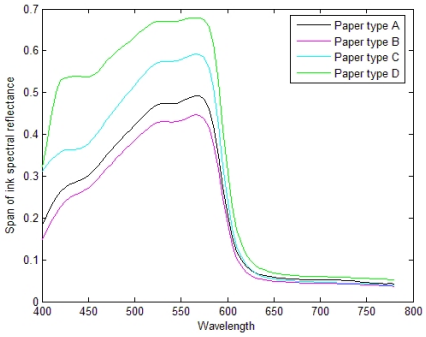

Figure 74: Spectral reflectance span for magenta inks.

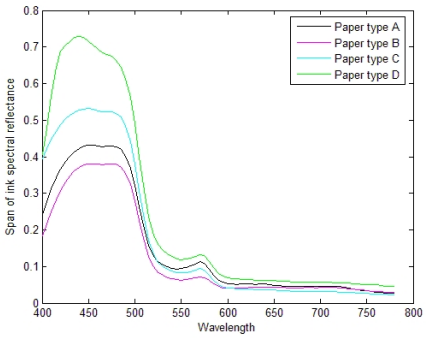

Figure 75: Spectral reflectance span for yellow inks.

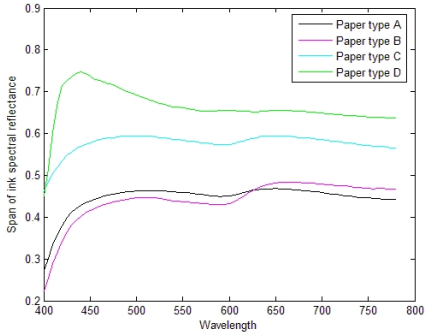

Figure 76: Spectral reflectance span for black inks.

The largest spectral reflectance spans correspond to the paper type D and paper type C (good quality papers) in comparison to the remaining kinds of paper. We also expect to get higher color gamut for papers with large spectral reflectance spans than with small ones. Thus, good quality papers have higher color gamut than low quality papers.

3.6 Dot gain characterization

Dot gain is a phenomenon associated with halftoning where printing dots can be larger or lighter than initially intended, mainly due to the characteristics of paper, inks, paper-ink interactions and printing process (including printing conditions and halftone techniques used). The literature generally consider two kinds of dot gain: physical and mechanical dot gain [5] [7].

Physical dot gain is actual growth in colorant area coverage (printing dot size) mainly due to spreading of ink on the paper surface. The ink drop can spread when applying to a substrate or due to ink penetration into the substrate surface [5].

Optical dot gain (also known as the Yule-Nielsen effect) is defined as the increase of dot size due to light scattering in the paper. Light that enters through bare substrate (is not reflected) may be scattered and exit underneath a dot. Similarly, light that enters through a dot surface may be scattered and exit through bare surface. These scattering causes that the bare surface is visually darker than expected and dots appear larger and lighter than intended. The overall scattering effect result in darker final output [5].

The reflectance of a binary halftone pattern can be predicted by the Murray-Davies equation [9] [5]:

$$R_\lambda = aR_{\lambda,ink} + (1-a)R_{\lambda,s} \tag{23}$$

, where the λ subscripts denote a wavelength, R_λ is predicted spectral reflectance, a is fractional dot area coverage of ink ink, $R_{\lambda,ink}$ is the spectral reflectance of ink ink at full area coverage, and $R_{\lambda,s}$ is the spectral reflectance of the base substrate. This equation suggests that the measured spectral reflectance of printed area, where a printing ink at fractional dot area coverage equal to a has been applied should be equal to the predicted spectral reflectance of the area using Equation (23) which bases on the spectral reflectance of the ink at full area coverage, fractional dot area coverage a, and the spectral reflectance of plain paper substrate.

The Murray-Davies equation assumes that the base substrate and the ink are of uniform color (the spectral properties of ink and paper do not change throughout the area of interest). Furthermore the area coverage denoted by a in Equation (23) should be the effective dot area (denoted later by a_{eff}) to achieve better prediction results, i.e. an estimated value which accurately predicts the spectral reflectance R in Equation (23). On the other hand, the theoretical area (denoted later by

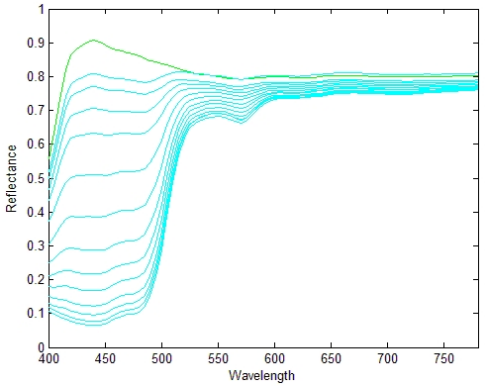

Figure 77: Cyan inks for paper type D at different densities.

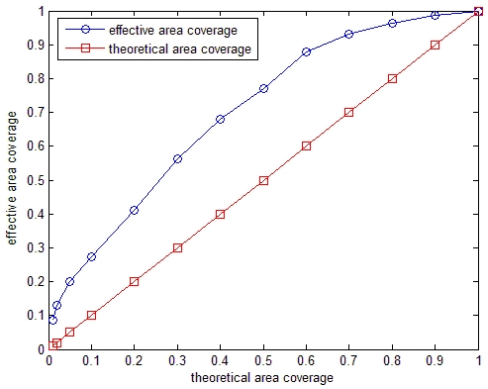

Figure 78: Theoretical versus effective dot coverage area.

a_{the}) is the actual value sent to the printer driver. The spectrum prediction based on the theoretical area coverage is inaccurate due to the assumption of square pixel shape, and the predicted reflectance of halftone images using Equation (23) is much higher than measured reflectance.

In particular, the Murray-Davies equation can be transformed to predict the effective dot area coverage [5]:

$$a_{eff} = \frac{R_{\lambda=min} - R_{\lambda=min,s}}{R_{\lambda=min,ink} - R_{\lambda=min,s}} \tag{24}$$

, where a_{eff} is the effective dot area coverage, and R_λ is a measured spectral reflectance of ink *ink* at a particular density. Let us notice that all spectral reflectance values are subscripted by $\lambda = min$ to indicate that it is not a spectral calculation, but one made at a single wavelength. [5] suggests that the choice of *min* should be the minimum value of reflectance R (it varies the most when dot area coverage is changed).

Furthermore, the dot gain can be calculated as a the difference between the effective and theoretical dot area coverage, i.e.

$$dot\ gain = a_{eff} - a_{the} \tag{25}$$

, where a_{the} denotes theoretical dot area, and a_{eff} can be calculated using Equation (24). Using this equation we take into account both varieties of dot gain.

Figure 77 shows example cyan ink at different densities for paper type D. Green curve represents the plain paper reflectance. Figure 78 shows theoretical versus effective dot area coverage for cyan ink from Figure 77. Equation (24) was used to calculate the effective dot area coverage.

As mentioned earlier, the printing dots appear larger for two reasons: ink spread out on the paper (physical dot gain), and the light scattering in the paper

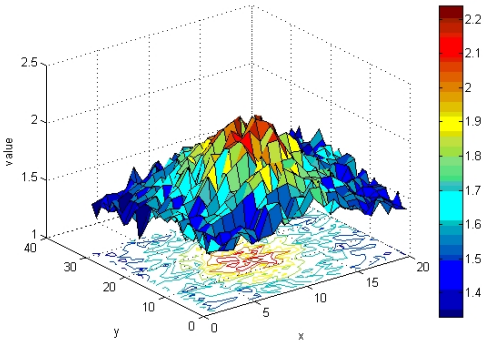

Figure 79: Cyan dot at 20% density.

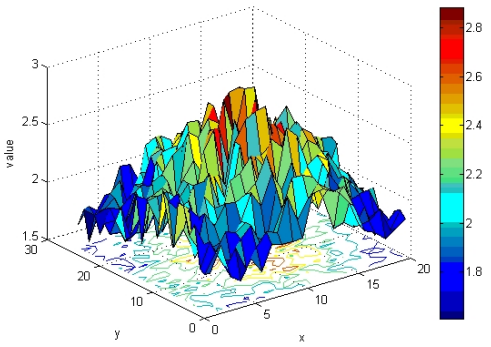

Figure 80: Cyan dot at 40% density.

(optical dot gain). A real dot has a diameter depending on the printer resolution, ink volume (density) and the ink spread characteristic on the paper. A dot irregular shape depends mainly on the ink spread characteristic on the substrate, what in particular causes that the dot color distribution is not uniform, especially when comparing the middle region and the edge region of the dot [10]. Upon striking the substrate, an ink must dry as quickly as possible to minimize the spread effect. The extent to which spreading occurs depends mainly on the surface tension and viscosity of the ink [11].

Now we will see how the ink spreading and light scattering affect the printing ink density distribution and color variation throughout a dot area. To visualize this we will utilize the following scheme to a spectral image of a printing dot:

1. let R be the spectral reflectance for a spatial location (x, y) of the spectral image;
2. compute mean value $\overline{R} = \frac{1}{N} \sum_{i=1}^{N} R_i$;
3. compute final value for the spatial location as $value = 1/\overline{R}$.

Figures 79 and 80 show 3D representations of two cyan dots at 20% and 40% densities, respectively. Based on the images we clearly see the uneven distribution (print density) of color throughout the dot area. In particular, the difference is the most visible when comparing the edge region and the middle part of the dots.

The uneven distribution of color throughout a printing dot area will have some unwanted implications on concentration prediction and color separation.

4 Mottling characterization

In this chapter we will investigate if there exists any spatial correlation between the spectral reflectance of plain paper and printed paper in exactly the same spatial locations where different kinds of mottling have been applied. Next we will check if there exist any differences between spatial correlation of prints to plain papers for different types of mottling for a particular kind of paper. In particular we will answer the following question: "Does some type of mottling have better spatial correlation to plain paper than the others".

In the experimental part related to mottling, the papers will be measured under D65 and UV illuminations, and in particular, we will try to check if UV illumination can be used for better characterization of paper and print in comparison to measurements under D65.

4.1 Print unevenness

Mottling is an important printing defect in modern printing using coated papers. Mottling can be defined as undesired unevenness in perceived print density especially visible in solid areas of a printed paper [2].

Uneven appearance (small dark and light areas appearing in the surface of paper) in solid portions of a printed paper is mainly influenced by the type of paper used. Spatial variations in the surface of paper (especially spatial variations of absorption and smoothness parameters) play an important role in the mottle characteristics. The mottling phenomena is also influenced by many parameters during the printing process including the type of ink used, the color sequence, the construction of printing press, faulty press adjustments, the selection of the wrong ink for the particular type of paper, and press speed.

In this thesis we will divert our attention from these minor causes of mottling phenomena, and we will focus our attention on spatial variation in the surface of paper as the main cause of printing mottling.

Figure 82 shows the mottling phenomena. Visually, the printed image appears non-uniform and it is the result of uneven ink distribution or non-uniform ink absorption across the paper surface. It is mainly caused by spatial variations in the paper surface showed on Figure 81.

As mentioned earlier, in our further investigation we will find out if there exists any spatial correlation between the spectral reflectance of plain paper and printed paper in exactly the same spatial areas for different kinds of mottling. We will check if there exist any differences between spatial correlation of prints to plain papers for different types of mottling. In particular, we will examine if some types of mottling have better spatial correlation to plain paper than the others.

The spatial correlation of different kinds of mottling will be computed for different types of papers used in the experiment measured under D65 illumination.

4.2 Measurements under D65 illumination

In this section we will investigate the spatial correlation of prints to plain papers measured for different kinds of mottling under D65 illumination.

The spatial correlation of a plain paper to its printed version will be computed as follows:

1. let S_{BEFORE} and S_{AFTER} be spectral images of the same paper sheet before (blank paper) and after printing process (printed paper). Select a region R of interest from spectral image S_{AFTER}, and for each spatial location (x, y) of region R do:
   (a) denote by x spectral reflectance in location (x, y) of image S_{AFTER};
   (b) find the same spatial location corresponding to location (x, y) of image S_{AFTER} in image S_{BEFORE} and denote its spectral reflectance by y;
   (c) calculate the correlation between spectral reflectances x and y which is the correlation for spatial location (x, y);
2. having correlation values for each spatial location draw a 3D surface which a function from spatial locations to their corresponding correlation values.

The correlation between spectral reflectance vectors x and y will be computed according to the following equation:

$$\rho_{x,y} = \frac{cov(x, y)}{\sigma_x \sigma_y} \tag{26}$$

, where $x = (x_1, ..., x_N)$, $y = (y_1, ..., y_N)$, and $cov(x, y)$ is the covariance between two vectors x and y, σ_x is the standard deviation of vector x, and σ_y is the standard deviation of vector y. Furthermore we define covariance $cov(x, y)$ as:

$$cov(x, y) = \frac{\sum_{i=1}^{N}(x_i - \overline{x})(y_i - \overline{y})}{N} \tag{27}$$

, and standard deviation σ_x as:

$$\sigma_x = \sqrt{\frac{1}{N}\sum_{i=1}^{N}(x_i - \overline{x})^2} \tag{28}$$

, where $\overline{x}$ and $\overline{y}$ are the mean values of vector x and y respectively.

The measurements of blank papers and their printed counterparts were done by the ImSpector V10 spectral camera under D65 illumination. Each region of interest was measured in the range from 400 nm to 1000 nm with 5 nm quantization step, what gave 121 values for each spectral reflectance value. However, in the spatial correlation scheme described above we took into account only the first 71 values corresponding to range from 400 nm to 780 nm. The values were limited

to the visible spectrum due to very high correlation between spectra x and y outside the visible range in comparison to their correlation in the range from 400 nm to 780 nm. Taking into account the infrared region would give higher spatial correlation between vectors x and y, what could diminish the "real" spatial correlation accuracy in the visible spectrum.

In particular, the 3D surfaces showing the spatial correlations for different types of mottling and papers do not correspond to real ones. For better result visualization the Gaussian smoothing has been applied to the original 3D surfaces. The following discrete approximation of 2D Gaussian function with $\Sigma = 1.4$ has been used as the pixel filter (mask) [32]:

$$mask = \frac{1}{115} \begin{vmatrix} 2 & 4 & 5 & 4 & 2 \\ 4 & 9 & 12 & 9 & 4 \\ 5 & 12 & 15 & 12 & 5 \\ 4 & 9 & 12 & 9 & 4 \\ 2 & 4 & 5 & 4 & 2 \end{vmatrix}.$$

Since the smoothing operation has been applied to all 3D surfaces, the results coming from visual assessments are valid and correct. The mean, variance, and standard deviation values presented for each type of paper and mottling kind are computed based on the original spatial correlations and do not correspond to the smoothed versions of the original images.

The smoothing operation has been applied for all 3D surfaces showing the spatial correlations under D65 illuminant. The operation has not been applied to 3D images showing paper surface before or after printing process under D65 and UV illuminants.

4.2.1 Paper type B

In this section we will investigate spatial correlation of paper type B for different types of mottling to their corresponding plain papers under D65 illumination.

Figure 81 shows paper type B before printing process, and Figure 82 shows the same paper area as in Figure 81 after the printing process has been applied.

Figure 83 shows 3D representation of paper type B surface corresponding to Figure 81, and Figure 84 presents 3D representation of paper type B surface which corresponds to Figure 82.

Figures 85 - 88 show correlations of plain paper type B to their corresponding printed papers under D65 illumination.

Figure 85 shows 3D representation of spatial correlation of paper type B in the case when water-ink-BT-BT printing process has been applied to plain paper area. Similarly, Figure 86 shows 3D representation of spatial correlation of paper type B in the case when dry-ink-BT-BT printing process has been applied, Figure 87 when dry-ink-dry-dry printing process has been applied, and Figure 88 when water-ink-dry-dry printing process has been applied.

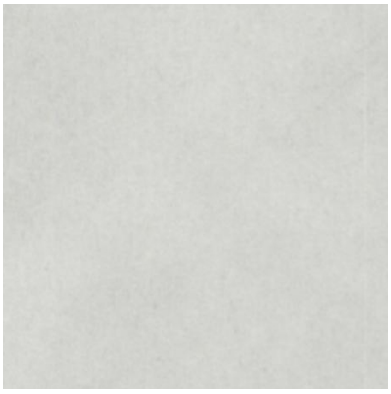

Figure 81: Blank paper type B under D65 illumination.

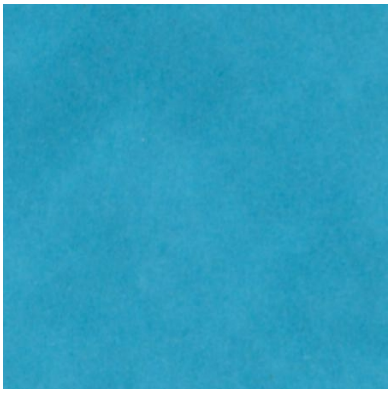

Figure 82: Printed paper type B under D65 illumination.

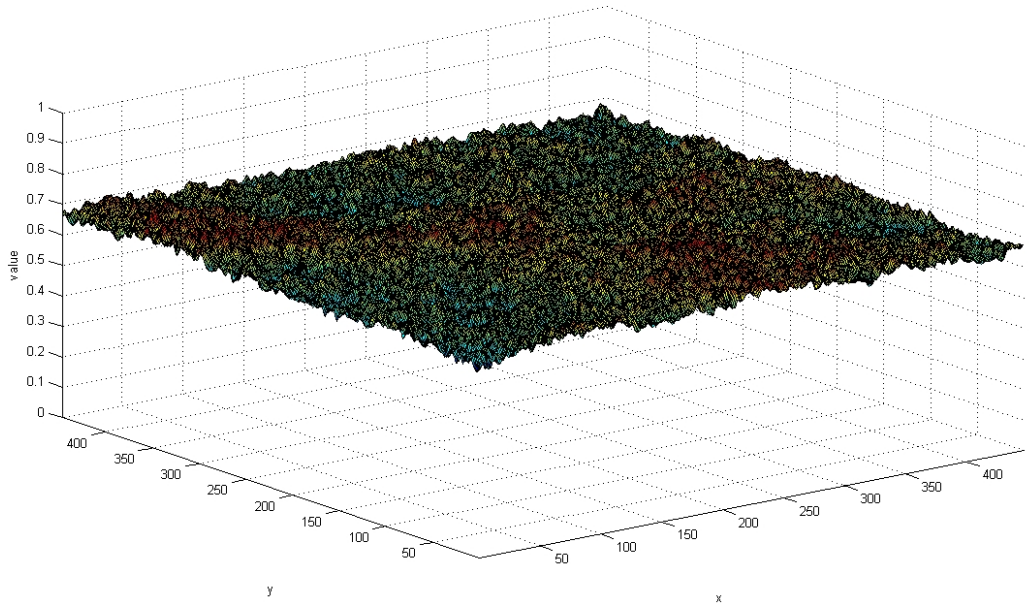

Figure 83: Paper type B surface before printing process. Water-ink-BT-BT printing process will be applied to the paper area.

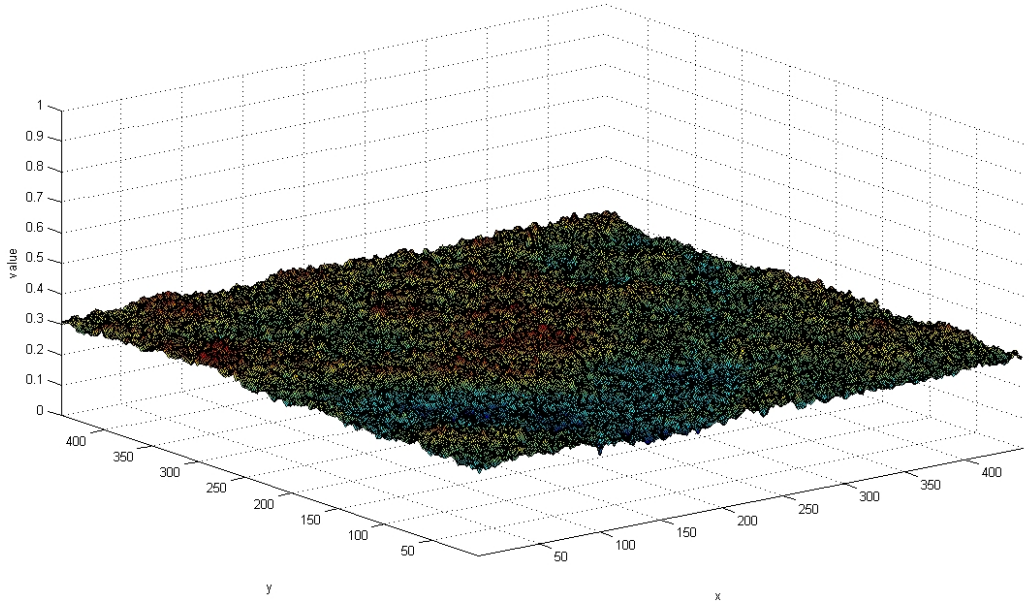

Figure 84: Paper type B surface after water-ink-BT-BT printing process has been applied.

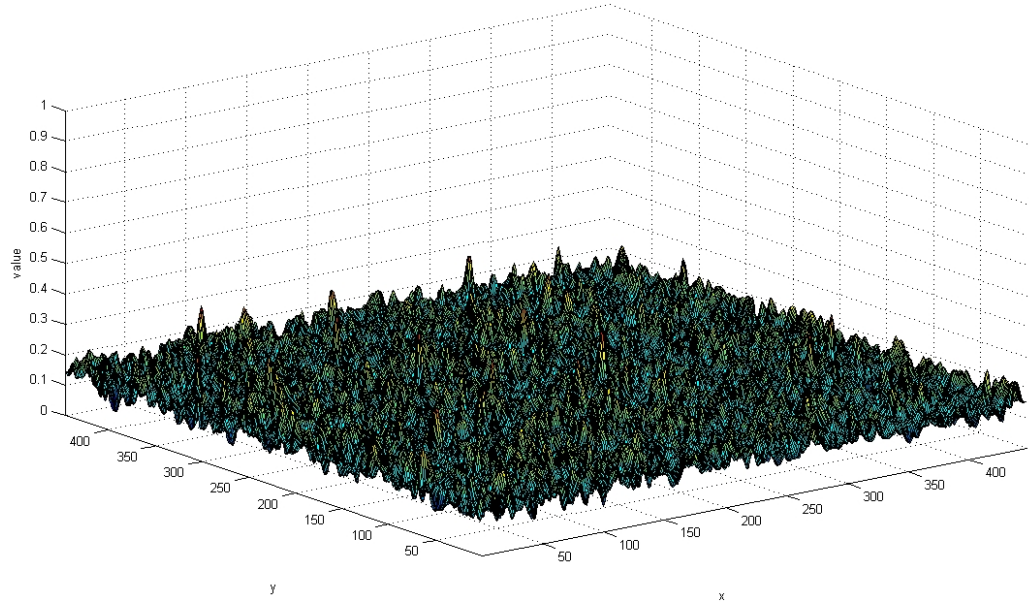

Figure 85: Spatial correlation for paper type B in the case when water-ink-BT-BT printing process has been applied.

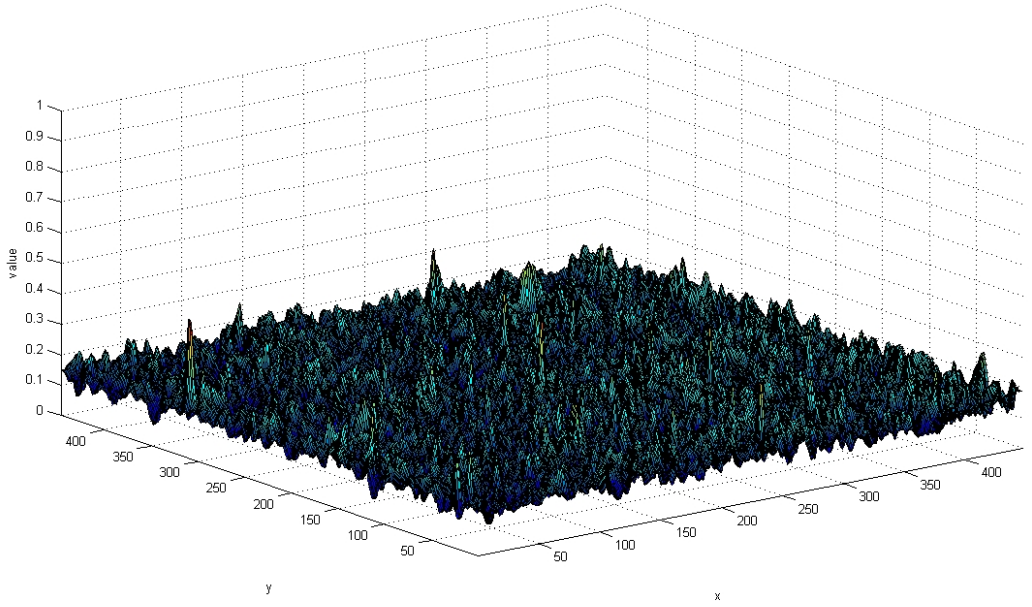

Figure 86: Spatial correlation for paper type B in the case when dry-ink-BT-BT printing process has been applied.

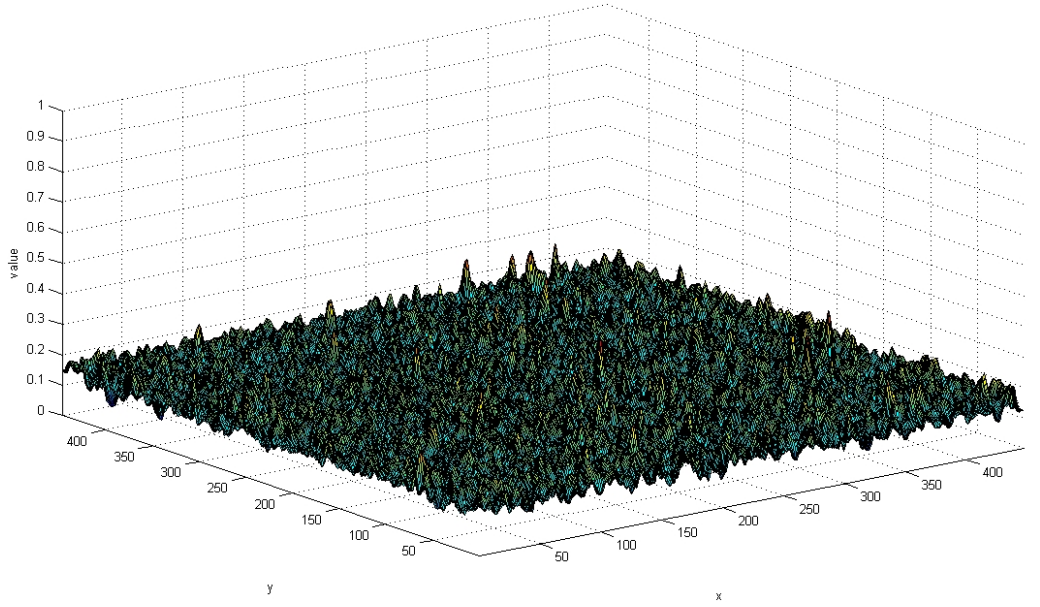

Figure 87: Spatial correlation for paper type B in the case when dry-ink-dry-dry printing process has been applied.

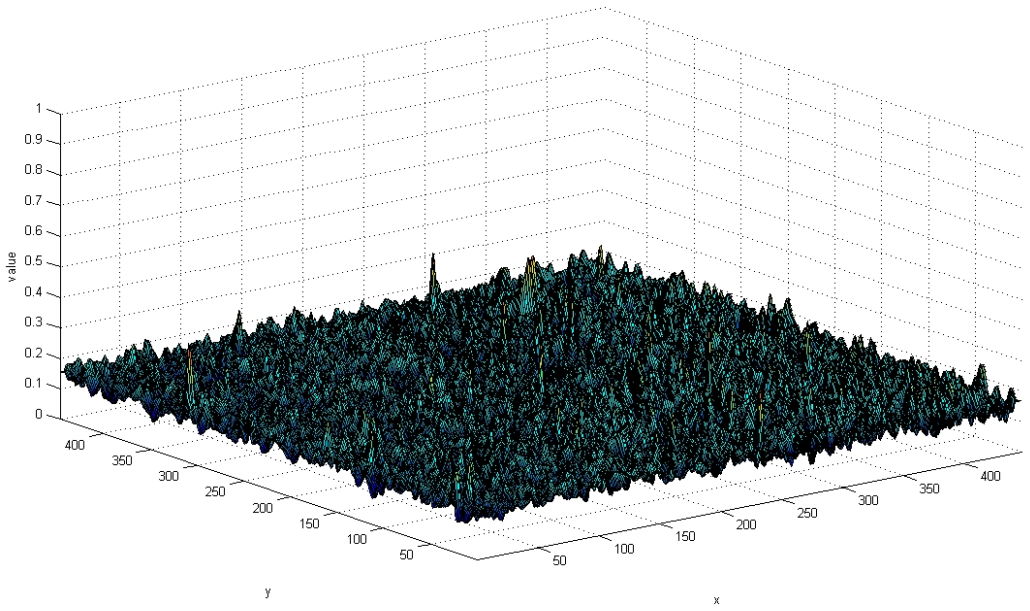

Figure 88: Spatial correlation for paper type B in the case when water-ink-dry-dry printing process has been applied.

Table 11 is a summary of spatial correlations for different types of mottling to their corresponding plain paper areas for paper type B. Based on Figures 85 - 88 and results contained in Table 11 we come to the following conclusions:

- there is no noticeable difference in spatial correlations between various kinds of mottling applied to paper type B. 3D surfaces of spatial correlations seem to be very similar, and no apparent differences between them exist;
- mottling type prediction based on mean value, variance or standard deviation is rather not possible. The only significant difference is visible in standard deviation value between dry-ink-dry-dry mottling and other kinds of mottling (see Table 11). However, small values of standard deviation for all spatial correlations for different types of mottling suggest that it can not be reliable way for mottling kind prediction;
- none of considered types of mottling has better or worse spatial correlation to plain paper than other types of mottling.

4.2.2 Paper type D

In this section we will investigate spatial correlation of paper type D for different types of mottling to their corresponding plain papers under D65 illumination.

Table 11: Spatial correlation summary for different kinds of mottling for paper type B.

Mottling kind	Mean	Variance	Standard deviation
water-ink-BT-BT	0.1099	0.0012	0.0353
dry-ink-BT-BT	0.1086	0.0014	0.0373
dry-ink-dry-dry	0.1080	0.0011	0.0326
water-ink-dry-dry	0.1102	0.0013	0.0358

Figure 89: Blank paper type D under D65 illumination.

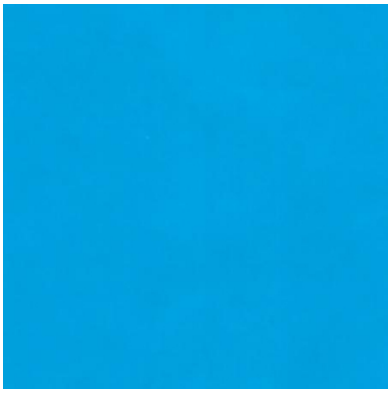

Figure 90: Printed paper type D under D65 illumination.

Figure 89 shows paper type D before printing process, and Figure 90 shows the same paper area as in Figure 89 after the printing process has been applied.

Figure 91 shows 3D representation of paper type D surface corresponding to Figure 89, and Figure 92 shows 3D representation of paper type D surface which corresponds to Figure 90.

Figures 93 - 96 show correlations of plain papers type D to their corresponding printed papers under D65 illumination.

Figure 93 shows 3D representation of spatial correlation of paper type D in the case when water-ink-BT-BT printing process has been applied to plain paper area, Figure 94 when dry-ink-BT-BT printing process has been applied, Figure 95 when dry-ink-dry-dry printing process has been applied, and Figure 96 when water-ink-dry-dry printing process has been applied.

Table 12 is a summary of spatial correlations for different types of mottling to their corresponding plain paper areas for paper type D. Based on Figures 93 - 96 and results contained in Table 12 we come to the following conclusions:

- there are no noticeable differences in spatial correlation between various kinds of mottling applied to paper type D - 3D surfaces of spatial correlations seem to be very similar;

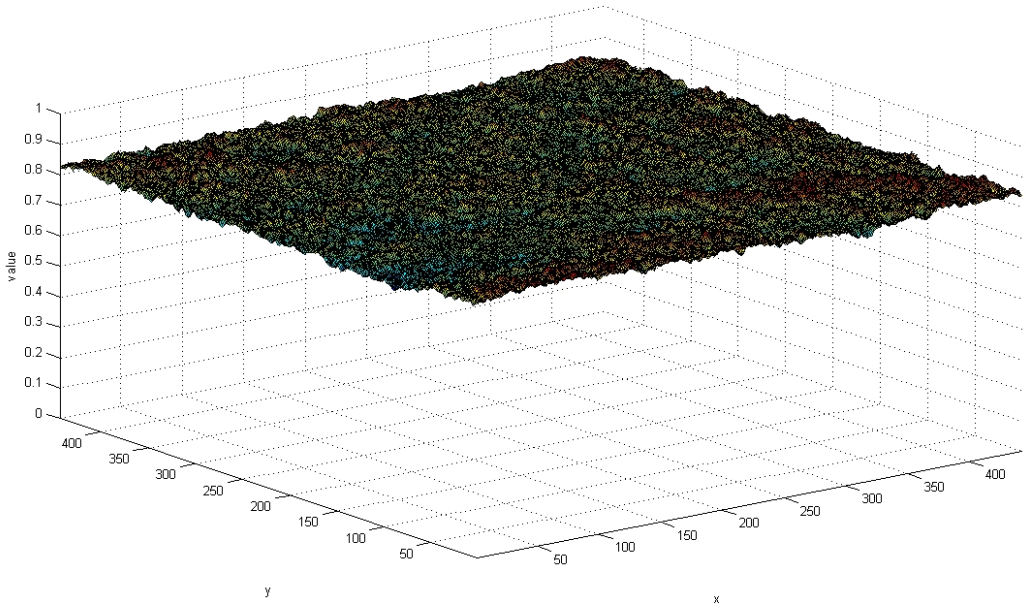

Figure 91: Paper type D surface before printing process. Water-ink-BT-BT printing process will be applied to the paper area.

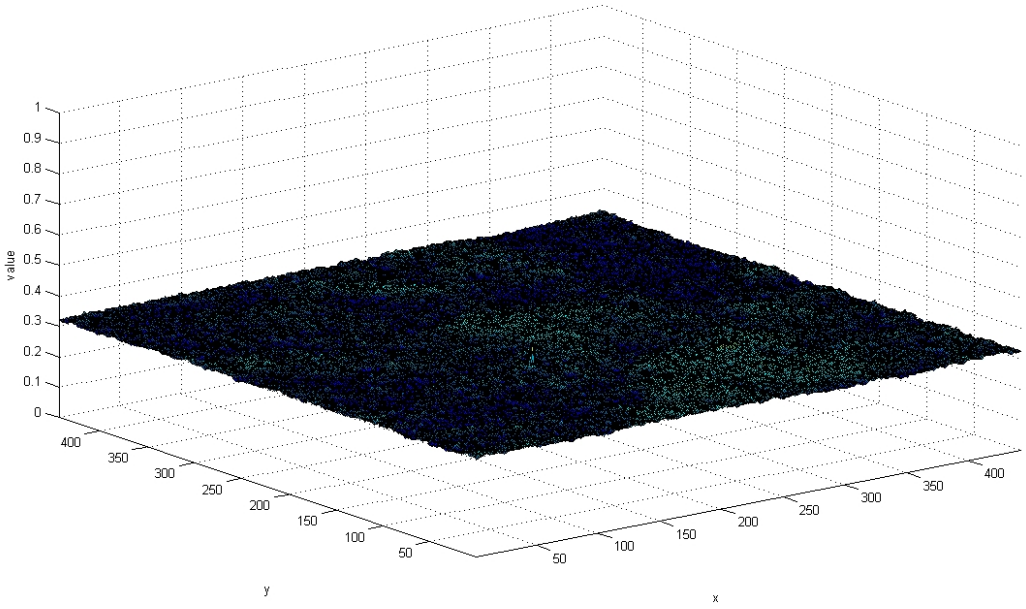

Figure 92: Paper type D surface after water-ink-BT-BT printing process has been applied.

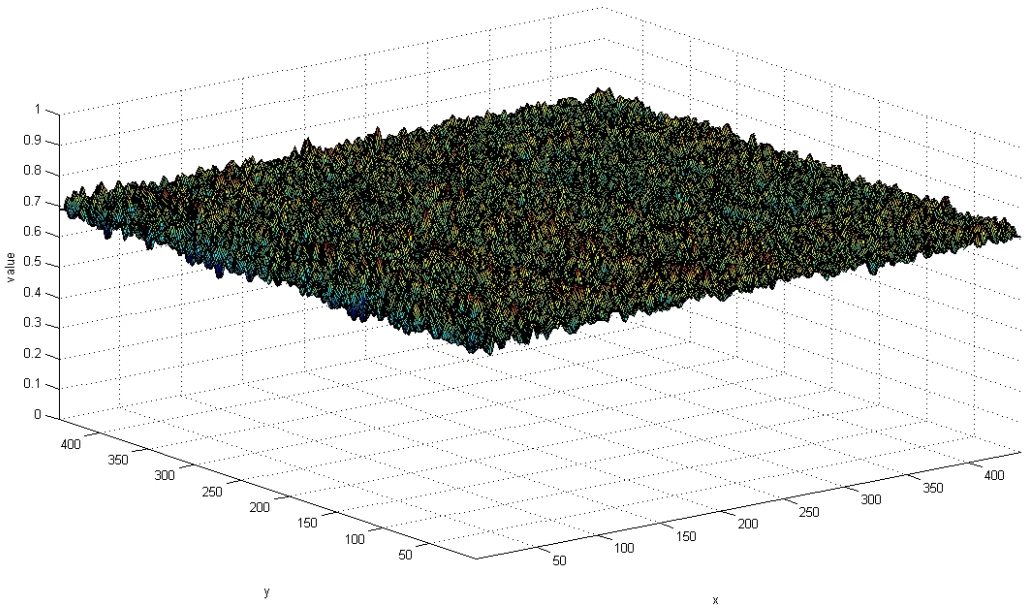

Figure 93: Spatial correlation for paper type D in the case when water-ink-BT-BT printing process has been applied.

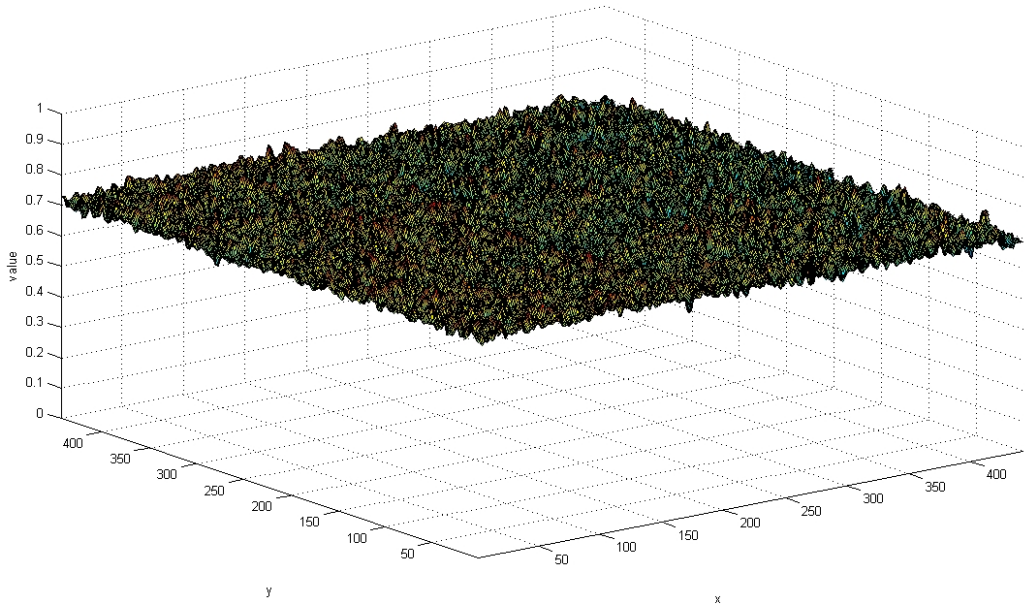

Figure 94: Spatial correlation for paper type D in the case when dry-ink-BT-BT printing process has been applied.

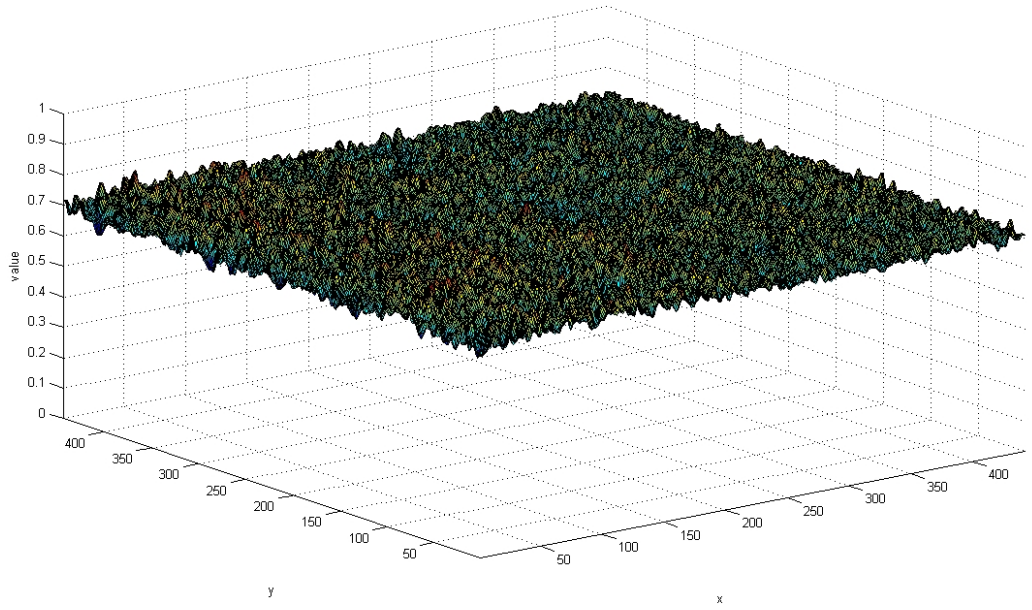

Figure 95: Spatial correlation for paper type D in the case when dry-ink-dry-dry printing process has been applied.

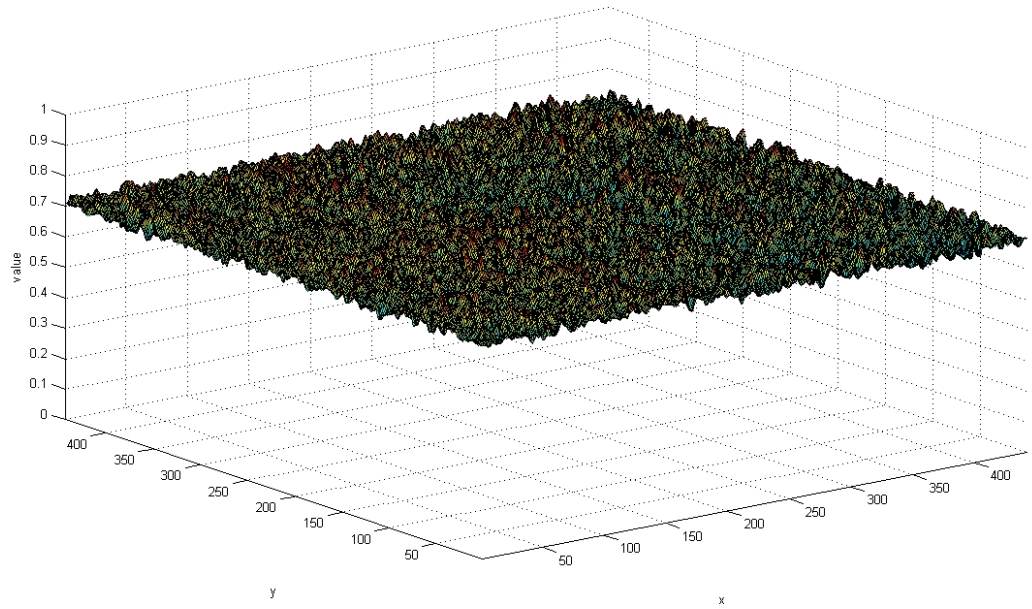

Figure 96: Spatial correlation for paper type D in the case when water-ink-dry-dry printing process has been applied.

- similarly like for paper type B, mottling type prediction based on mean value, variance or standard deviation is rather not possible. The standard deviations of spatial correlations for different types of mottling for paper type D are much more closer (almost identical) to each other than in the case of paper type B (the same conclusion applies for variances and mean values);

- none of considered types of mottling has better or worse spatial correlation to plain paper than other types of mottling.

Table 12: Spatial correlation summary for different kinds of mottling for paper type D.

Mottling kind	Mean	Variance	Standard deviation
water-ink-BT-BT	0.5152	0.0013	0.0359
dry-ink-BT-BT	0.5145	0.0013	0.0363
dry-ink-dry-dry	0.5128	0.0013	0.0363
water-ink-dry-dry	0.5145	0.0014	0.0368

Now we will investigate the mean differences between various wavelength planes for different types of mottling for paper type D under D65 illumination. Strictly speaking, for each pair of mottling type (corresponding spectral images are denoted by M_1 and M_2) we will perform the following procedure (the scheme must be repeated for each spectral reflectance plane of interest):

1. take a spectral reflectance plane for mottling M_1 and M_2 at wavelength λ denoted by $P_{M_1,\lambda}$ and $P_{M_2,\lambda}$, respectively.

2. calculate the difference spectral image $DI = |P_{M_1,\lambda} - P_{M_2,\lambda}|$;

3. calculate mean value $\overline{DI}$ of the difference spectral image DI, which is the mean difference between wavelength planes $P_{M_1,\lambda}$ and $P_{M_2,\lambda}$ for mottling types denoted by M_1 and M_2.

Figure 97 shows the above procedure applied for paper type D under D65 illumination for wavelength planes in the range between 400 nm and 580 nm with 5 nm sampling step. Each kind of mottling versus all other kinds of mottling was considered.

Based on the results shown in Figure 97 we can conclude that there exist some differences between mean differences of wavelength planes for various kinds of mottling. In particular we can see that:

1. there are big differences between D-I-BT-BT and D-I-D-D mottling kinds (cyan curve) especially in the range from 400 nm to 520 nm. In this case,

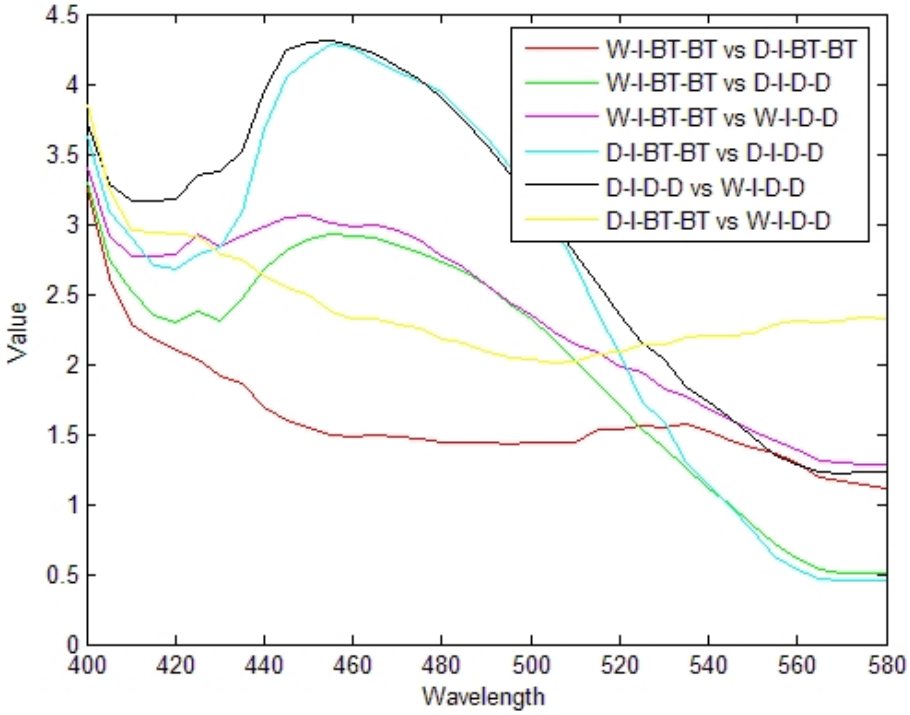

Figure 97: Mean difference analysis of various wavelength planes for different kinds of mottling for paper type D. Short cuts: D = dry, W = water, I = ink, BT = back-trap.

the wavelength range can be divided into two regions: the first from 400 nm to 520 nm with big differences, and the second from 520 nm to 580 nm with small differences. Similar observations can be made for D-I-D-D and W-I-D-D mottling pair (black curve);

2. similar observations (concerning the uneven distribution of differences between the region from 400 nm to 520 nm and the region from 520 nm to 580 nm) can be made for W-I-BT-BT and W-I-D-D mottling pair (magenta curve), and W-I-BT-BT and D-I-D-D mottling pair (green curve). However, for these mottling pairs the differences in the region from 400 nm to 520 nm are smaller in comparison to mottling pairs pointed out in point 1;

3. two remaining pairs of mottling, namely D-I-BT-BT and W-I-D-D pair (yellow curve), and D-I-D-D and W-I-D-D pair (black curve), have much more even distribution of the differences between planes than other pairs.

The aim for this study was to examine how much different types of mottling differ one from another when the mean differences between corresponding spectral reflectance planes of a mottling pair will be considered.

4.3 Measurements under UVA illumination

In Section 4.2 we introduced a procedure to compute the correlation between two reflectance spectra under D65 illumination, and we mentioned that the spectral reflectance vectors are 71 dimensional what corresponds to wavelengths from 400 nm to 780 nm with 5 nm step. In the case of measurements under UV illumination the setup for measurements under UV illuminant introduced in Section 2.5.2 was used. In particular, the values coming from the ImSpector V10 spectral camera were not corrected after the image acquiring phase, and these are actually the spectral radiance values in the range from 288 nm to 1181 nm with 0.7 nm sampling step.

To show 3D representations of the paper surface under UV illumination the radiance data were quantized into the region from 380 nm to 780 nm with 5 nm step. Then the same procedure as described in Section 3.2 was used to generate the 3D images, where the input values to the procedure were spectral radiance vectors instead of spectral reflectance vectors.

To show the RGB representations of the samples measured under UV illumination the radiance data were quantized into the region from 380 nm to 780 nm with 5 nm step. Then the quantized data were assumed to be the spectral reflectance data, and the X, Y, Z tristimulus values were calculated under the assumption of the CIE D65 standard illuminant and with the 1931 CIE Standard Observer. The RGB values were calculated on basis of the tristimulus values (see Section 2.1.4).

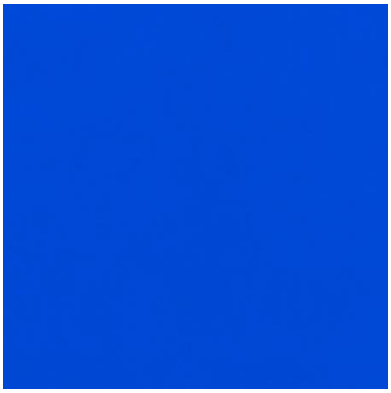

Figure 98: Blank paper type D under UVA illumination.

Figure 99: Printed paper type D under UVA illumination.

4.3.1 Papers under UV illumination

In this section we will investigate the surface of paper type D before and after printing process under UVA illumination.

Figure 98 shows paper type D before printing process, and Figure 99 the same paper area as in Figure 99 after the printing process has been applied, both under UV illuminant.

Figure 100 shows 3D representation of paper type D surface corresponding to Figure 98, and Figure 101 presents 3D representation of paper type D surface after printing process which corresponds to Figure 99.

Figures 102 - 107 show remaining kinds of paper under UV illumination. Due to low content of fluorescent and whitening agents in the paper surfaces the spectral radiance values under UV illumination are extremely small, and finally the RGB representations of the spectral radiance images are very dark. In particular, the selection of a particular region from the spectral radiance images becomes impossible, and thus further processing of these images is difficult.

4.3.2 Spectral variation of different kinds of mottling under D65 and UVA illuminants.

In this section we will examine average spectral reflectance of different kinds of mottling for different kinds of paper under D65 and UV illuminants. In particular, this study will show if we can distinguish between different kinds of mottling based on average spectral reflectance values. Next we will examine average spectra of different kinds of plain and printed papers under UVA illumination.

The average spectrum was calculated as mean value of spectral reflectance values (for measurements under D65 illumination) or spectral radiance values (for measurements under UV illumination) over a region of size 45 mm by 45 mm. In the case of measurements under D65 illumination the spectral reflectance values

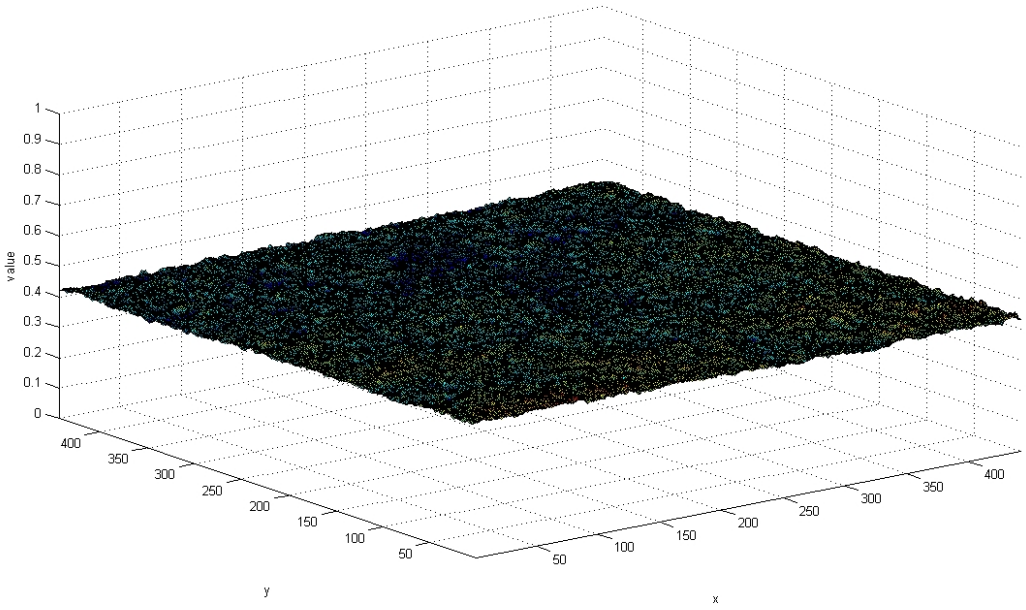

Figure 100: Paper type D surface before printing process. Water-ink- BT-BT printing process will be applied to the paper area.

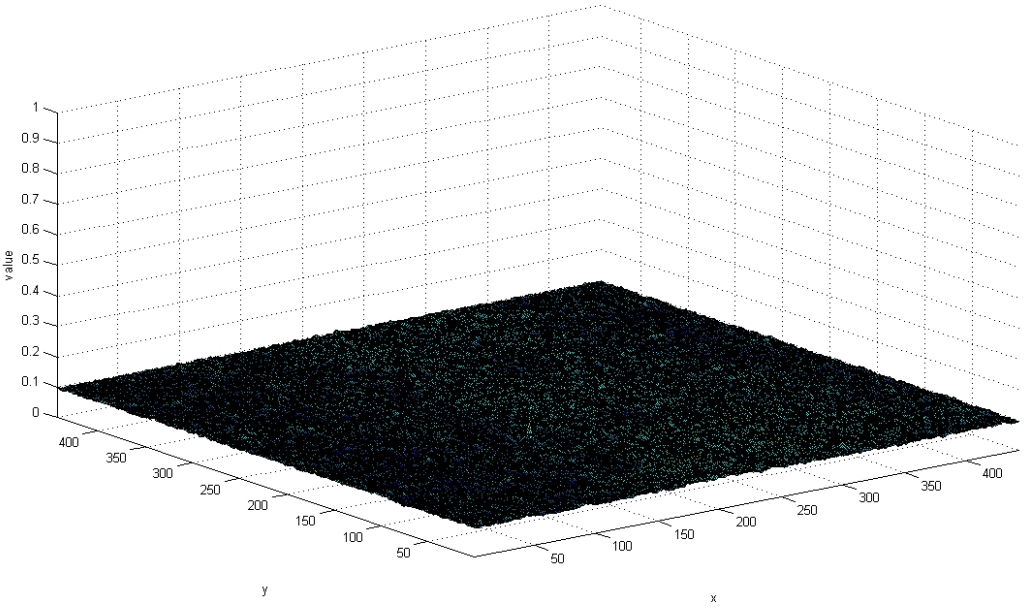

Figure 101: Paper type D surface after water-ink-BT-BT printing process has been applied.

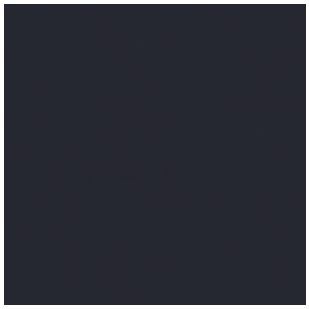

Figure 102: Blank paper type B under UVA illumination.

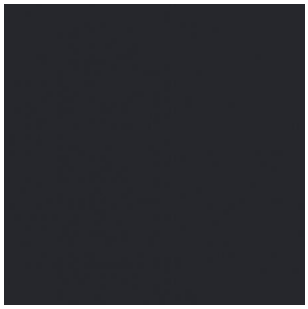

Figure 103: Printed paper type B under UVA illumination.

Figure 104: Blank paper type A under UVA illumination.

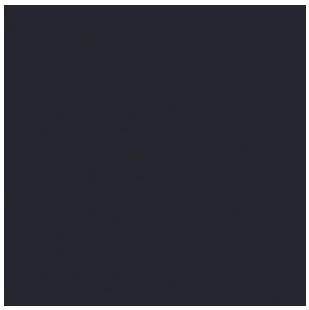

Figure 105: Printed paper type A under UVA illumination.

Figure 106: Blank paper type C under UVA illumination.

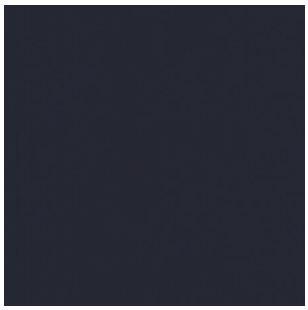

Figure 107: Printed paper type C under UVA illumination.

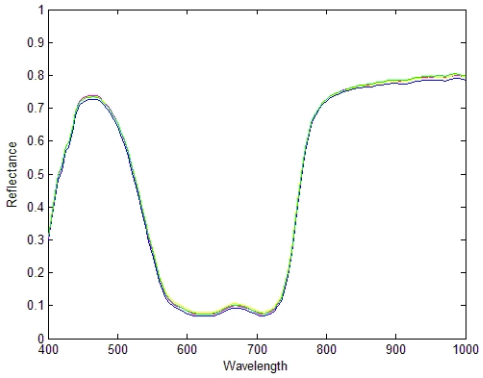

Figure 108: Average spectra of different kinds of mottling for paper type D under D65 illumination.

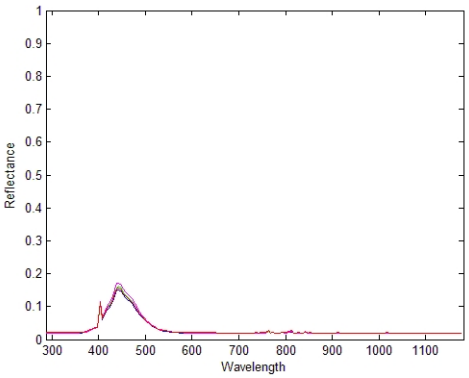

Figure 109: Average spectra of different kinds of mottling for paper type D under UVA illumination.

in the range from 400 nm to 1000 nm with 5 nm step were used. In the of measurements under UV illumination the spectral radiance values in the range from 288 nm to 1181 nm with 0.7 nm step were used [8]. All the spectral images were acquired with the ImSpector V10 spectral camera.

Figure 108 shows average spectra of different kinds of mottling (including water-ink-BT-BT, dry-ink-BT-BT, dry-ink-dry-dry and water-ink-dry-dry) for paper type D under D65 illumination.

Figure 109 shows average spectra of different kinds of mottling for paper type D under UV illumination.

Figure 110 presents average spectra of different kinds of plain papers under UV illumination, and Figure 111 shows average spectra of different kinds of printed paper under UV illumination.

Based on the results shown in Figures 108 - 111 we come to the following conclusions:

1. there is no difference in average reflectance spectra between various kinds of mottling (water-ink-BT-BT, dry-ink-BT-BT, dry-ink-dry-dry and water-ink-dry-dry) under D65 illumination. The type of mottling can not be recognized based on the average reflectance spectra.

2. there is no difference in average spectral radiance between various kinds of mottling (water-ink-BT-BT, dry-ink-BT-BT, dry-ink-dry-dry and water-ink-dry-dry) under UV illumination. The type of mottling can not be recognized based on the average spectral radiance;

[8] In the plots of spectral radiance values contained in the thesis the Y axis is named "Reflectance". In reality, these are spectral radiance values, i.e. spectral reflectance values where the influence of the ambient illumination was not removed.

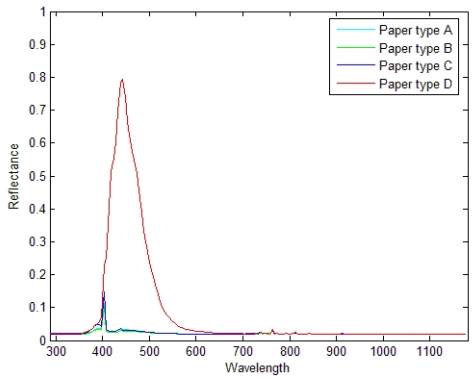

Figure 110: Average spectra of different kinds of plain paper under UVA illumination.

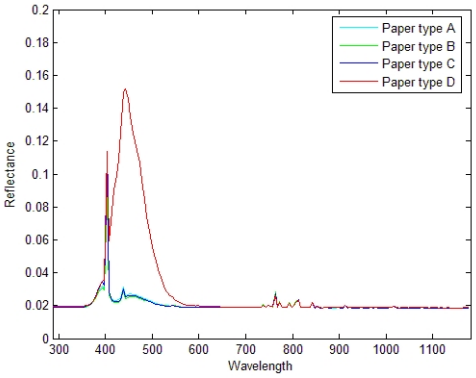

Figure 111: Average spectra of different kinds of printed paper under UVA illumination.

3. paper type D contains much more fluorescent and whitening agents than the other papers (gives much higher spectral radiance responses than other kinds of paper). It is the only paper which can be easily post-processed when measured under UV illumination (the RGB representation of the images are not black or very dark).

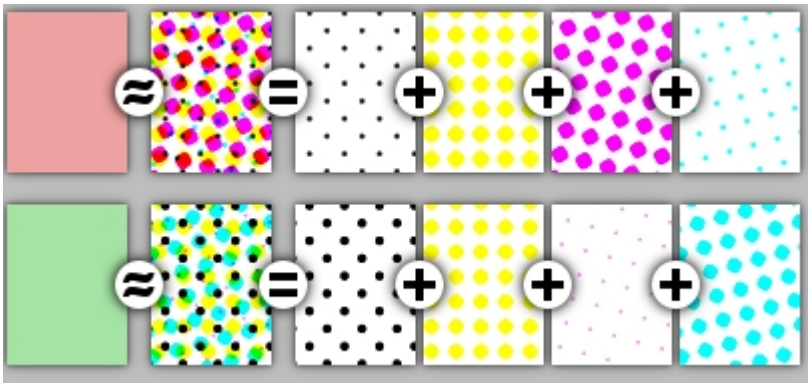

Figure 112: Examples of inverse color separation process (Image taken from [30]).

5 Printing dot separation

In this chapter we will examine whether the inverse color separation process of multicolor printing inks is possible based on spectral reflectance data, i.e. given a spectral reflectance data of a printing dot image we will try to separate it into four RGB images, where each of them corresponds to one of the printing inks used and contains only printed dots of the same color[9]. In particular, this study will show whether concentration prediction (what printing inks and in what densities were used to create a particular region) of printing inks is possible based on spectral reflectance data. We will also investigate if it is possible to determine missing or partially missing printed dots in dot overlapping areas based on spectral reflectance.

Figure 112 shows examples of inverse color separation process. From left to right: the printed image when view by the human eye from a sufficient distance, the halftone dot pattern at high magnification, the cyan separation, the magenta separation, the yellow separation and the black separation (these separations are the four RGB images which are the output of the inverse color separation process).

5.1 Concentration prediction of overprinted inks

In this section we will study whether the concentration prediction process (what printing inks and in what densities) of printing inks is possible based on spectral reflectance data. Firstly, we will discuss some problems related to the concentration prediction, and then we will use the Kubelka-Munk theory to predict ink concentrations in dot overlapping areas.

The ImSpector V8 spectral camera was used to acquire spectral images of

[9]In this thesis the inverse color separation process will be also called color separation process if it does not cause any misunderstandings.

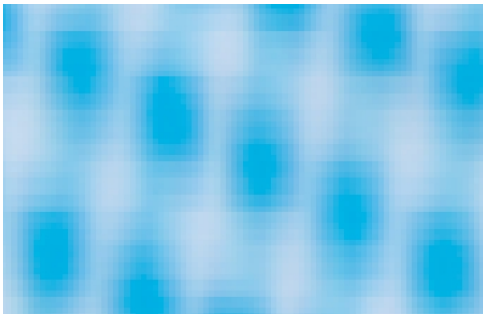

Figure 113: Cyan printing dots at 30% density.

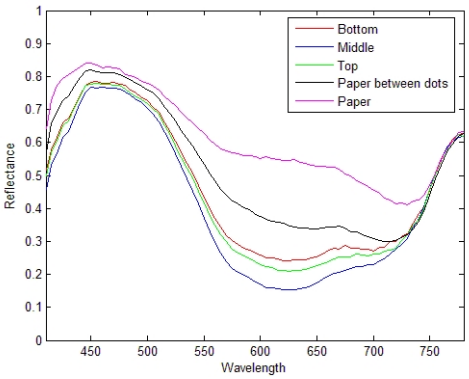

Figure 114: Average paper and dot spectral reflectance variations.

printing dots. The description of its setup and the justification for using the spectral camera for printing dot measurements were given in Section 2.5.2.

5.1.1 Printing dot spectrum

In Section 3.6 we introduced the dot gain phenomena, and we explained that the dot color (amount of ink applied to the substrate) is spread out very unevenly throughout the dot area. Figures 79 and 80 suggest that the highest amount of ink (print density) is located in the middle part of the dot with decreasing tendency towards the outer boundary of the dot. Now we will show how these color (spectral reflectance) variations affect ink concentration prediction and color separation processes.

Figure 113 shows a cyan printing ink at 30% density. We can see by naked eye that the highest amount of cyan ink is located in the middle part of the dots, and it decreases continuously to the edges of the dots. Let us also notice that there exist significant variations of paper reflectance. Especially spaces between dots in horizontal direction are more whitish in comparison to spaces in vertical direction (which are more bluish).

Figure 114 shows several example spectra of paper and dots taken from Figure 113. Magenta and black curves correspond to spectral reflectances of paper, and red, blue and green curves correspond to spectra in different locations of a single printing dot. In particular, these spectral variations can cause some problems related to ink concentration prediction of overprinted areas and color separation including:

- where the spectrum of a dot at particular density should be taken from? (possibly it can be the average spectrum taken throughout the whole dot area);

- where the paper spectrum should be taken from? (both whitish and bluish regions between printing dots shown in Figure 113 should be predicted as paper in color separation process. Possibly the best choice is the average spectrum of the whitish and bluish regions of paper surface);

- concentration prediction will give various values for different pixels belonging to a printing dot due to significant spectral variations of color within the dot area;

- inability to distinguish between paper surface and dot areas due to spectral variations of paper located between dots (whitish and bluish regions), and the closeness of paper spectral reflectance (in bluish areas) to spectral reflectance of inks at low densities or outer areas of dots. As the result, the paper surface will be considered as a dot area, or the outer regions of dots will be considered as paper surface, what finally will lead to wrong color separation.

Now we will investigate how the selection of spectral reflectance for paper surface influences the ability to recognize paper and dot areas. Algorithm 1 is a simple sketch of a procedure which we will help us to evaluate the color separation of cyan dots at different densities from the paper areas.

Algorithm 1 considers each spatial location (i, j) of spectral image SI. Based on the comparison of the spectral reflectance $r_{i,j}$ of spatial location (i, j) with a fixed set of spectra R, it decides whether the spatial location (i, j) should be classified as a paper area or dot area. The result of the algorithm is a black-white image I, where white areas denote paper (regions of spectral image SI which were classified as paper areas) and black parts denote dot areas (regions of spectral image SI which were classified as dot areas).

For clarity, the fixed set of spectra R consists of the spectral reflectance R_S of paper surface and cyan dot spectra at different densities, where C_{dens} denotes average cyan dot spectrum at density *dens*. The classification of each spatial location as paper or dot area is based on the Root Mean Square Error (abbreviated as RMSE) computed as follows:

$$RMSE(r_1, r_2) = \sqrt{\frac{\sum_{i=1}^{N}(r_1(i) - r_2(i))^2}{N}} \tag{29}$$

, where r_1 and r_2 are two reflectance spectra which are to be compared, and N is the dimensionality of a spectrum.

For each spatial location (i, j) the algorithm chooses spectrum *bestSpectrum* which fits the best spectrum $r_{i,j}$ according to RMSE error (*bestSpectrum* minimizes the RMSE error for spectrum $r_{i,j}$).

For simplicity, the fixed set R of spectral reflectances in Algorithm 1 includes only paper spectral reflectance and cyan dot spectral reflectances at different densities. In general case, however, we assume that the set R contains also magenta,

Alg. 1 Simple recognition of spectral reflectances.

Input: SI, $R = \{R_S, R_{C_{10}}, R_{C_{20}}, ..., R_{C_{100}}\}$.
Output: Black-white image I.

```
1   begin
2       for each spatial location (i, j) in image SI
3           error = ∞;
4           r_{i,j} = SI(i, j);
5           bestSpectrum = R_S;
6           for all reflectance spectra r ∈ R
7               temp = RMSE(r, r_{i,j});
8               if (temp ≤ error) then
9                   error = temp;
10                  bestSpectrum = r;
11          if (bestSpectrum == R_S) then I(i, j) = 1;
12          else I(i, j) = 0;
13  end
```

yellow and black dot spectral reflectances at different densities. Algorithm 2 is a sketch of a procedure which employs extended set R. Variables I_C, I_M, I_Y and I_K are black-white images for cyan, magenta, yellow and black dots respectively, which are assumed to be white when the algorithm starts.

Alg. 2 Simple recognition of spectral reflectances with extended set R.

Input: SI, R.
Output: Black-white images I_C, I_M, I_Y, I_K.

```
1   begin
2       for each spatial location (i, j) in image SI
3           r_{i,j} = SI(i, j);
4           find r ∈ R such that RMSE(r, r_{i,j}) is minimal
5           if (r == reflectanceOfCyanInk) then I_C(i, j) = 0;
6           elseif (r == reflectanceOfMagentaInk) then I_M(i, j) = 0;
7           elseif (r == reflectanceOfYellowInk) then I_Y(i, j) = 0;
8           else (r == reflectanceOfBlackInk) then I_K(i, j) = 0;
9   end
```

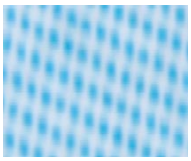

Figure 115: Cyan dots at 20% density.

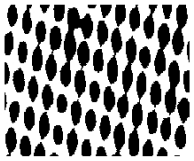

Figure 116: Separation result for whitish spectrum.

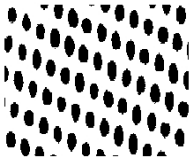

Figure 117: Separation result for cyanic spectrum.

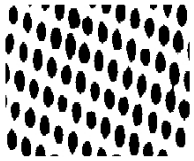

Figure 118: Separation result for cyanic-whitish spectrum.

The result of Algorithm 2 are four black-white images I_C, I_M, I_Y and I_K. For each image I_{ink} (where ink denote a color of a printing ink) the following conditions are satisfied:

1. white areas correspond to spatial locations of spectral image SI which were classified as paper or areas coved by an ink which is different from ink;
2. black areas which correspond to spatial locations of spectral image SI which were classified as coved by ink ink.

It is easy to notice that Algorithm 2 does not work for dot overlapping areas (appropriate algorithm will be presented later).

Now we will employ Algorithm 2 to perform a simple color separation. For a given spectral image three different spectra will be considered as paper spectral reflectances:

- whitish spectrum - average spectrum was taken form a white-looking region which should be considered as paper area in the separation process;
- cyanic spectrum - average spectrum was taken form a cyan-looking region which should be considered as paper area in the separation process;
- cyanic-whitish spectrum - average spectrum was taken simultaneously form a white-looking and cyan-looking regions which should be considered as paper area in the separation process.

In particular, this experiment will show how the choice of paper reflectance spectrum influences the color separation process. We will also discuss some limitations which can be imposed on the set R to improve the separation results.

Figure 115 shows cyan dot image at 20% density. We will try to separate the cyan dots from the paper areas using Algorithm 2 with three different spectra as paper reflectances. The reflectance spectra of printing dots at different densities are the average spectra taken throughout the dot areas.

Figures 116 - 118 show the separation results for cyan dots at 20% density, where different spectra were considered as paper spectrum. In all three cases we can distinguish the shape of the dots and:

- separation result with whitish spectrum produces dots which are joined together (interconnections between dots in vertical direction). Dots seem to be bigger than their actual sizes are;
- separation result with cyanic spectrum produces dots which are not joined together. Dots are smaller than their actual sizes are;
- separation result with cyanic-whitish spectrum produces dots which are not joined together. Printing dots are about right sizes and the separation process seems to be correct.

Figure 119 shows cyan dot image at 40% density. We will try to separate the cyan dots from the paper areas using Algorithm 2 with three different spectra as paper reflectances. Figures 120 - 122 show the separation results for cyan dots at 40% density, where different spectra were considered as paper spectrum. Based on the results we make the following observations:

- the separation process with whitish and cyanic spectra as paper spectrum produces images with dots which are joined together. Interconnections between dots in all directions give unacceptable separation. Dots are much bigger than their actual sizes are and we can not clearly distinguish the shapes and locations of printing dots;
- the separation process with cyanic-whitish spectrum produces dots which are joined together. Interconnections between dots exist mainly in horizontal direction and do not exclude the possibility to distinguish the shapes and ranges of dots. Printing dots are about their right sizes.

Figures 123 - 134 present RGB representations of spectral images of cyan printing dots at different densities.

Based on Figures 123 - 134 we come to the following conclusions:

- Figures 123 - 127 should be a good subject for color separation process due to low distortion of paper spectral reflectance (there are no paper regions with intensive cyan color which should be considered as paper in the color separation process);
- Figure 128 can be also a subject for color separation process if the paper reflectance is chosen carefully. Due to high degree of distortion of paper spectral reflectance (cyanic interconnections between dots mainly in vertical direction) the separation process can result in unacceptable output if the paper reflectance is not selected correctly;

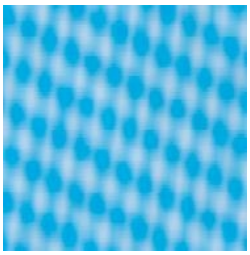

Figure 119: Cyan dots at 40% density.

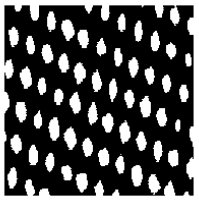

Figure 120: Separation result for whitish spectrum.

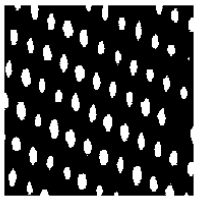

Figure 121: Separation result for cyanic spectrum.

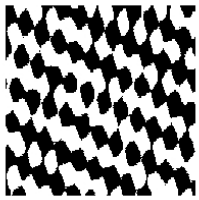

Figure 122: Separation result for whitish-cyanic spectrum.

Figure 123: Cyan dots at 2%.

Figure 124: Cyan dots at 5%.

Figure 125: Cyan dots at 10%.

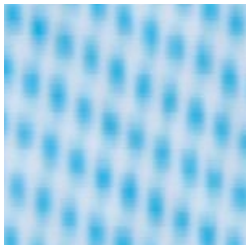

Figure 126: Cyan dots at 20%.

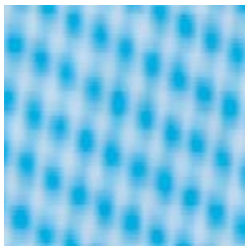

Figure 127: Cyan dots at 30%.

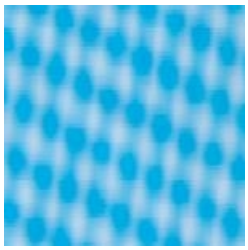

Figure 128: Cyan dots at 40%.

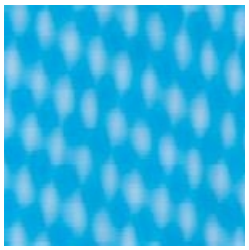

Figure 129: Cyan dots at 50%.

Figure 130: Cyan dots at 60%.

Figure 131: Cyan dots at 70%.

Figure 132: Cyan dots at 80%.

Figure 133: Cyan dots at 90%.

Figure 134: Cyan dots at 100%.

- color separation for printing dots shown in Figures 129 - 134 is not possible due to high distortion of paper reflectance.

Let us now to sum up the main conclusions derived from examples and results presented in this section:

1. the color separation process is significantly influenced by the selection of current paper reflectance spectrum and spectra of printing dots at different densities;

2. inappropriate selections of paper reflectance spectrum or printing dot spectra can cause additional interconnections between printing dots resulting in distortion of their shapes and real sizes in the final outcome (inability to distinguish between paper surface and dot areas);

3. with the increase of dot density, the difficulty with appropriate selection of paper reflectance increases (for example with the increase of cyan dot density the distortion of plain paper areas by cyan color increases and makes it harder to appropriately select paper reflectance);

4. the ability for correct color separation decreases when the dot density increases (more areas with spectral reflectance distortion occur);

5. distinction between paper area and dot at very low densities or outer regions of printing dots at low densities can be impossible or difficult to carry out;

6. what is the best reflectance spectrum of a printing dot at particular density? (possibly the average spectra of the whole dot area);

7. how to make the best selection of paper reflectance spectrum? (how to find the best area for spectrum selection automatically?).

5.1.2 Kubelka-Munk theory and concentration prediction

The Kubelka-Munk (KM) theory has been mainly used to predict the reflectance of translucent colorants. However, it can also model transparent and opaque colorants as special cases. In particular, the Kubelka-Munk theory has been used to predict the reflectance of textiles, plastics, paints, inks and other materials [12]. The KM theory has been also used for prediction of reflectance of printing inks. However, one of the difficulties in applying the theory for printer characterization is in determining the scattering and absorption coefficients for each printing ink used (two-constant Kubelka-Munk theory). [13] suggests some methods to determine the coefficients, but unfortunately the methods can not be applied in our case. Therefore, we will employ a variation of the KM theory called single-constant Kubelka-Munk theory in which only ratios of absorption by scattering coefficients for each colorant are known.

Originally, Kubelka and Munk considered a translucent colorant layer on top of an opaque background. Within the colorant layer both scattering and absorption occur. They also assumed that the light flux travels either up or down, and the light inside the colorant layer is completely diffuse. Therefore, the reflected light from the surface of the material depends on the scattering and absorption coefficients of the colored materials, the background reflectance, and the thickness of the colorant layer [15][12].

For opaque color materials (the colorant layer is sufficiently thick that the reflectance of background has no effect on the colorant layer reflectance), the theory transforms the spectral reflectance factor R_λ into an approximately linear space defined as $(K/S)_\lambda$, where K denotes the absorption and S the scattering coefficients respectively [14]. Equations (30) and (31) give the relationships between R_λ and $(K/S)_\lambda$:

$$(K/S)_\lambda = (1 - R_\lambda)^2/2R_\lambda \tag{30}$$

$$R_\lambda = 1 + (K/S)_\lambda - \sqrt{(K/S)_\lambda^2 + 2(K/S)_\lambda} \tag{31}$$

In order to predict the reflectance R_λ for a mixture of colorants with spectral reflectances $R_1, ..., R_k$ and effective concentrations $c_1, ..., c_k$ we perform the following steps [12]:

1. compute $(K/S)_{\lambda,i}$ for each colorant according to Equation (30), where i denotes the i-th colorant;

2. compute the spectral reflectance of unit concentration $(k/s)_{\lambda,i}$ for each colorant based on already computed $(K/S)_{\lambda,i}$;

3. compute $(K/S)_\lambda$ for the mixture (denoted by $(K/S)_{\lambda,mix}$) according to the following equation:

$$(K/S)_{\lambda,mix} = c_1(k/s)_{\lambda,1} + c_2(k/s)_{\lambda,2} + ... + c_k(k/s)_{\lambda,k}; \tag{32}$$

4. compute spectral reflectance R_λ of the mixture according to Equation (31).

Let us notice that in order to predict the reflectance of a mixture of colorants, the $(k/s)_\lambda$ coefficients are determined for each mixture component. Then under the assumption of linearity of the $(k/s)_\lambda$ coefficients, the value $(K/S)_\lambda$ for the mixture is computed. The last step is to transform the $(K/S)_\lambda$ value for the mixture to its spectral reflectance using Equation (31).

In our algorithms for concentration prediction we will use the single-constant Kubelka-Munk theory for opaque materials. The use of the double-constant Kubelka-Munk theory and other versions of single-constant Kubelka-Munk theory can not be applied in our case.

Based on the Kubelka-Munk theory we will now introduce an algorithm for concentration prediction of overprinted areas where two inks were used. Algorithm 3 depicts the procedure, where R is a spectral reflectance of an overprinted area for which colorants are to be found, and X and Y are two lists of reflectance spectra such that:

1. the list X corresponds to spectra of one ink denoted by ink_1 and the set Y corresponds to spectra of another ink denoted by ink_2, where $ink_1 \neq ink_2$;
2. the list X contains spectra of different printing dot densities of ink ink_1;
3. the list Y contains spectra of different printing dot densities of ink ink_2.

Alg. 3 Two-ink concentration prediction of overprinted areas.

Input: R, $X = \{X_1, ..., X_k\}$, $Y = \{Y_1, ..., Y_l\}$.
Output: $error$, $index_X$, $index_Y$.

```
1   begin
2       error = 1; index_X = −1; index_Y = −1;
3       for each spectrum X_i in set X
4           for each spectrum Y_j in set Y
5               ks_X = KS(X_i);
6               ks_Y = KS(Y_j);
7               ks_mix = ks_X + ks_Y;
8               R_mix = R(ks_mix);
9               temp = RMSE(R_mix, R);
10              if temp ≤ error then
11                  error = temp;
12                  index_X = i;
13                  index_Y = j;
14      return [error, index_X, index_Y]
15  end
```

The algorithm uses the Kubelka-Munk theory to find two spectra which after mixing fit the best the initial spectrum R according to root mean square error. It must be noted here that the found spectra are from different lists (X and Y), and the algorithm returns the following values: $error$ - the RMSE error of the two found spectra and the initial spectrum R, $index_X$ - index of the chosen spectrum from list X, and $index_Y$ - index of the chosen spectrum from list Y.

The algorithm implicitly computes three functions: $RMSE()$ - computes root mean square error between two spectra, $KS()$ - computes (K/S) coefficient for a given spectrum (see Equation (30)), and $R()$ - computes spectral reflectance for a given (K/S) coefficient (see Equation (31)).

In the case of the four-color printing process Algorithm 3 must be executed for each pair of printing inks, i.e. $\mathrm{C}_4^2 = \binom{4}{2} = 6$ times to find two spectra which after mixing fit the best the initial spectrum R. The procedure is depicted in the form of Algorithm 4. The input to the algorithm are: R - spectrum for which colorants are to be found, C - set of cyan dot spectra at different densities, M - set of magenta dot spectra at different densities, Y - set of yellow dot spectra at different densities and K - set of black dot spectra at different densities.

Alg. 4 Full two-ink concentration prediction of overprinted areas.

Input: R, C, M, Y, K.
Output: $error$, $index_X$, $index_Y$, $index_{PAIR}$.

```
1    begin
2        CM = KM2(C, M); index_PAIR = 1
3        CY = KM2(C, Y); index_PAIR = 2
4        CK = KM2(C, K); index_PAIR = 3
5        MY = KM2(M, Y); index_PAIR = 4
6        MK = KM2(M, K); index_PAIR = 5
7        YK = KM2(Y, K); index_PAIR = 6
8        S = solution with minimum error among {CM, CY, CK, MY, MK, YK};
9        return [S, index_PAIR]
10   end
```

The algorithm considers all pairs of printing inks and for each ink pair it examines all possible combinations of spectra corresponding to different densities. $KM2$ denotes the procedure depicted by Algorithm 3. The best pair of inks is denoted by $index_{PAIR}$ and their corresponding concentrations and their error are stored in S. Thus, the algorithm returns two spectra of two different inks at particular densities which after mixing process fit the best spectrum R.

Algorithm 5 is a straightforward extension of Algorithm 3 for three-ink concentration prediction of overprinted areas. R is a spectral reflectance of an overprinted area for which colorants are to be found. X, Y and Z are three lists of printing dot spectra at different densities such that:

1. the list X corresponds to spectra of one ink denoted by ink_1, the list Y corresponds to spectra of the second ink denoted by ink_2 and the set Z

corresponds to spectra of the third ink denoted by ink_3, where $ink_1 \neq ink_2 \neq ink_3$;

2. the list X contains spectra of different printing dot densities of ink ink_1;
3. the list Y contains spectra of different printing dot densities of ink ink_2;
4. the list Z contains spectra of different printing dot densities of ink ink_3.

Alg. 5 Three-ink concentration prediction of overprinted areas.

Input: R, $X = \{X_1, ..., X_l\}$, $Y = \{Y_1, ..., Y_m\}$, $Z = \{Z_1, ..., Z_n\}$.
Output: $error$, $index_X$, $index_Y$, $index_Z$.

```
1   begin
2       error = 1; index_X = −1; index_Y = −1; index_Z = −1;
3       for each spectrum X_i in set X
4           for each spectrum Y_j in set Y
5               for each spectrum Z_k in set Z
6                   ks_X = KS(X_i);
7                   ks_Y = KS(Y_j);
8                   ks_Z = KS(Z_k);
9                   ks_mix = ks_X + ks_Y + ks_Z;
10                  R_mix = R(ks_mix);
11                  temp = RMSE(R_mix, R);
12                  if temp ≤ error then
13                      error = temp;
14                      index_X = i;
15                      index_Y = j;
16                      index_Z = k;
17      return [error, index_X, index_Y, index_Z]
18  end
```

The algorithm looks for three spectra which after mixing fit the best the initial spectrum R according to root mean square error. It must be noted here that the found spectra are taken from different lists, i.e. they correspond to different printing inks at particular densities.

In the case of the four-color printing process then Algorithm 5 must be executed for each triple of printing inks, i.e. $C_4^3 = \binom{4}{3} = 4$ times to find tree spectra which after mixing fit the best the initial spectrum. The overall procedure is depicted

Alg. 6 Full three-ink concentration prediction of overprinted areas.

Input: R, C, M, Y, K.
Output: $error$, $index_X$, $index_Y$, $index_Z$, $index_{TRIPLE}$.

```
1    begin
2        CMY = KM3(C, M, Y); index_TRIPLE = 1
3        CMK = KM3(C, M, K); index_TRIPLE = 2
4        MYK = KM3(M, Y, K); index_TRIPLE = 3
5        CYK = KM3(C, Y, K); index_TRIPLE = 4
6        S = solution with minimum error among {CMY, CMK, MYK, CYK};
7        return [S, index_TRIPLE]
8    end
```

in the form of Algorithm 6. The input to the algorithm is exactly the same as for Algorithm 4.

Algorithm 6 assumes that spectrum R is a mixture of three inks and searches all triples of inks and for each ink triple it examines all spectra corresponding to various dot densities to find out what the best colors of the inks and their densities are. The algorithm returns three spectra of three different inks at particular densities which after mixing process fit the best spectrum R. $KM3$ denotes the procedure depicted by Algorithm 5. The best triple of inks is denoted by $index_{TRIPLE}$, and their corresponding concentrations and their error are stored in S.

Algorithm 7 is a straightforward extension of previous algorithms presented in this section to four-ink concentration prediction of overprinted areas. R is a spectral reflectance of an overprinted area for which colorants are to be found. X, Y, Z and W are four lists of spectra which definitions are similar to these introduced earlier.

The algorithm considers the only quartette of printing inks (in the case of the four-color printing process), and for each printing ink it examines all possible spectra corresponding to its different dot densities. The Algorithm assumes that spectrum R is a mixture of four inks and for each ink it searches all spectra at various densities to find out what the best density for the ink is. The algorithm returns one spectrum for each printing ink which corresponds to a particular density of the ink. After mixing, the selected spectra give a spectrum which fits the best spectrum R.

Let us now to combine Algorithms 4, 6, and 7 into one algorithm which predicts number of inks, their colors and concentrations which were probably used to create a particular spectrum. Algorithm 8 depicts the procedure.

The input values to the algorithm are: R - spectral reflectance of an overprinted area for which colorants are to be found, C - spectral reflectances of cyan ink at

Alg. 7 Full four-ink concentration prediction of overprinted areas.

Input: R, X, Y, Z, W.
Output: $error$, $index_X$, $index_Y$, $index_Z$, $index_W$.

```
1   begin
2       error = 1; index_X = −1; index_Y = −1; index_Z = −1;
3       for each spectrum X_i in set X
4           for each spectrum Y_j in set Y
5               for each spectrum Z_k in set Z
6                   for each spectrum W_l in set W
7                       ks_X = KS(X_i);
8                       ks_Y = KS(Y_j);
9                       ks_Z = KS(Z_k);
10                      ks_W = KS(W_l);
11                      ks_mix = ks_X + ks_Y + ks_Z + ks_W;
12                      R_mix = R(ks_mix);
13                      temp = RMSE(R_mix, R);
14                      if temp ≤ error then
15                          error = temp;
16                          index_X = i;
17                          index_Y = j;
18                          index_Z = k;
19                          index_W = l;
20      return [error, index_X, index_Y, index_Z, index_W]
21  end
```

different dot densities, M - spectral reflectances of magenta ink at different dot densities, Y - spectral reflectances of yellow ink at different dot densities, and K - spectral reflectances of black ink at different dot densities. The output values of the algorithms are: $numberOfInks$ - number of inks probably used to create the overprinted area, and S which gives information about the color of the inks and their densities. $KM2_{FULL}$ denotes Algorithm 4, $KM3_{FULL}$ refers to Algorithm 6 and $KM4_{FULL}$ corresponds to Algorithm 7.

Algorithm 8 starts to search the best colorant selection within two-ink combinations. The best found solution is stored in $KM2_R$, and then it starts to look for the best colorants within three-ink combinations. The best solution is saved in $KM3_R$, and next it examines the best density combinations for all printing inks which possibly were used to create the overprinted area. The result is stored in $KM4_R$, and the algorithm chooses the best solution among $KM2_R$, $KM3_R$ and

Alg. 8 Concentration prediction of overprinted areas.

Input: R, C, M, Y, K.
Output: S, $numberOfInks$.

```
1    begin
2        KM2_R = KM2_FULL(C, M, Y, K);
3        KM3_R = KM3_FULL(C, M, Y, K);
4        KM4_R = KM4_FULL(C, M, Y, K);
5        S = solution with minimum error among {KM2_R, KM3_R, KM4_R};
6        numberOfInks =number of selected inks;
7        return [S, numberOfInks]
8    end
```

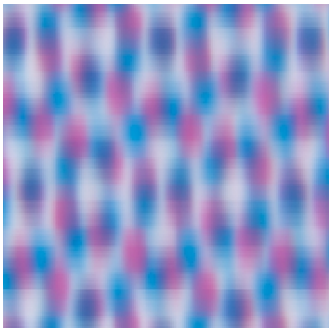

Figure 135: Cyan and magenta dots at 30% density.

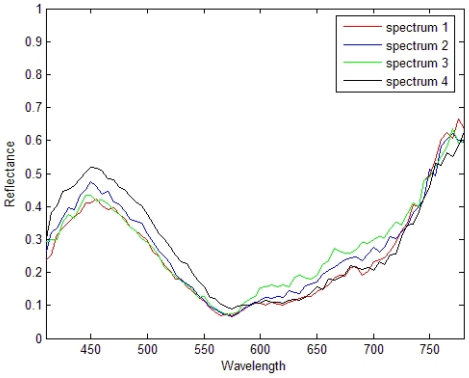

Figure 136: Spectral variations in dot overlapping regions.

$KM4_R$ based on the root mean square error values. The optimal combination of inks which yields the minimum error is returned as the output of the algorithm.

Now we will apply Algorithm 8 for concentration prediction of a couple of example spectra. Figure 135 shows cyan and magenta dots at 30% density, and Figure 136 depicts some spectral reflectance curves of some overprinted areas of magenta and cyan inks. In particular, let us notice that spectral reflectance curves vary a lot even though, they were taken from overprinted areas of cyan and magenta inks at 30% density. Clearly, it has a very close connection with the issues described in Section 5.1.1 concerning uneven distribution of color (spectral reflectance) within printing dots. In particular, uneven distribution of color within printing dot area can be caused by uneven structure of the substrate and non-uniform distribution of whitening agents in the paper surface.

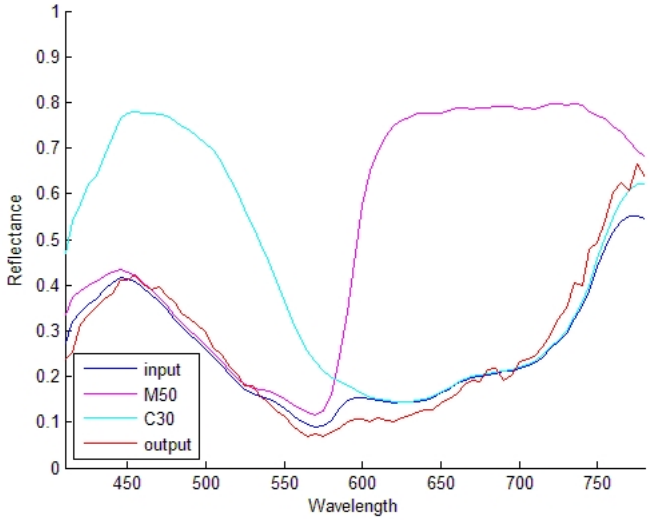

Figure 137: Concentration prediction example for a spectrum (blue curve) taken from an overlapping area where magenta and cyan at 30% density were applied. Results: magenta at 50% density (spectrum denoted by magenta curve), cyan at 30% density (spectrum denoted by cyan curve), RMSE = 0.0392, and the predicted reflectance of the mixture denoted by red line.

Figure 137 shows an output of an application performing concentration prediction. The figure presents the result of the application when applied for spectral reflectance curve denoted by *spectrum* 1 in Figure 136. The input spectrum is shown by blue curve, and the result of the application are magenta at 50% density and cyan at 30% density denoted by magenta and cyan curves respectively. The reflectance of the mixture of magenta at 50% density and cyan at 30% predicted based on the Kubelka-Munk theory is shown by red line.

Table 13 contains results of employing Algorithm 8 for spectra shown in Figure 136. Even though, these example spectra were taken from overprinted regions of magenta and cyan inks at 30% density the predicted concentrations vary a lot. It must be also noticed that the spectral variations in dot overlapping regions did not result in bad colorant predictions, i.e. for all example spectra cyan and magenta inks were predicted.

Figure 138 shows cyan and yellow dots at 30% density, and Figure 136 depicts some spectral reflectance curves of some overprinted areas of yellow and cyan inks. Let us notice that the spectral reflectance curves vary a lot even though, they were taken from overprinted areas of cyan and yellow inks at 30% density. We will now apply Algorithm 8 to see what inks and what densities possibly were used to create the spectra.

Table 14 contains results of employing Algorithm 8 for spectra shown in Figure 139. Even though, these example spectra were taken from overprinted regions of

Table 13: Influence of spectral variations in dot overlapping regions on concentration prediction for cyan and magenta inks at 30% density.

Sample	Magenta conc.	Cyan conc.	RMSE
spectrum 1	50%	30%	0.0392
spectrum 2	40%	30%	0.0353
spectrum 3	50%	20%	0.0321
spectrum 4	30%	30%	0.0285

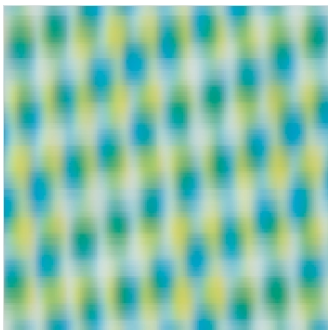

Figure 138: Cyan and yellow dots at 30% density.

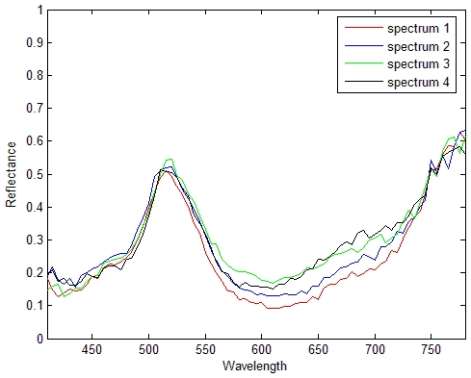

Figure 139: Spectral variations in dot overlapping regions.

yellow and cyan inks at 30% density the predicted concentrations vary. In the table, there is no result for *spectrum* 4, because the application did not predict right ink colors for this spectrum.

Table 14: Influence of spectral variations in dot overlapping regions on concentration prediction for cyan and yellow inks at 30% density.

Sample	Yellow conc.	Cyan conc.	RMSE
spectrum 1	40%	30%	0.0457
spectrum 2	30%	30%	0.0364
spectrum 3	40%	20%	0.0421
spectrum 4	-	-	-

Figure 140 shows the output of the prediction process for *spectrum* 4. The input spectrum is denoted by blue curve, and the algorithm resulted in the following output: cyan at 20%, magenta at 10% and yellow at 30% densities shown by cyan, magenta and yellow curves respectively. The mixture of cyan at 20%, magenta at 10% and yellow at 30% densities predicted by Kubelka-Munk theory is shown

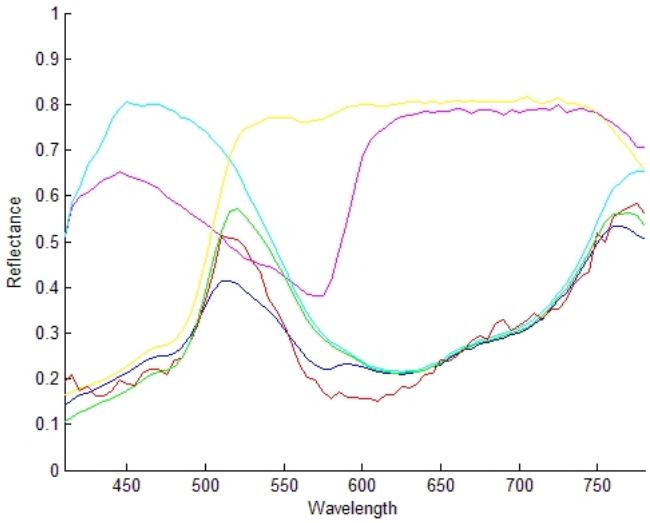

Figure 140: Concentration prediction example for a spectrum taken form cyan and yellow overlapping area at 30% density (an example of wrong ink colors prediction).

by red line. On the other hand, if Algorithm 4 is applied to the spectrum, then the results are as follows: cyan ink at 20% and yellow ink at 40% densities, and their predicted mixture is shown by green line. In this case the colors of the inks were predicted correctly, but the number of inks in any combinations was limited to two by Algorithm 4 in comparison with Algorithm 8.

Table 15 shows results of concentration prediction of Algorithms 8 and 4 applied to *spectrum* 4. Algorithm 8 did not predict the right number of colorants used to create spectrum *spectrum* 4. If Algorithm 4 is used, then ink colors are predicted correctly. However, it must be noted that Algorithm 4 limits the number of inks which can be used in any combination to two. Let us also notice that the difference between errors computed by Algorithm 8 and Algorithm 4 is relatively small ($RMSE\ error \in [0, ..., 1]$).

Table 15: Concentration prediction of spectrum 4 using two different schemes.

Scheme	Cyan conc.	Magenta conc.	Yellow conc.	Black conc.	RMSE
Alg. 8	20	10	30	-	0.0415
Alg. 4	20	-	40	-	0.0551

Figure 141 shows magenta and yellow dots at 30% density, and Figure 142 depicts some spectral reflectance curves of some overprinted areas of yellow and magenta inks at 30% density.

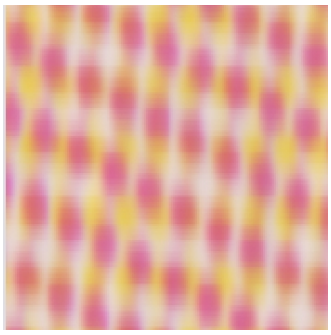

Figure 141: Magenta and yellow dots at 30% density.

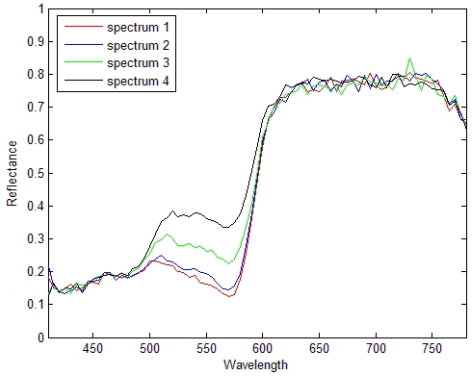

Figure 142: Spectral variations in dot overlapping regions.

Table 16 contains results of employing Algorithm 8 for spectra shown in Figure 142. Even though, these example spectra were taken from overprinted regions of magenta and yellow inks at 30% density, the predicted concentrations vary a lot. It must be also noticed that the spectral variations in dot overlapping regions did not result in bad colorant predictions, i.e. for all spectra cyan and magenta inks were predicted. Let us notice also that the predicted concentrations of yellow ink do not vary unlike to concentrations of magenta ink.

Table 16: Influence of spectral variations in dot overlapping regions on concentration prediction for magenta and yellow inks at 30% density.

Sample	Magenta conc.	Yellow conc.	RMSE
spectrum 1	50%	30%	0.0427
spectrum 2	40%	30%	0.0477
spectrum 3	30%	30%	0.0447
spectrum 4	20%	30%	0.0525

Figure 143 shows magenta, cyan and yellow dots at 30% density, and Figure 144 depicts some spectral reflectance curves of some overprinted areas of yellow, cyan and magenta inks at 30% density.

Table 17 contains results of employing Algorithm 8 for spectra shown in Figure 144. The spectral variations in dot overlapping regions did not result in bad colorant predictions. Let us notice that the concentrations of a particular ink do not vary a lot.

Based on the results presented above we can come to the following conclusions:

1. spectral reflectance variations in dot overlapping areas are significant, what makes exact concentration prediction impossible. Usually the colors of inks used to create the overlapping areas can be predicted correctly;

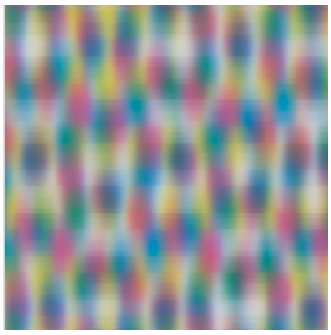

Figure 143: Magenta, cyan and yellow dots at 30% density.

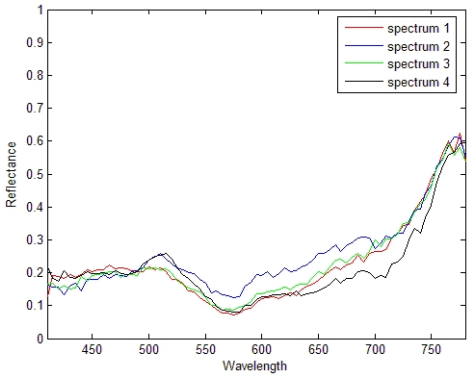

Figure 144: Spectral variations in dot overlapping regions where three inks were used.

Table 17: Influence of spectral variations in dot overlapping regions on concentration prediction for magenta, cyan and yellow inks at 30% density.

Sample	Magenta conc.	Yellow conc.	Cyan conc.	RMSE
spectrum 1	50%	30%	30%	0.0386
spectrum 2	40%	30%	20%	0.0262
spectrum 3	50%	30%	20%	0.0354
spectrum 4	40%	30%	30%	0.0309

2. spectral reflectance variations in dot overlapping areas can make correct colorant prediction impossible (for example three instead of two inks can be predicted). This is mainly caused by some distortion of spectral information made by the spectral camera during the measurement phase and the inaccuracy of the opaque version of the single-constant Kubelka-Munk theory for prediction of spectral reflectance of printing inks.

These results suggest problems in color separation process. It must be noticed that probably most of these problems are caused by incorrect color information coming from the spectral camera (see "Printing dot measurements" in Section 2.5.2). In particular, the distortion of spectra and spectral noise makes it difficult to evaluate the correctness and accuracy of presented algorithms. Nevertheless, later we will gives some possible improvements for concentration prediction process which can make it be more accurate.

5.2 Color separation based on spectra comparison

In this section we will utilize algorithms presented in Sections 5.1.1 and 5.1.2 to design an algorithm for printing dot separation process.

Algorithm 9 is a simple extension of Algorithm 2 presented in Section 5.1.1. The input of the algorithm has the same meaning as for previous algorithms.

Alg. 9 Full one-ink concentration prediction.

Input: R, C, M, Y, K.
Output: S

```
1    begin
2        error = 1; index = 1; ink = 1
3        for each spectrum C_i in set C
4            temp = RMSE(R, C_i);
5            if (temp ≤ error) then
6                                error = temp;
7                                index = i;
8        for each spectrum M_i in set M
9            temp = RMSE(R, M_i);
10           if (temp ≤ error) then
11                               error = temp;
12                               index = i;
13                               ink = 2;
14       for each spectrum Y_i in set Y
15           temp = RMSE(R, Y_i);
16           if (temp ≤ error) then
17                               error = temp;
18                               index = i;
19                               ink = 3;
20       for each spectrum K_i in set K
21           temp = RMSE(R, K_i);
22           if (temp ≤ error) then
23                               error = temp;
24                               index = i;
25                               ink = 4;
26       return [error, ink, index]
27   end
```

For each printing ink the algorithm goes through all spectra corresponding to

various densities of printing dots, and for each spectrum it computes the root mean square error between the current processed spectrum and the input spectrum R. A spectrum which fits the best the input spectrum R is saved in the form of two identifiers (ink, $index$) and spectra for the next printing ink are processed. The output of the algorithm is the spectrum which corresponds to a printing ink of color ink at density $index$. The spectrum yields the minimum error among all other considered spectra for all printing inks.

Algorithm 10 is a straightforward scheme which combines Algorithms 8 and 9 to perform concentration prediction based on spectra comparison. R is a spectral reflectance of an area where single ink was applied, an overprinted area where various inks were applied, or the paper surface. The input values to the algorithm also are sets of spectra C, M, Y and K, where spectra contained in each of the sets correspond to a particular printing ink at various densities.

Alg. 10 Concentration prediction based on spectra comparison.

Input: R, C, M, Y, K, P.
Output: S, $numberOfInks$.

1 **begin**
2 $KM1_R = KM1_{FULL}(R, C, M, Y, K)$;
3 $KM_R = PRED_{FULL}(R, C, M, Y, K)$;
4 $P_R = RMSE(R, P)$;
5 S = solution with minimum error among $\{KM1_R, KM_R, P_R\}$;
6 $numberOfInks$ =number of selected inks;
7 return $[S, numberOfInks]$
8 **end**

After the algorithm is done it returns the number of inks stored in $numberOfInks$ which probably were used to create the input spectrum R. Furthermore, it gives information about which inks and what density for each of the inks were used to create the input spectrum R. In the case when R corresponds to the paper surface, the number of inks $numberOfInks$ is equal to zero.

Let us also notice that the color separation process is usually performed on a spectral image of printing dots. In this case, the procedure described by Algorithm 10 must be executed for each spatial location of the spectral image. The extension is straightforward and we will be skipped here.

Now we will assess how well Algorithm 10 performs color separation process. Figure 145 shows cyan and magenta dots which are to be separated. Figures 146 and 147 represent the separation result.

Figures 146 and 147 suggest that the separation process for Figure 145 failed.

Figure 145: Cyan and magenta dots which are to be separated.

Figure 146: Cyan dot separation.

Figure 147: Magenta dot separation.

In particular, the cyan and magenta dot separation became impossible for overlapping and nonoverlapping regions (where one ink was applied). The paper surface was recognized properly, but it must be noticed that the paper spectrum was selected manually and passed to Algorithm 10 (the influence of paper spectrum selection on color separation was discussed in Section 5.1.1).

The color separation process for spectral images of printing dots failed. We strongly believed that it is mainly caused by problems discussed in Sections 5.1.1 and 5.1.2 which are directly caused by the color noise which exist in the acquired spectral images. In particular, we think that the color separation results can be considerably improved when working with spectral images of good quality. Furthermore, the correctness and accuracy of presented algorithms can not be properly evaluated due to noisy spectral images. Nevertheless, we strongly believe that the proposed algorithms using the Kubelka-Munk theory can be used successfully to solve the color separation problem.

Time complexity considerations Let us now analyse the time complexity of Algorithm 10 when applied to a spectral image S of size $n \times m$ with spectral dimension d. The number of known spectra passed to the algorithm is denoted by k (usually $k = 41$, what means that for each printing ink there are 10 spectra which correspond to densities from 10% to 100% with 10% step, and the paper surface spectrum). For each pixel p with spectral reflectance r the algorithm performs the following steps:

1. *step* $KM1$ - RMSE error is calculated k times;
2. *step* $KM2$ - RMSE error is calculated $\binom{inks=4}{pair=2}(\frac{k-1}{4})^2$ times;
3. *step* $KM3$ - RMSE error is calculated $\binom{inks=4}{triple=3}(\frac{k-1}{4})^3$ times;
4. *step* $KM4$ - RMSE error is calculated $\binom{inks=4}{quartette=4}(\frac{k-1}{4})^4$ times.

The above steps must be done for each of $n \times m$ pixels in the spectral image, and these steps contain mainly matrix calculations. This suggests that any color

separation scheme based the proposed scheme may be computationally demanding, and causing the color separation process to be impractical.

Table 18 presents some time complexity requirements of Algorithm 10 for color separation process when applied to spectral images of different spatial sizes.

Table 18: Time complexity of Algorithm 10 for spectral images of different sizes.

Spectral image size	Time in sec.
6×6	28.7
11×11	95.0
21×21	345.1

Each of the spectral images is 75 dimensional, and the measurements were done on a computer working under Windows XP with 512 MB of RAM memory and AMD Athlon 64-bit 3200+ processor. For comparison, let us notice that the spectral image shown in Figure 145 has 84×47 spatial size, and in this situation the required time would be considerably longer.

Thus, another approach is needed to deal with the low accuracy of spectral images and time complexity problems of the inverse color separation process.

Possible improvements in the color separation algorithm In Section 5.1.2 we introduced Kubelka-Munk theory known as single-constant Kubelka-Munk theory. In this case, we know the (K/S) ratios for each colorant at each wavelength λ computed by using Equation (30) based on spectral reflectance of the colorant.

Unlike to single-constant Kubelka-Munk theory, in two-constant Kubelka-Munk theory the scattering S and absorption K coefficients are know for each colorant. Similarly to single-constant Kubelka-Munk theory, double-constant Kubelka-Munk theory assumes that the additivity is valid for the scattering S and absorption K coefficients [15]:

$$K_{\lambda,mix} = c_1 k_{\lambda,1} + c_2 k_{\lambda,2} + ... + c_k k_{\lambda,k} \tag{33}$$

$$S_{\lambda,mix} = c_1 s_{\lambda,1} + c_2 s_{\lambda,2} + ... + c_k s_{\lambda,k} \tag{34}$$

Dividing Equation (33) by Equation (34) we will get the $\frac{K}{S}$ ratio for a mixture:

$$\frac{K}{S}_{\lambda} = \frac{c_1 k_{\lambda,1} + c_2 k_{\lambda,2} + ... + c_k k_{\lambda,k}}{c_1 s_{\lambda,1} + c_2 s_{\lambda,2} + ... + c_k s_{\lambda,k}} \tag{35}$$

Then Equation (31) is used to calculate the spectral reflectance of the mixture. Let us notice that the single-constant Kubelka-Munk theory makes a simplifying assumption that the scattering coefficient in Equation (35) is constant yielding

Equation (30). The single-constant version is usually used for materials where the colorants have negligible scattering coefficients in comparison to the background support (for example paper) [12].

A comparison of single and double constant Kubelka-Munk theories to predict mixtures of acrylic paints was made by [15] with noticeable superiority of double-constant Kubelka-Munk theory. [13] explains that for translucent printing inks printed on paper, the reflectance of the paper substrate makes a contribution to the reflectance of the system and therefore Equation (31) should be replaced by:

$$R = \frac{(R_g - R_\infty)/R_\infty - (R_\infty R_g - 1)\exp\left((1/R_\infty - R_\infty)Sx\right)}{(R_g - R_\infty) - (R_g - 1/R_\infty)\exp\left((1/R_\infty - R_\infty)Sx\right)} \tag{36}$$

, where R_g is the spectral reflectance of the substrate, the coefficient S is defined for a unit thickness of the colorant layer, x is the thickness of the colorant layer, and R_∞ is defined as in Equation (31).

In our case, the difficulties in applying the two-constant Kubelka-Munk theory and Equation (36) lie in determining the K and S coefficient for each colorant (printing ink) and colorant thickness. [13] suggests the following methods for determining the S and K coefficients for printing inks:

1. print each colorant of interest over two different kinds of paper or substrates, for example over white and black paper at a particular thickness;

2. based on Equation (36) make a set of two simultaneous equations with two variables S and K;

3. solve the system of two simultaneous equations.

Due to the failure of color separation process based on spectra comparisons, we will try to overcome problems presented in Section 5.1.1 and 5.1.2, and in the next section we will try to develop an alternative method for color separation. The proposed method is based on plane selections of a spectral image to perform color separation process.

5.3 Color separation based on by plane selection

In Section 2.3.1 we introduced spectral images and spectral imaging systems, and in Section 2.1.7 we described the subtractive color mixing model. In this section we will utilize this information for printing dot color separation.

A spectral image can be represented as ordered sequence of planes. Each plane corresponds to a sampled wavelength of the visible spectrum and contains spectral reflectance values at the wavelength for each spatial location of imaged scene. Furthermore, if we take a particular plane p corresponding to wavelength λ and color c, then high spectral reflectance values of plane p corresponds to regions of the spectral image which possess significant amount of color c. For example, if we

take a plane corresponding to wavelength 650 nm (red color), then high spectral reflectance values will correspond to these regions of the spectral image which possess significant amount of reddish.

Let us now consider four inks of the four-color printing process: cyan, magenta, yellow and black. Figures 56 - 71 show spectral reflectance curves for different inks and different kinds of paper. To make color separation possible we will utilize the theory underlying spectral imaging and ink properties.

Let us choose a particular ink color (except for black) and denote the ink by c. We are looking for plane p (corresponding to wavelength λ) with the following properties (from now we consider plane p as gray color image):

- all regions corresponding to printing dots of color c will be shown in dark color;
- all other regions (corresponding to paper and printing dots of color different from c) will be shown in white color;
- overlapping areas where printing ink of color c has been applied will be shown in dark color;
- missing parts of printing dots of color c in overlapping areas will not be shown in dark color (missing dots in overlapping areas will be detected).

At this point the main question is: "What plane should be selected to see printing dots of a particular ink?". It is clear that the selected plane should satisfy properties given above. Furthermore, the experimental study showed that:

- plane corresponding to wavelength 435 nm should be selected to see yellow printing dots;
- plane corresponding to wavelength 510 nm should be selected to see magenta printing dots;
- plane corresponding to wavelength 635 nm should be selected to see cyan printing dots;

Figure 148 presents cyan and yellow dots at 30% density. According to the above procedure to see cyan and yellow printing dots the planes at 635 nm and 435 nm should be selected respectively. The result of color separation is shown in Figures 149 and 150 for cyan and yellow dots respectively.

Figure 151 presents cyan and magenta dots at 30% density. According to the given procedure to make the color separation of cyan and magenta printing dots, the planes at 635 nm and 510 nm should be selected respectively. The result of color separation is shown in Figures 152 and 153 for cyan and magenta dots respectively.

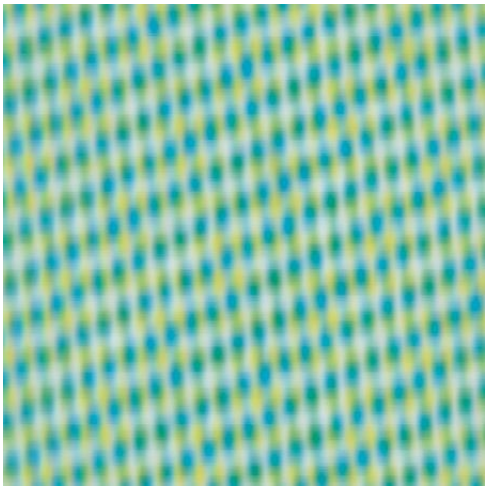

Figure 148: Cyan and yellow dots at 30% density.

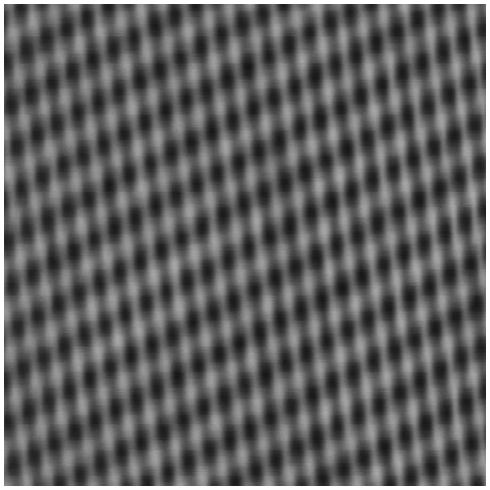

Figure 149: Cyan dot separation.

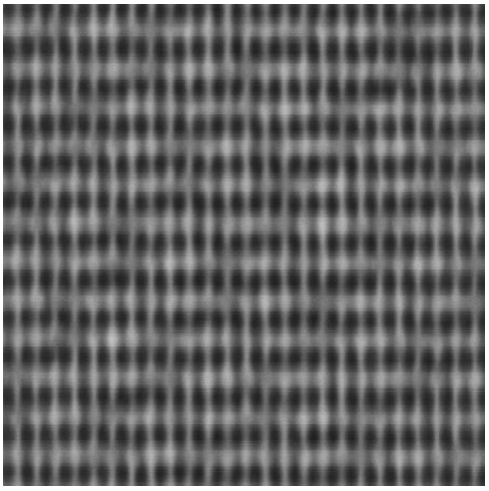

Figure 150: Yellow dot separation.

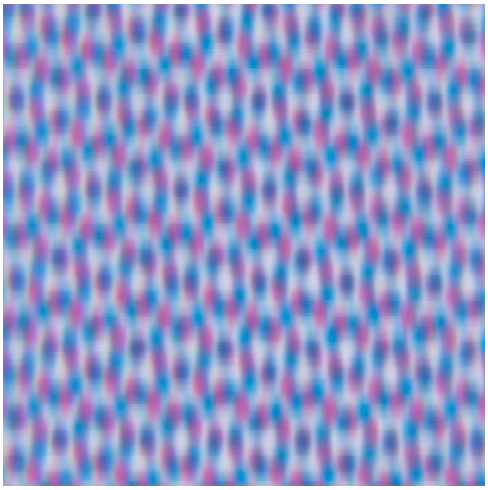

Figure 151: Cyan and magenta dots at 30% density.

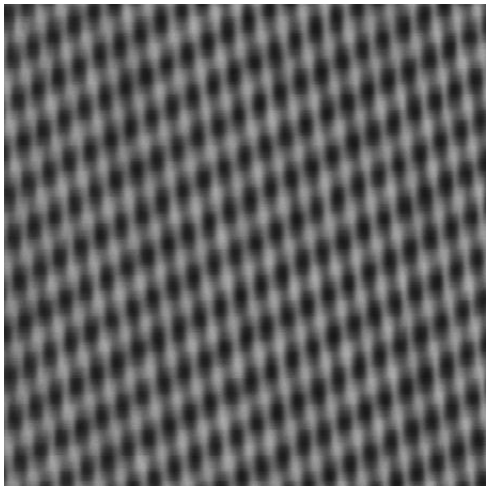

Figure 152: Cyan dot separation.

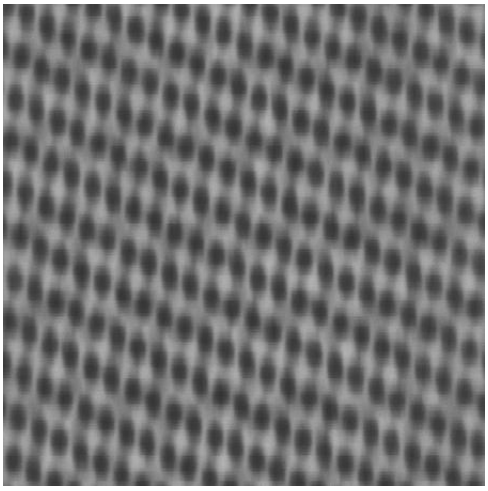

Figure 153: Magenta dot separation.

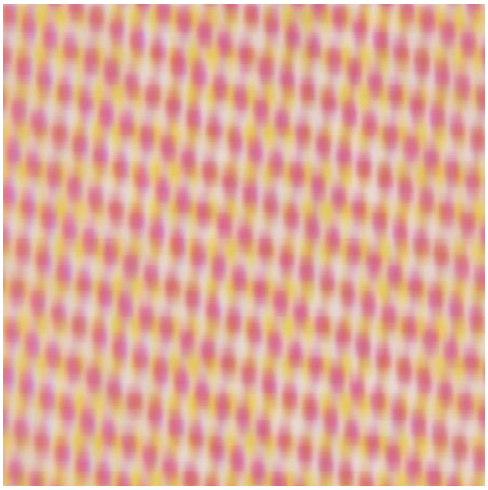

Figure 154: Yellow and magenta dots at 30% density.

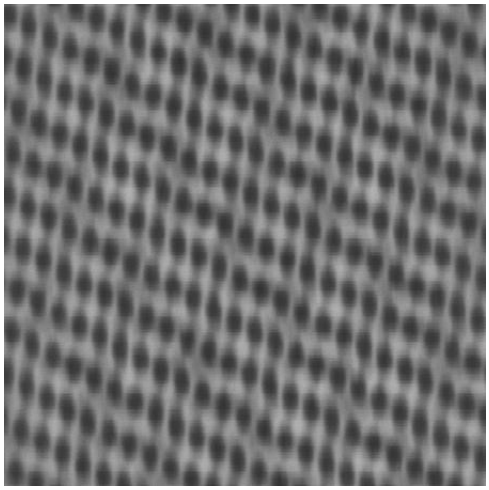

Figure 155: Magenta dot separation.

Figure 154 shows yellow and magenta dots at 30% density. According to our scheme to make the color separation of yellow and magenta printing dots, the planes at 435 nm and 510 nm should be selected respectively. The result of color separation is shown in Figures 156 and 155 for yellow and magenta dots respectively.

Figure 157 shows a little bit more complicated example of printing for color separation process. Magenta, cyan and yellow dots were applied at 30% density to create this output. Let us notice that there exist some regions where three inks were overprinted. According to our scheme to make the color separation for magenta, cyan and yellow printing inks, the planes at 510 nm, 635 nm and 435 nm should be selected respectively. The result of color separation is shown in Figures 158, 159 and 160 for cyan, magenta and yellow dots respectively.

Figure 161 shows a printing output where yellow and black inks were applied at 30% density. According to our scheme to make the color separation for yellow ink the plane at 435 nm should be selected. Unfortunately, there is no plane selection for black ink. The result of color separation is shown in Figure 162.

Let us notice that Figure 162 contains yellow and black printing dots causing the color separation process to fail. It is easy to see that the problem lies in the black ink - the regions with black printing dots will appear in each selected plane making the separation impossible. This is the only reason why the above color separation procedure excludes the black ink. Nevertheless, the exclusion does not solve the problem and another scheme for dealing with prints containing black ink is needed.

Let us now assume that we have a spectral image S of printing dots where at least 3 printing inks were used including black ink. In this situation the problem

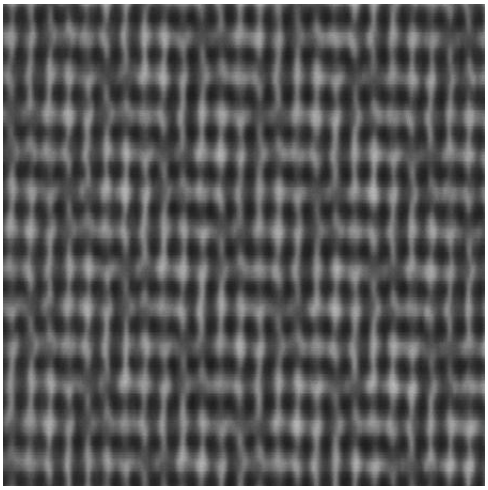

Figure 156: Yellow dot separation.

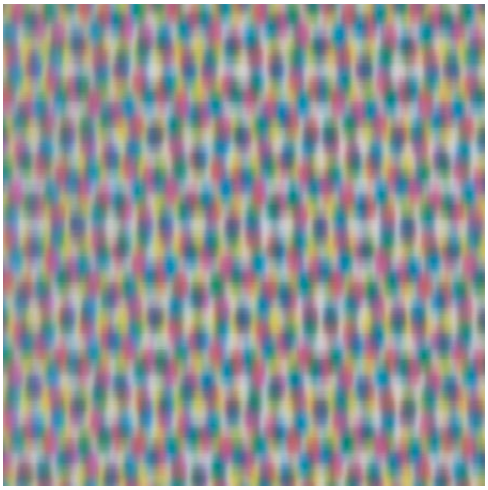

Figure 157: Yellow, cyan and magenta dots at 30% density.

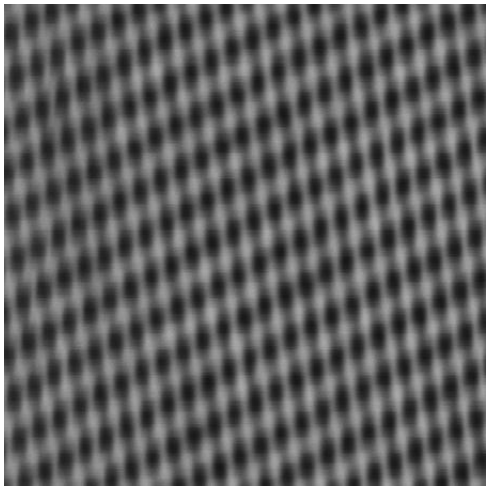

Figure 158: Cyan dot separation.

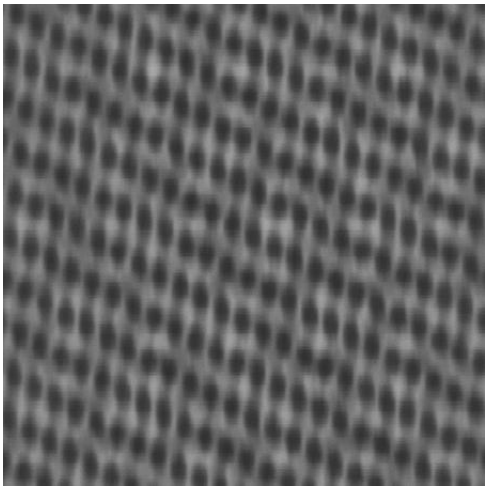

Figure 159: Magenta dot separation.

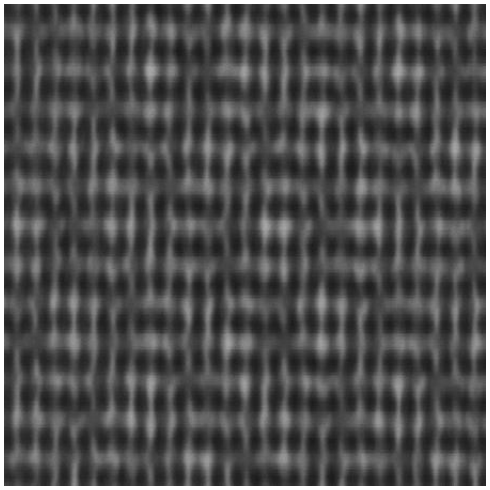

Figure 160: Yellow dot separation.

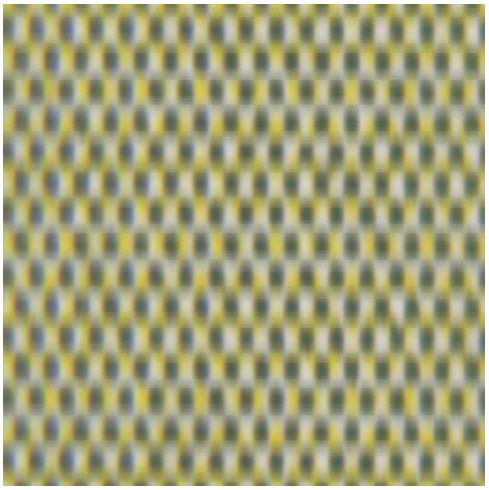

Figure 161: Yellow and black dots at 30% density.

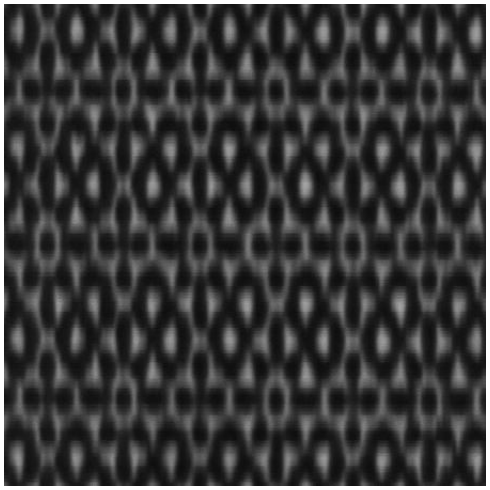

Figure 162: Yellow dot separation.

with prints containing black ink can be easily solved according to the following procedure:

1. make color separation of all inks used in the image S according to the plane selection scheme;
2. choose any two gray color images (denoted by $I1$ and $I2$) produced by the separation process. Let us noticed that the black dots exist in images $I1$ and $I2$;
3. find locations of black dots based on images $I1$ and $I2$. Remove the locations corresponding to black dots from images $I1$ and $I2$;
4. create black dot separation image based on locations of black dots computed in the previous step.

In this situation, when two inks where used to create a spectral image S including black ink, we can use the algorithms proposed in Section 5.1.2. In the case of two-ink spectral images including black ink the algorithms should work well and should separate the dots of different colors correctly.

Let us now to sum up the scheme for color separation based on plane selection in the form of Algorithm 11. The input values to the algorithm are:

1. R is a spectral image for which color separation process is to be performed;
2. $INKS$ is a set of colors of printing inks which were used to create image R.

The output of the algorithm are gray color images which represent color separation result. Each of the images corresponds to an ink (let us say ink) of the input set $INKS$ and contains all printing dots of color ink which exist in the input spectral image S. It must be also noticed that the algorithm requires the user to give the inks of interest for which the color separation must be done. The set $INKS$ should not contain any printing inks which were not used to create the input image R. The output images can be further post-processed, for example they can be converted to black-white images.

Alg. 11 Color separation based on plane selection.

Input: S, $INKS$.
Output: gray-color images representing color separation

```
1    begin
2        for each ink ink in set INKS
3            if (ink == cyan) then
4                    show plane at 435 nm as gray color image
5            ifelseif (ink == magenta) then
6                    show plane 510 nm as gray color image
7            ifelseif (ink == yellow) then
8                    show plane 635 nm as gray color image
9            else return;
10       return;
11   end
```

6 Conclusions

In this thesis, a detailed study concerning spectral imaging and spectral measurement of paper and print was done. We investigated the pros and cons of spectral imaging on the example of spectral characterization of paper and print and showed how the spectral imaging can be used in the field of paper and color printing industries. This final chapter briefly reviews the main results coming from the experimental part of the thesis, our contributions to the thesis and discusses possible future research concerning this area. The research done in the thesis consists of the following parts:

- **Basic spectral characterization for paper and print.** We investigated and showed how spectral imaging can be used for basic spectral characterization of paper and print including the determination of average spectra and spectral variances of different kinds of blank paper, spatial variation of blank paper surface, black color formations for different kinds of paper, average spectra and spectral variances of printing inks and dot gain characteristic. Each of these issues has been studied deeply and some applications and procedures were developed to visualize the results coming from the experimental part.
- **Mottling characterization and prediction.** In part we investigated if there exists any spatial correlation between the spectral reflectance of plain paper and printed paper in exactly the same spatial areas where different

kinds of mottling have been applied. We also examined if there exist any differences between spatial correlation of prints to plain papers for different types of mottling.

The conclusions concerning these issues were done on the basis of data coming from sample measurements under D65 illumination. The derived conclusions are the same for different kinds of mottling for different types of paper. A number of applications were developed to visualize the spatial correlation results, and special schemes to treat and visualize the spectral radiance values (being output of measurements under UV illuminant) have been proposed.

In this part we also examined average spectral reflectance of different kinds of mottling for different kinds of paper under D65 and UV illuminants. We investigated if we can distinguish different kinds of mottling based on average spectral reflectance values.

We also encountered some problems concerning measurements under UV illumination. The power of the UV light turned out to be too weak to successfully measure papers with small amount of fluorescent and whitening agents including paper type B, paper type A and paper type C. Nevertheless, on the basis of other measurements and derived results, we believe that the conclusions for these papers are the same as for paper type D. The simplest solution to the problem is to employ stronger UV illuminant and repeat the sample measurement phase.

- **Inverse color separation process.** We studied whether the concentration prediction process of printing inks is possible based on spectral reflectance data with the use of the Kubelka-Munk theory to predict ink concentrations in dot overlapping areas. Next we developed an algorithm for color separation process based on spectra comparison.

  In the sample measurement phase, we also encountered some problems related to the quality of spectral images. We tried to acquire spectral images of printing dots with our spectral imaging system. In this situation, the ImSpector V8 spectral camera was equipped with a magnification optics and lens and located at very close distance to the imaged sample to be able to see the structure of printing dots. This causes some noise and distortion of spectral reflectance data and consequently the resulting spectral images were not very accurate and of bad quality. The implications of these problems on the color separation process were deeply discussed in the thesis.

  The concentration prediction process in dot overlapping areas based on the Kubelka-Munk theory encountered some problems - inaccurate predictions of printing inks and their concentrations. We strongly believe that this inaccuracy of concentration prediction is related to the noise in acquired spectral images and our algorithms can perform better if applied to spectral images

of good quality. The direct consequence of the inaccuracy of concentration prediction process is the inaccuracy of color separation process based on spectra comparison.

The thesis also suggested some improvements for higher accuracy of the concentration prediction process including:

- hardware improvements - the concept of spectral microscopy would be a excellent solution for the problem of noisy spectral images. The connection of spectral camera and a microscope will result in high quality and high resolution spectral images;
- software improvements - the double constant Kubelka-Munk theory could be used to get better prediction accuracy. This involves determining the absorption and scattering coefficients for each printing ink (some numerical methods for determining the coefficients were described in the thesis and in particular, they required each ink to be printed on carefully selected two different substrates). Furthermore, the equation for translucent materials instead of opaque materials could be used to improve the prediction accuracy. In this case, however, some methods for determining the thickness of the colorant layer must be developed.

Due to the inaccuracy of color separation process based on spectra comparison and its high computational cost, an alternative method for color separation process has been developed. This method is based on plane selections of a spectral image which reveal some information about the placement and structure of printing dots.

Future research concerning spectral characterization of paper and print should mainly done in the field of color separation process. Firstly, some spectral images should be taken with the help of spectral camera attached to a microscope, and then the real accuracy of proposed algorithms should be evaluated. Secondly, some new samples should be prepared in a special way (described in the thesis) which allows for determining the absorption and scattering coefficient for each colorant. Also some methods for determining the colorant thickness or overprinted area thickness should be developed. Then, the double constant Kubelka-Munk theory for translucent inks could be applied for concentration prediction process and for inverse color separation process.

A RGB images of printing dots

Figures 163 - 174 show RGB images of printing dots taken by Epson Perfection V700 scanner.

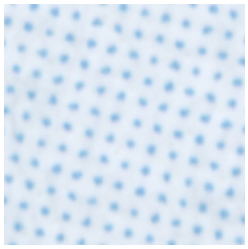

Figure 163: Cyan dots at 2%.

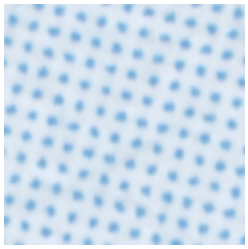

Figure 164: Cyan dots at 5%.

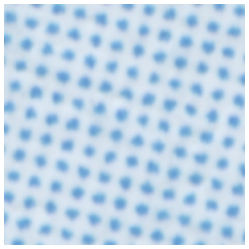

Figure 165: Cyan dots at 10%.

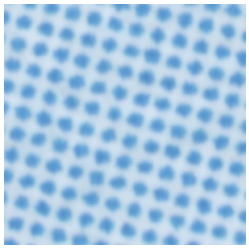

Figure 166: Cyan dots at 20%.

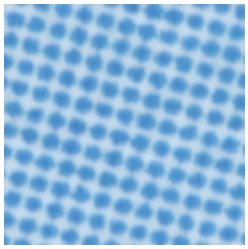

Figure 167: Cyan dots at 30%.

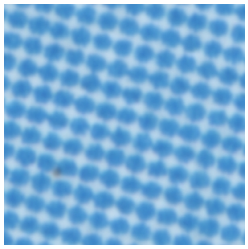

Figure 168: Cyan dots at 40%.

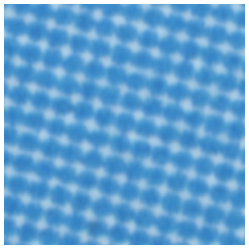

Figure 169: Cyan dots at 50%.

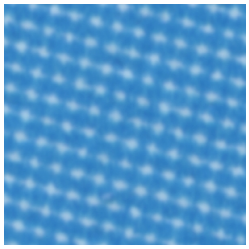

Figure 170: Cyan dots at 60%.

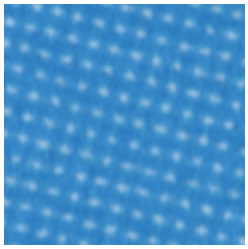

Figure 171: Cyan dots at 70%.

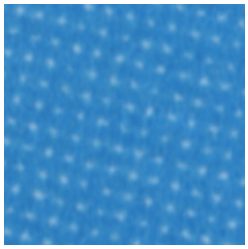

Figure 172: Cyan dots at 80%.

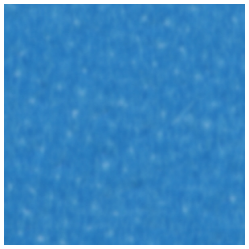

Figure 173: Cyan dots at 90%.

Figure 174: Cyan dots at 100%.

References

[1] P. Oittinen, H. Saarelma: *Printing*. Papermaking Science and Technology, 1998.

[2] A. Sadonikov, P. Salmela, L. Lensu, J. Kamarainen, H. Kälviäinen: *Mottling Assessment of Solid Printed Areas and Its Correlation to Perceived Uniformity*. In Proc. of the 14th Scandinavian Conference of Image Processing, pp. 411-418, 2005.

[3] C. Fahlcrantz: *On the Evaluation of print mottle*. Doctoral thesis, Computer science and communication, Royal Institute of Technology, Stockholm, 2005.

[4] *http://en.wikipedia.org/wiki/CMYK_color_model*

[5] S. Berns, D. Wyble: *A Critical Review of Spectral Models Applied to Binary Color Printing*. Journal of Color Research and Application, Vol. 25, No. 1, pp. 4-19, 2000.

[6] G. Sharma, W. Wu, E. Dalal: *The CIEDE2000 color-difference formula: Implementation notes, supplementary test data, and mathematical observations*. Color Research and Application, accepted for publication in April 2004. Available at: *http://www.ece.rochester.edu/˜gsharma/ciede2000/ciede2000noteCRNA.pdf*

[7] H. Kang: *Digital Color Halftoning*. SPIE–The International Society for Optical Engineering, 1999.

[8] M. Mohammadi, M. Nezamabadi, L. Taplin, R. Berns: *Pigment Selection Using Kubelka-Munk Turbid Media Theory and Non-Negative Least Square Technique*. Available at: *http://www.cis.rit.edu/mcsl/research/reports.php*

[9] R. Bala: *Device Characterization, Chapter 5 in Digital Color Imaging Handbook by G. Sharma*. CRC Press, 2003.

[10] C. Koopipat, N. Tsumura, Y. Miyake, M. Fujino: *Effect of Ink Spread and Opitcal Dot Gain on the MTF of Ink Jet Image*. The Journal of Imaging Science and Technology, Vol. 46, No. 4, pp. 321-325, 2002.

[11] B. Smith, E. Simonson: *Inkjet printing for textiles*. Computer printing 19, pp. 23-29, 1987.

[12] R. Berns: *Billmeyer and Saltzman's Principles of Color Technology*. John Wiley & Sons, 2000.

[13] S. Westland, C. Ripamonti: *Computational Colour Science using MATLAB*. John Wiley & Sons, 2004.

[14] D. Tzeng, R. Berns: *Spectral-Based Ink Selection for Multiple-Ink Printing I. Colorant Estimation of Original Object*. In Proc. of the IS&T/SID Sixth Color Imaging Conference: Color Science, Systems, and Applications, pp. 106-111, 1998.

[15] M. Mohammadi, R. Berns: *Verification of the Kubelka-Munk turbid media theory for artist acrylic paint*. Munsell Color Science Laboratory Technical Report, 2004. Available at: *http://www.art-si.org*

[16] G. Sharma: *Digital Color Imaging Handbook*. CRC, 2002.

[17] G. Field: *Color and Its Reproduction*. Graphic Arts Technical Foundation, 1988.

[18] M. Yamaguchi: *Introduction of Natural Vision*. Imaging Science and Engineering laboratory, Tokyo Institute of Technology. Available at: *http://www.isl.titech.ac.jp/˜guchi/NV*

[19] M. Fairchild, M. Rosen, G. Johnson: *Spectral and Metameric Color Imaging*. Munsell Color Science Laboratory, Center for Imaging Science, Rochester Institute of Technology.

[20] *SPECIM. Spectral Camera. User manual (Version 1.1)*. September 2001. Available at: *http://www.specim.fi/*

[21] H. Trussell, M. Kulkarni: *Sampling and processing of color signals*. IEEE Trans. Image Processing, Vol. 5, pp. 677–681, 1996.

[22] J. Parkkinen, T. Jaaskelainen, E. Torniainen. *Do we really need spectral imaging?* Electronic imaging, Vol. 15, pp. 2, 2004.

[23] T. Jaaskelainen, J. Hiltunen, H. Laamanen, J. Parkkkinen: *Accurate spectral measurement and reconstruction*. Second International Symposium on multispectral imaging and high accurate color reproduction, pp. 79-88, 2000.

[24] A. Tremeau: *Lecture onColor Vision and Color Science*. LIGIV Laboratory, Saint Etienne University, France.

[25] D. Malacara: *Color Vision and Colorimetry: Theory and Applications*. Spie Press, 2002.

[26] *http://en.wikipedia.org/wiki/CIE_1931_color_space*

[27] *http://en.wikipedia.org/wiki/Standard_illuminant*

[28] M. Stone: *Color in information display principles, perception, and models*. ACM SIGGRAPH 2004 Course Notes, ACM Press.

[29] *http://www.ipaper.com/*

[30] *http://en.wikipedia.org/wiki/Halftone#Multiple_screens_and_colour_halftoning*

[31] *http://en.wikipedia.org/wiki/Lab_color_space*

[32] R. Gonzalez, R. Woods: *Digital Image Processing*. Addison-Wesley, 1992.

[33] J. Adams, P. Dolin: *Printing Technology*. Thomson Delmar Learning, 2001.

[34] T. Daly: *The Digital Color Printing Handbook: A Photographer's Guide to Creative Color Management and Printing Techniques*. Amphoto Books, 2005.